# NEURAL CIRCUITS AND SYNAPSES FOR EARLY STAGE VISUAL PROCESSING

**by**

**Michael B. Manookin**

**A dissertation submitted in partial fulfillment**
**of the requirements for the degree of**
**Doctor of Philosophy**
**(Neuroscience)**
**in The University of Michigan**
**2009**

**Doctoral Committee:**

**Associate Professor Jonathan B. Demb, Chair**
**Professor Peter F. Hitchcock**
**Professor Richard I. Hume**
**Associate Professor Gina R. Poe**
**Assistant Professor Geoffrey G. Murphy**

## Table of Contents

## List of Figures

**Figure**

## Abstract

**NEURAL CIRCUITS AND SYNAPSES FOR EARLY STAGE VISUAL PROCESSING**

**by**

**Michael B. Manookin**

**Chair: Jonathan B. Demb**

Ganglion cells are the output neurons of the retina and send visual information through the optic nerve to various targets in the brain. There are ~20 types of ganglion cell, and most types encode contrast, the variance in light intensity around the mean level. This thesis investigates how retinal circuits and synapses encode contrast. At the first level of light processing, cone photoreceptors release glutamate onto ON and OFF bipolar cells, which respond to objects brighter or darker than the background and release glutamate onto the corresponding type of ganglion cell. This thesis demonstrates how excitatory and inhibitory synapses work in concert to encode light information in three ganglion cell types: ON Alpha, OFF Alpha, and OFF Delta cells.

First, I demonstrate that excitatory synapses adapt following prolonged stimulation. Following a switch from high to low contrast, a ganglion cell rapidly decreases its responsiveness and recovers slowly over several seconds. This slow adaptation arises from reduced glutamate release from presynaptic bipolar cells. Glutamate released from bipolar cells binds to $\alpha$-amino-3-hydroxyl-5-methyl-4-isoxazole-propionate (AMPA) and N-methyl-D-aspartic acid (NMDA) receptors on ganglion cell dendrites. NMDA-mediated responses were present in multiple ganglion cell types but absent in one type, the ON Alpha cell. OFF Alpha and Delta cells used NMDA receptors for encoding different contrast ranges: the full range (Alpha), including near-threshold responses, versus a high range (Delta). The Delta cell expresses the NR2B subunit, consistent with an extra-synaptic NMDA receptor location that is activated by glutamate spillover during high contrast stimulation. The contrast-independent role for NMDA receptors in OFF Alpha cells correlated with two circuit properties: high contrast sensitivity and low presynaptic basal glutamate release.

In addition to excitatory glutamate synapses, OFF ganglion cells are driven by the removal of synaptic inhibition (disinhibition). Experiments implicate the AII amacrine cell, better known for its role in rod vision, as a critical circuit element through the following pathway: cone → ON cone bipolar cell → AII cell → OFF ganglion cell. These results show a new role for disinhibition in the retina and suggest a new role for the AII amacrine cell in daylight vision.

# Chapter 1

# Introduction

## Light processing in the retina

The retina constitutes the first stage of visual information processing. In vertebrates, such as humans and guinea pigs, photons of light pass through the retinal layers where it may be absorbed by a photoreceptor. Photoreceptors are separated into two classes: rods and cones. Generally, rods subserve dim light vision, conditions where few photons are present. Cones operate under daylight conditions, and the cone circuitry is the focus of this thesis.

Cones release glutamate onto bipolar cells and horizontal cells (Figure 1.1). In darkness, cones are depolarized and continuously release glutamate; a bright stimulus has the opposite effect: cones hyperpolarize, causing an attenuation of glutamate release. Cones release glutamate onto two classes of cone bipolar cell: ON and OFF cells. ON and OFF bipolars express different classes of glutamate receptor causing opposite responses to cone glutamate release. ON bipolar cells express a metabotropic glutamate receptor (mGluR6) on their dendrites (Nomura et al., 1994), and when glutamate activates the receptor, it closes a cation channel, causing the ON cell to hyperpolarize. Thus, a flash of light that would hyperpolarize cones suppresses glutamate release onto an ON bipolar cell and, subsequently, depolarize the cell. OFF bipolars

express ionotropic glutamate receptors, specifically AMPA and kainate receptors. The same light flash removes glutamate release from OFF bipolar dendrites and causes a hyperpolarization.

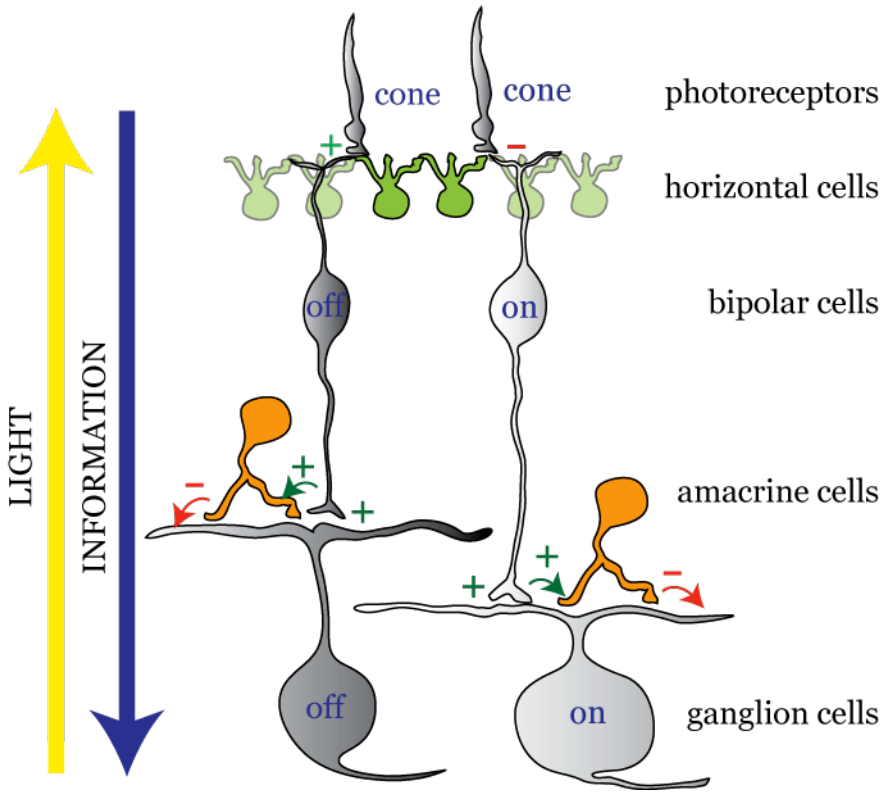


**Figure 1.1. Schematic of the vertebrate retina.**

At the next level of signaling, bipolar cells release glutamate onto ganglion cells. Ganglion cells generally express AMPA and NMDA receptors (Fletcher, Hack, Brandstatter, & Wassle, 2000; Grunert, Haverkamp, Fletcher, & Wassle, 2002; Kalloniatis, Sun, Foster, Haverkamp, & Wassle, 2004), which allow glutamate release from bipolar cells to preserve the stimulus sign established in the bipolar cells. Thus, an ON ganglion cell receives glutamatergic input from ON bipolar cells, and vice versa. Bipolar cells can also excite an amacrine cell, a

type of inhibitory interneuron. An amacrine cell can, in turn, inhibit bipolar cell terminals (i.e., feedback inhibition) or ganglion cells (i.e., feedforward inhibition). Ganglion cells integrate excitatory and inhibitory inputs and transmit visual signals down their axons, which form the optic nerve.

## Contrast processing and adaptation

Humans can see and behave across a wide range of lighting conditions. For example, one can navigate through the woods on a starry night, where each rod photoreceptor absorbs a photon only about once per minute; and yet one can also navigate across the beach on a cloudless day, where cone photoreceptors absorb thousands of photons per second. The mean luminance between these extreme examples can differ by ~100-million-fold. This wide range of intensities poses a computational problem for the retina, because a ganglion cell can fire only about 20 action potentials (spikes) in the ~100 msec integration time of a postsynaptic neuron. Thus, the ganglion cell must continually adjust its sensitivity so that the wide range of light levels (~8 log units) can be encoded with the narrow range of output signals (~1-2 log units).

To deal with the mismatch between input and output, the retina adjusts its sensitivity depending on the mean intensity, through mechanisms of light adaptation. These mechanisms are varied and include: the switch between rod photoreceptors (for night vision) and cone photoreceptors (for day vision); intrinsic properties of each receptor type that alter sensitivity depending on mean intensity; and post-receptoral mechanisms within the retinal circuitry. The

apparent purpose of light adaptation is to adjust the ganglion cell's response to report, not the absolute intensity, but rather the *contrast*, or the *percentage deviations* from the mean intensity (Troy & Enroth-Cugell, 1993).

The contrast of a visual stimulus is a more robust property than the absolute intensity. To illustrate this point, consider a simple example, where an observer gazes at a bird on a background of leaves. Assume that the bird reflects 50% more light towards the observer's eye compared to the leaves (and ignore color in this example). Now imagine that the light reflected to the eye is reduced either by the observer's action (i.e., putting on a pair of sun glasses) or by a change in the light source reflecting off the objects (i.e., a cloud passes overhead, obscuring the sunlight). In either case, the light reflected into the eye is reduced 10-fold or more. However the *relative* reflectance is unchanged: the bird still reflects 50% more light than the leaves. Hence, it follows that the retina (and most of the visual system) is designed to encode contrast or the relative reflectance of objects within the same scene: the relative reflectance of objects represents a stable property of natural scenes, whereas absolute reflectance does not. Physiological measurements of retinal ganglion cells confirm this idea, showing that responses to a given contrast level are relatively constant over several orders of mean light level.

## Contrast adaptation

Ganglion cells are sensitive to an approximately 100-fold variance in contrast level, and processing such a wide range of contrasts is challenging.

Hanglion cells face a fundamental problem: at low contrast, they must increase sensitivity to utilize their response range (~0-20 spikes) while preserving the signal-to-noise ratio, whereas, at high contrast, they must decrease sensitivity to avoid saturating the response (Baccus & Meister, 2004; Demb, 2002). To face this challenge, the circuit adapts to the relevant range of contrast using mechanisms of plasticity. These mechanisms adjust their responses on different time scales: a fast adaptation that acts over tens to hundreds of milliseconds and a slow adaptation that acts over several seconds.

Slow adaptation occurs when a cell is stimulated strongly with a few seconds of high contrast. This period of high-contrast stimulation causes a cell to depolarize and spike. When the stimulus returns to a low-contrast, the cell subsequently hyperpolarizes below the previous resting membrane potential. During this afterhyperpolarization (AHP), spiking is suppressed while the membrane potential depolarizes back to the baseline level. Slow contrast adaptation occurs at several levels of visual processing, including the visual cortex and retina. Previous research suggests that slow contrast adaptation in some cortical neurons and retinal ganglion cells arises from intrinsic mechanisms (Baccus & Meister, 2002; Sanchez-Vives, Nowak, & McCormick, 2000a, 2000b; Solomon, Peirce, Dhruv, & Lennie, 2004).

Previous studies of slow contrast adaptation in mammalian retina used extracellular recording (Brown & Masland, 2001; Chander & Chichilnisky, 2001; Smirnakis, Berry, Warland, Bialek, & Meister, 1997; Solomon et al., 2004). We studied slow adaptation in retinal ganglion cells using a more powerful technique,

intracellular recording. We found that slow adaptation results from a slowly recovering AHP, as shown for cortical neurons and salamander ganglion cells. However, these experiments showed that slow adaptation in ganglion cells does not arise primarily from an intrinsic property of the cell. Rather, ganglion cell adaptation arises from an emergent mechanism of the retinal network: reduced glutamate release from presynaptic (nonspiking) bipolar cells (Chapter 2; Manookin and Demb, 2006). This presynaptic mechanism complements intrinsic mechanisms for slow adaptation found at later stages of the visual pathway.

## The spatial receptive field

A ganglion cell calculates contrast over a specific retinal region known as its spatial receptive field. There are approximately 20 different types of ganglion cell. Each type encodes different aspects of visual information, and some are highly selective for features such as wavelength of light or the direction of moving objects. Here, we focused on three types of ganglion cell (ON $\alpha$, OFF $\alpha$, and OFF $\delta$) that have relatively conventional receptive fields, consisting of an excitatory center region and an inhibitory surround region.

A ganglion cell's excitatory center is coextensive with its dendritic tree. Thus, the photoreceptors overlaying the span of the ganglion cell's dendritic tree contribute to driving the excitatory center. These photoreceptors synapse onto both ON and OFF bipolar cells. However, most ganglion cell types collect synapses from either ON-type bipolar cells or OFF-type bipolar cells and then inherit the ON- or OFF-center property from these presynaptic bipolar cells.

A ganglion cell's inhibitory surround corresponds to the retinal region that extends beyond the dendritic tree. For example, an OFF-center cell that is excited by light decrements coincident with the dendrites is inhibited by light decrements in the surround region, beyond the dendrites. The center and surround combine to report the relative contrast over space. The center is commonly stronger than the surround, so that a large object covering both the center and surround will drive a center response (e.g., a large bright object will provide some excitation to an ON-center cell). For some cell types (e.g., the $\beta$/X-type ganglion cell of the cat or the midget/Parvocellular-projecting ganglion cell of the monkey), the center and surround combine in an approximately linear fashion (Enroth-Cugell & Robson, 1966). Thus, the response to center plus surround stimulation can be predicted reasonably well by summing the separate responses to center and surround measured individually. For other cell types (e.g., the $\alpha$/Y-type of the cat) there is a nonlinear combination of center and surround regions. For these nonlinear receptive fields, the presynaptic bipolar cells may be described by relatively linear receptive fields; the major nonlinearity of the ganglion cell receptive field may arise at the level of the synaptic output of the bipolar cells as they converge onto the ganglion cell (Demb, Zaghloul, Haarsma, & Sterling, 2001). In general, a ganglion cell's excitatory center is driven by the presynaptic bipolar cells, whereas the surround arises at two levels: the horizontal cells in the outer retina and the amacrine cells in the inner retina.

My thesis research found two cell types that challenge this canonical view (Manookin, Beaudoin, Ernst, Flagel, & Demb, 2008). Presenting an OFF

ganglion cell with a dark spot in the receptive field center excited the cell. Whole-cell recordings revealed that the excitatory center of OFF $\alpha$ and $\delta$ ganglion cells is formed from a combination of bipolar cell excitation and removed inhibition (i.e., disinhibition). Thus, tonic inhibition at steady mean luminance was increased or decreased depending on stimulus sign. Experiments revealed the source of the disinhibition to be the AII amacrine cell, which plays a fundamental role in encoding dim-light (photopic) vision (Bloomfield & Dacheux, 2001; Singer, 2007). Our research demonstrates a new role for disinhibition in the retina and suggests a function for the AII amacrine cell in daylight vision (Chapter 3; Manookin et al., 2008).

**Physical limits to contrast sensitivity**

Under optimal conditions, humans can detect small spots with contrasts of 1-3%(Dhingra, Kao, Sterling, & Smith, 2003). Studies using similar methods to detect the threshold of ganglion cells have arrived at similar threshold values under optimal conditions (Dhingra et al., 2003). Thus, there may be certain conditions where perceptual thresholds are driven by a small number of ganglion cells, and there may be relatively little information lost between the retina and the visual cortex. However, there is a loss between the contrast threshold that could (theoretically) be computed at the level of photon absorptions by the photoreceptors and the threshold measured in the ganglion cell. Recent computational analysis suggests that, under certain conditions, this loss may be a factor of ~10-20 (Borghuis, Sterling, & Smith, 2009).

The ability to detect contrast depends on the statistics of photon arrival and the statistical properties of various cellular processes. Photon arrival follows Poisson statistics, where the mean and the variance are equal. For example, consider a case where a ganglion cell integrates signals over 20 photoreceptors across the retina and over a 100 msec 'integration time' and where the mean rate of photoisomerizations (i.e., absorbed photons) is 50 isomerizations (R*) per photoreceptor per second (i.e., 5 R*/photoreceptor/integration time). In this case, the mean R* rate over the spatial/temporal integration (20 x 100 x 5) is 10,000 and the variance (across multiple 'trials') would be the same. Thus, the SD (or noise level) would be the square root or 100 R*. The signal-to-noise ratio (mean/SD per integration time) would then be 10,000/100 = 100. Therefore, the cell in question would have difficulty detecting a difference of less than 1/100 (i.e., SD/mean) or 1% deviation from the mean level (i.e., 1% contrast). The contrast threshold would be worse (i.e., higher) when the mean luminance is lower, the number of integrated photoreceptors is fewer, or the temporal integration time decreases.

Similar limitations on contrast sensitivity arise at the bipolar cell → ganglion cell synapse. Similar to photon arrival, glutamate release from bipolar cells obeys Poisson statistics. Glutamate is released from a presynaptic bipolar cell axon terminal and can bind to ionotropic glutamate receptors (AMPA and NMDA) on the postsynaptic ganglion cell dendrite. AMPA and NMDA receptors differ on a number of fundamental properties (for review, see (Dingledine, Borges, Bowie, & Traynelis, 1999; Erreger, Chen, Wyllie, & Traynelis, 2004)). For

example, AMPA receptors have fast kinetics (deactivation time of <3 ms), whereas NMDA receptors have slower kinetics (deactivation time of >30 ms). Thus, the ability of synapses to transfer information at low contrast depends on the release rates onto AMPA, NMDA, and inhibitory receptors and the number of synapses that are integrated by a given neuron. The threshold of a cell would be best (i.e., lowest) in the presence of high release rates and a large number of integrated synapses (i.e., high degree of synaptic convergence within the circuitry).

In Chapter 4, we show that different cell types utilize different release and receptor-expression strategies for visual encoding. The ON Alpha cell receives a high rate of presynaptic glutamate release. Under these high release rates, NMDA receptors and desensitizing AMPA receptors would be saturated at baseline and would thus be ineffective at contrast encoding (Figure 4.8). The ON Alpha cell avoids this problem by expressing non-desensitizing AMPA receptors and not expressing NMDA receptors. Unlike ON Alpha cells, OFF Alpha cells do not receive a high rate of presynaptic glutamate release at baseline. OFF cells employ a different mechanism for maintaining a high sensitivity at low contrast. They express synaptic NMDA receptors, which are highly sensitive to small increases in presynaptic glutamate release, such as those observed at low contrast. These and other findings presented in Chapter 4 demonstrate a new role for NMDA receptors in information encoding in the nervous system.

This thesis focuses on the circuits and synapses involved in contrast processing at the level of ganglion cells. Specifically, the following chapters

explore the network mechanisms involved in the formation of a ganglion cells receptive field center, which involves presynaptic mechanisms (i.e., bipolar cell and amacrine cell input) and postsynaptic mechanisms, such as glutamate receptor expression and localization relative to synaptic release sites. Together, these findings advance previous knowledge and understanding about information processing in the retina with potential applications to synapses in other brain areas.

## Chapter 2

## Presynaptic Mechanism for Slow Contrast Adaptation in Mammalian Retinal Ganglion Cells


### Summary

Visual neurons, from retina to cortex, adapt slowly to stimulus contrast. Following a switch from high to low contrast, a neuron rapidly decreases its responsiveness and recovers over 5–20 s. Cortical adaptation arises from an intrinsic cellular mechanism: a sodium-dependent potassium conductance that causes prolonged hyperpolarization. Spiking can drive this mechanism, raising the possibility that the same mechanism exists in retinal ganglion cells. We found that adaptation in ganglion cells corresponds to a slowly recovering afterhyperpolarization (AHP), but, unlike in cortical cells, this AHP is not primarily driven by an intrinsic cellular property: spiking was not sufficient to generate adaptation. Adaptation was strongest following spatial stimuli tuned to presynaptic bipolar cells rather than the ganglion cell; it was driven by a reduced excitatory conductance, and it persisted while blocking GABA and glycine receptors, K(Ca) channels, or mGluRs. Thus, slow adaptation arises from reduced glutamate release from presynaptic (nonspiking) bipolar cells.

## Introduction

The natural environment contains a wide range of possible lighting conditions. To operate across these conditions, the visual system must adapt its sensitivity to the statistics of the immediate environment. At the first stage of vision, the retina adapts to the mean intensity, a process also called ‘‘light adaptation,’’ through intrinsic photoreceptor properties as well as postreceptoral mechanisms (Pugh, Nikonov, & Lamb, 1999; Troy & Enroth-Cugell, 1993; Walraven, Enroth-Cugell, Hood, Macleod, & Schnapf, 1990). The retina further adapts to the range of intensities relative to the mean, also called ‘‘contrast adaptation.’’ A common hypothesis suggests that, at low contrast, the retina increases sensitivity to improve the signal-to-noise ratio, whereas, at high contrast, the retina decreases sensitivity to avoid saturating the response (Baccus & Meister, 2004; Demb, 2002). Contrast adaptation is largely absent in photoreceptors and therefore must arise through either network mechanisms or intrinsic properties of ganglion cells (Baccus & Meister, 2002; Rieke, 2001; Sakai, Wang, & Naka, 1995).

At multiple levels of the visual system, including the retina, cells adapt to contrast over at least two time scales: a fast adaptation that acts in tens to hundreds of milliseconds, and a much slower adaptation that acts over several seconds (Baccus & Meister, 2002; Carandini & Ferster, 1997; Maffei, Fiorentini, & Bisti, 1973; Movshon & Lennie, 1979; Smirnakis et al., 1997; Solomon et al., 2004). The slow form of contrast adaptation was recently demonstrated in the primate magnocellular pathway in vivo (Solomon et al., 2004). Magnocellular

retinal or thalamic cells were stimulated with high contrast followed by a switch to low contrast or mean luminance. Following the switch, these cells showed a suppressed response that required a recovery period of over 10 s. To put this time period into perspective, consider that under steady contrast conditions, ganglion cell responses can be predicted based on the previous ~300 ms of the stimulus (Baccus & Meister, 2002; Chichilnisky, 2001; Kim & Rieke, 2001; Zaghloul, Boahen, & Demb, 2003). Thus, a 10 s period of adaptation is relatively long.

Slow contrast adaptation in magnocellular neurons required a high-contrast stimulus effective at driving the cell (Solomon et al., 2004). This apparent activity dependence suggested that the mechanism for adaptation is intrinsic to the ganglion cell. Indeed, there is good precedent for this hypothesis: some cortical neurons express an intrinsic property for slow contrast adaptation (Sanchez-Vives et al., 2000a). When a cortical cell is stimulated strongly, either by a visual stimulus or direct current injection, the cell depolarizes and fires spikes. At the offset of stimulation, the cell hyperpolarizes and this afterhyperpolarization (AHP) recovers slowly over seconds.

The AHP suppresses spiking responses to low-contrast stimuli (Carandini & Ferster, 1997; Sanchez-Vives et al., 2000a, 2000b). Ion substitution experiments demonstrated that the cortical AHP was caused largely by a potassium conductance sensitive to intracellular sodium (Sanchez-Vives et al., 2000a). This potassium conductance can apparently be activated by sodium influx caused by either synaptic input in the absence of spiking, or by spiking in

the absence of synaptic input (Carandini & Ferster, 1997; Sanchez-Vives et al., 2000a, 2000b; Vidyasagar, 1990). Thus, for a cortical cell, spiking is sufficient but not necessary to drive adaptation. A retinal ganglion cell might express a similar intrinsic mechanism for slow adaptation. However, ganglion cells also show adaptive effects to small stimulus patches, implicating a possible mechanism in presynaptic bipolar cells (Brown & Masland, 2001). Cortical cells in area MT also express adaptation that is primarily caused by a presynaptic mechanism (Kohn & Movshon, 2003, 2004).

Previous studies of slow contrast adaptation in mammalian retina used extracellular recording (Brown & Masland, 2001; Chander & Chichilnisky, 2001; Smirnakis et al., 1997; Solomon et al., 2004). Here we studied slow adaptation in mammalian ganglion cells using intracellular recording. We show that slow adaptation results from a slowly recovering AHP, as shown in cortical cells and salamander ganglion cells (Baccus & Meister, 2002; Carandini & Ferster, 1997; Sanchez-Vives et al., 2000b). However, slow adaptation in ganglion cells does not arise primarily from an intrinsic property of the cell. Rather, ganglion cell adaptation arises from a network mechanism: reduced glutamate release from pre-synaptic (nonspiking) bipolar cells. This presynaptic mechanism complements intrinsic mechanisms for slow adaptation found at later stages of the visual pathway.

## Results

### Demonstration of Slow Contrast Adaptation in Intracellular Recordings of Mammalian Ganglion Cells In Vitro

We tested for slow adaptation in brisk-transient (Y-type) ganglion cells in an intact (retinal pigment epithelium-attached) in vitro preparation of the guinea pig retina (Demb, Haarsma, Freed, & Sterling, 1999; Demb, Zaghloul, & Sterling, 2001). We targeted Y-type cells by recording from the largest cell bodies in the ganglion cell layer (see Experimental Procedures). We focused on Y-type cells because we could target them routinely and because they are probably homologous to magnocellular pathway cells (or a subset of these cells), which show strong adaptation in vivo (Kaplan & Shapley, 1982; Levitt, Schumer, Sherman, Spear, & Movshon, 2001; Solomon et al., 2004). A cell was stimulated with a drifting grating that alternated between high contrast (100%, 10 s) and low contrast (5%–40%, 20 s; see Experimental Procedures). At the offset of high contrast, the spiking response in a cell, recorded extracellularly, was completely suppressed and recovered over a 7.0 s period (Figure 2.1A). A whole-cell, voltage recording of the same cell showed that the period of suppressed spiking corresponded to a period of membrane hyperpolarization that slowly recovered—an afterhyperpolarization (AHP; Figure 2.1B), as reported in salamander cells (Baccus & Meister, 2002). Across cells, spiking was suppressed at the offset of high contrast and took 6.9 ± 0.9 s to recover (n = 10; see Experimental

Procedures). Each cell recorded intracellularly showed an AHP during the period of suppressed spiking (AHP amplitude, 28.8 ± 0.7 mV; n =4).

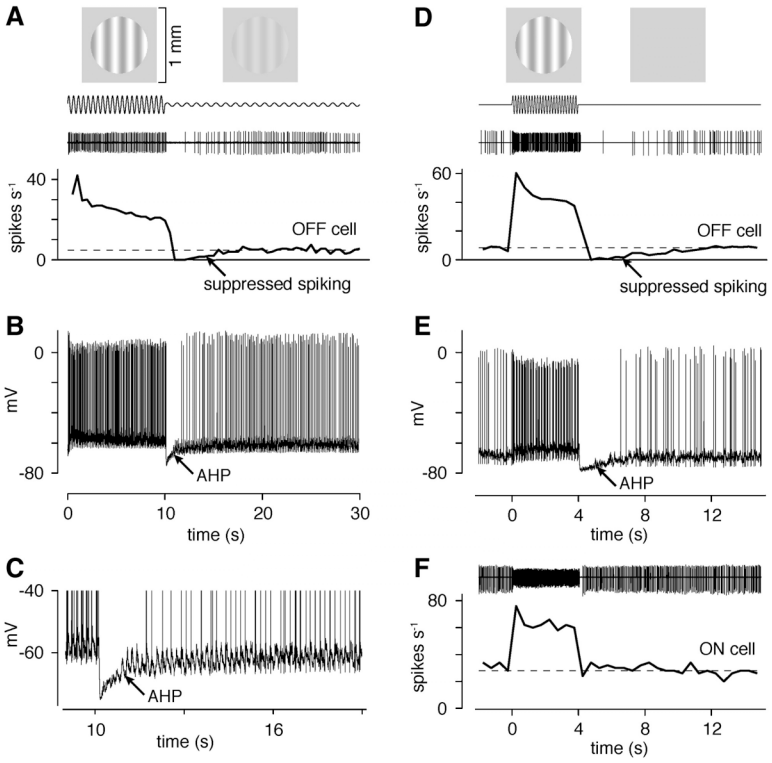


**Figure 2.1. OFF Ganglion Cells Show Reduced Spiking following High Contrast Due to a Slow Afterhyperpolarization**

(A) An OFF cell was stimulated with a drifting sine wave grating with contrast alternating between high (100%, 10 s) and low (20%, 20 s). Following high contrast, spiking was suppressed and required 7.0 s to recover to the baseline level (dashed line). Trace at top shows one cycle of the loose-patch, extracellular recording; poststimulus time histogram (psth) at bottom shows the average firing rate across four repeats (bin size, 500 ms). Grating spatial frequency was 6.7 cycles $mm^{-1}$ and drifted at 6 Hz (stimulus trace does not show 6 Hz). (B) Intracellular recording of the same cell and stimulus shown in (A). Following high contrast, the membrane potential showed an afterhyperpolarization (AHP) of -11.4 mV that required 5.5 s to recover to baseline.
The period of suppressed spiking corresponded to the period of the AHP.
(C) Enlarged area of (B) showing the AHP.
(D) An OFF cell showed a maintained discharge (7.8 Hz) that was suppressed following a 4 s, high-contrast stimulus (drifting grating, 6.7 cycles $mm^{-1}$, 6 Hz). Trace at top shows loose-patch record; psth at bottom shows the average firing rate across four repeats. The spike rate recovered over 6.5 s.
(E) Intracellular recording of the cell in (D) shows an AHP following the stimulus that required 4.0 s to return to the resting potential. (F) Extracellular recording of an ON cell does not show a prolonged reduction in spike rate following high contrast (drifting grating, 6.7 cycles $mm^{-1}$, 6 Hz). Following high contrast, spiking was suppressed for only ~100 ms, evident in the raw trace.

Many ganglion cells discharge continuously at mean luminance, and this discharge is suppressed following a period of high contrast. In one representative cell, maintained firing took 6.5 s to recover to the baseline rate (Figure 2.1D). An intracellular recording of the same cell showed that the period of suppressed spiking corresponded to the period of an AHP (Figure 2.1E). Under our conditions, suppressed spiking following high contrast was found in nearly all OFF-center Y-type cells but was weak or absent in most ON-center Y-type cells (Figure 2.1F; time to recovery, 0.5 ± 0.4 s; n = 6). However, we observed adaptation in several other types of ON-center or ON-OFF ganglion cells, suggesting that the ON pathway did express slow adaptation for certain cell types. For example, in three direction-selective ganglion cells (one ON-center type, two ON-OFF types) recorded intracellularly, the switch from a 4 s grating (6 Hz; 6.7 cycles $mm^{-1}$; 100% contrast) to mean luminance caused a large AHP (−9.5 ± 0.1 mV) that recovered over 6.2 ± 1.1 s (data not shown).

For periods of high contrast of either 1 or 8 s, the AHP amplitude increased from −4.0 ± 0.6 mV to −7.8 ± 0.9 mV and the recovery time increased from 3.6 ± 0.8 s to 7.9 ± 1.6 s (n = 6 OFF Y-type cells); the AHP integral increased from −5.0 ± 0.6 mV s to −20.9 ± 2.1 mV s (Figure 2.2). Thus, longer periods of contrast evoked larger and longer-lasting AHPs. In the following studies, we focused on OFF-center Y-type cells to investigate the mechanism for slow adaptation, because we could target these cells routinely and they showed strong adaptation as reflected by the AHP.

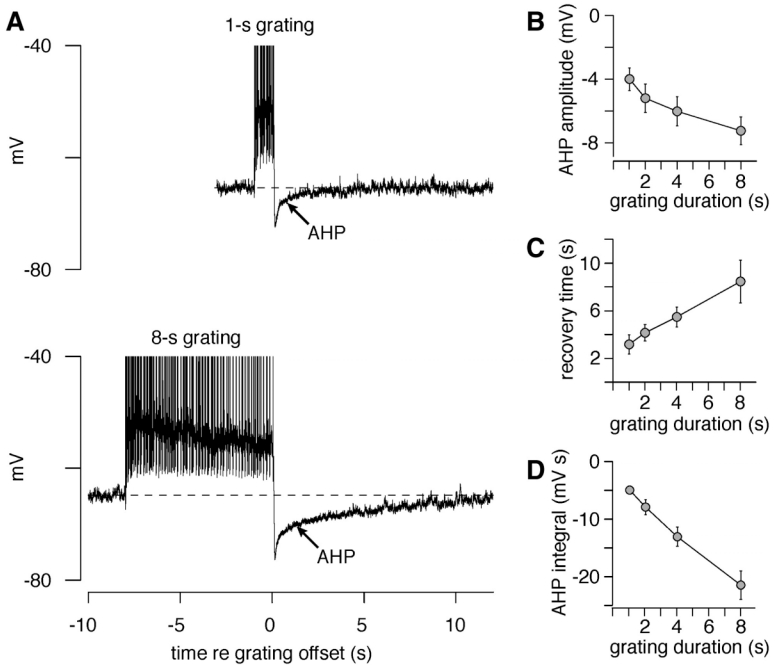


**Figure 2.2. Longer Periods of High Contrast Evoke Larger and Longer-Lasting Afterhyperpolarizations**

(A) An OFF cell was stimulated with either a 1 s or 8 s grating (100% contrast, 6.7 cycles $mm^{-1}$; 6 Hz) followed by mean luminance. Compared to the 1 s grating, the 8 s grating evoked a larger AHP (−6.9 mV versus −10.8 mV) that took longer to recover (2.0 s versus 5.7 s), resulting in a larger AHP integral (−5.5 mV s versus −25.2 mV s; see Experimental Procedures). Recovery was measured as the time required to return 90% back to the resting potential (see Experimental Procedures).

(B) Longer periods of high contrast increased the amplitude of the AHP (n = 6 cells). Error bars indicate SEM across cells.

(C) Longer periods of high contrast increased the time needed to recover to the resting potential.

(D) Longer periods of high contrast increased the AHP integral.

## Spiking Is Neither Sufficient nor Necessary to Generate the Visually Evoked Afterhyperpolarization

We first tested whether the AHP results from an intrinsic mechanism (e.g., potassium channel) in the ganglion cell that is sensitive to sodium influx, as found in cortex; a cortical cell adapts following either a visual stimulus or direct current

injection (Sanchez-Vives et al., 2000a). We stimulated the same ganglion cell with either the grating stimulus or a direct injection of current through the electrode (Figure 2.3A). Both the grating and the current step evoked a membrane depolarization and a train of spikes, and in fact the current step evoked a larger depolarization (8.3 ± 0.8 mV versus 7.0 ± 0.7 mV; a difference of 1.3 ± 0.6 mV, $p < 0.05$) and a higher spike rate (27.9 ± 4.7 spikes $s^{-1}$ versus 15.7 ± 1.8 spikes $s^{-1}$; a difference of 12.2 ± 3.3 spikes $s^{-1}$, $p < 0.005$). However, only the grating evoked a large and long-lasting AHP (Figure 2.3B). Across cells, the AHP amplitude ~300 ms after stimulus offset was −5.8 ± 0.6 mV following the grating versus −2.3 ± 0.2 mV following the current step (difference of 3.4 ± 0.5 mV, $p < 0.001$; $n = 9$). Four seconds after stimulus offset, the AHP persisted following the grating (−1.9 ± 0.3 mV) but was nearly back to baseline following the current step (−0.30 ± 0.15 mV; difference of 1.6 ± 0.3 mV; $p < 0.001$; sampling window, 1.0 s). Furthermore, the AHP integral was about four times larger following the visual stimulus (−18.9 ± 2.3 mV s) relative to the current step (−4.4 ± 1.4 mV s; difference, 14.5 ± 0.9 mV s; $p < 0.001$). We also tried sine-wave current injection at the stimulus frequency (6 Hz, +0.2 nA amplitude; Figure 2.3C). In this case ($n = 8$ cells), current injection evoked a higher spike rate (10.3 ± 1.1 spikes $s^{-1}$ versus 7.2 ± 1.2 spikes $s^{-1}$), but the grating evoked a larger AHP amplitude (−5.1 ± 0.5 mV versus −1.0 ± 0.3 mV) and a larger AHP integral (−17.3 ± 2.0 mV s versus −2.8 ± 2.0 mV s). Thus, even though current injection evoked a larger spiking response, the grating evoked a larger AHP, indicating that spiking alone is not sufficient to generate the full visually evoked AHP.

Apparently the mechanism for slow contrast adaptation differs between retina and primary visual cortex (Sanchez-Vives et al., 2000b).

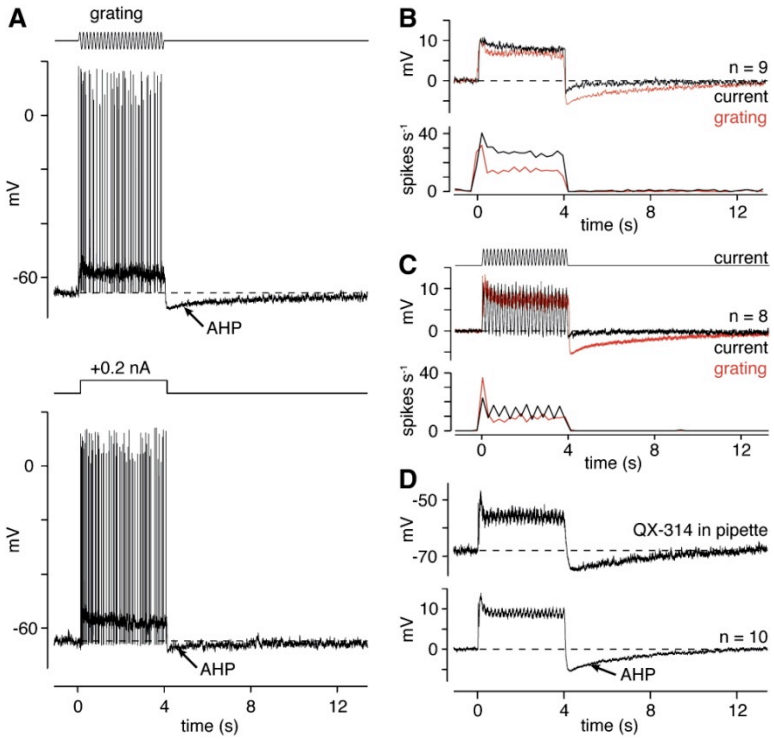


**Figure 2.3. Spiking Is Neither Sufficient nor Necessary to Generate the Afterhyperpolarization**

(A) An OFF cell was stimulated with either a 4 s grating (top; 100% contrast, 6 Hz, 6.7 cycles $mm^{-1}$) or a 4 s step of positive current (bottom; +0.2 nA). Both stimuli generated membrane depolarization and spiking. At the offset of the grating, there was a relatively large AHP (−5.5 mV), whereas at the offset of the current pulse, there was a smaller AHP (−3.2 mV).

(B) Average subthreshold membrane potential and spike rate for the grating stimulus and the current step (n = 9 cells; 100 Hz sampling). Membrane depolarization and spiking responses were larger following the current step, whereas the AHP was larger and longer lasting following the grating. Thus, spiking alone, as evoked by the current step, was not sufficient to generate the full visually evoked AHP. Stimulus responses were advanced 46 ms in time to align with the current responses. Spike rate was binned at 250 ms here and in (C).

(C) Same format as (B), except the current stimulus was a 4 s period of 6 Hz sine-wave stimulation with a peak of +0.2 nA (current injection protocol shown above response traces). Current injection evoked a higher spike rate, whereas the grating evoked a larger and longer-lasting AHP (n = 8 cells).

(D) An OFF cell was stimulated with a 4 s grating (100% contrast, 6 Hz, 6.7 cycles $mm^{-1}$) while applying QX-314 (5 mM) through the pipette to block spiking (top). On average (bottom, n = 10 cells), the AHP was similar to control conditions; thus, spiking was not necessary to generate the AHP.

We next asked whether spiking was necessary to generate the AHP. We included QX-314 (5 mM) in the pipette solution to block voltage-gated sodium channels in the recorded cell (Connors & Prince, 1982). Under these conditions, a grating stimulus evoked a membrane depolarization without spiking (n = 10; Figure 2.3D). Following stimulus offset, each cell showed an AHP that was, on average, −4.8 ± 0.4 mV in amplitude and required 6.2 ± 0.6 s to return to the resting potential (AHP integral, −14.4 ± 2.2 mV s). Thus, spiking was not necessary to generate the AHP.

## Spatial Sensitivity of the Afterhyperpolarization Suggests a Presynaptic, Bipolar Cell Mechanism

We hypothesized that the retinal basis for the AHP might arise from a presynaptic mechanism, possibly in the bipolar cells that release glutamate and excite the ganglion cell. In the above experiments, we routinely used a high spatial frequency grating, with bar width of ~80–100 μm. This bar width is much narrower than the ~600 μm receptive field center of the ganglion cell, but similar to the ~100 μm receptive field center of bipolar cells (D. Dacey et al., 2000; Demb, Zaghloul, & Sterling, 2001). We directly examined the effect of spatial frequency on the AHP amplitude. A low spatial frequency (0.3 cycles $mm^{-1}$) evoked a strong response at the 6 Hz drift rate of the grating (F1 amplitude; (Demb, Zaghloul, & Sterling, 2001; Hochstein & Shapley, 1976), as expected, but produced only a small AHP (Figure 2.4A). A high spatial frequency (6.7 cycles $mm^{-1}$) evoked a steady depolarization with a small 6 Hz modulation riding on top, followed by a large AHP (Figure 2.4A). Both spatial frequencies evoked a similar

average spike rate over time (F0 component; Figure 2.4B), and so, as shown above, the magnitude of the AHP did not directly correspond to the preceding spike rate.

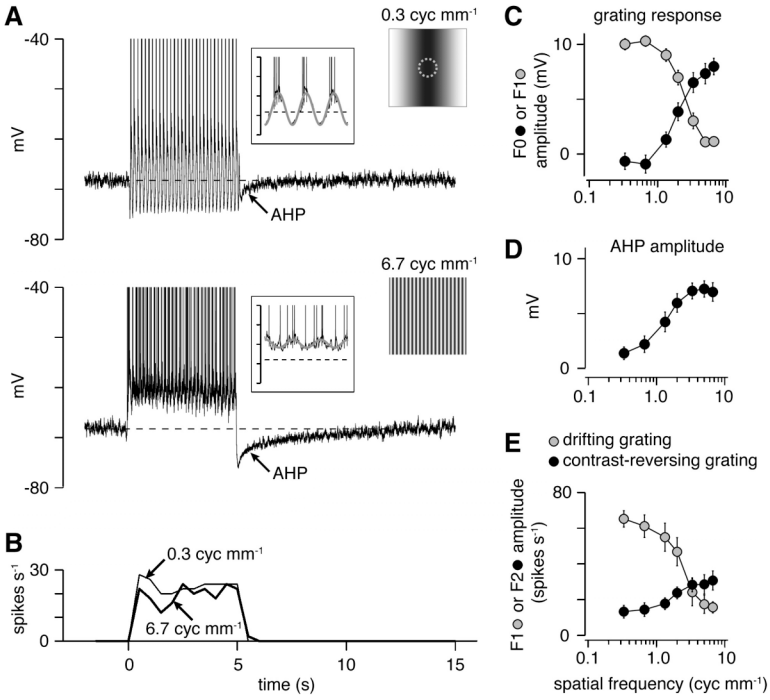


**Figure 2.4. The Afterhyperpolarization Is Evoked Most Effectively by High Spatial Frequencies**

(A) In an OFF cell, a low spatial frequency grating (0.3 cycles $mm^{-1}$) evoked a strong response at the 6 Hz drift rate followed by a small AHP. A high spatial frequency grating (6.7 cycles $mm^{-1}$) evoked a tonic depolarization plus a small 6 Hz modulation followed by a large AHP. Traces in the insets show 500 ms of response with a fitted 6 Hz sine wave (F1 response; y axis: −80 to −40 mV). In both insets, the cell fires 13 spikes (bursts of five, four, and four spikes to the low-frequency stimulus and 13 spikes dispersed over time to the high-frequency stimulus). Dashed line indicates the resting potential.

(B) A psth for the two conditions in (A) (bin size, 500 ms); mean firing rate for the two conditions was similar.

(C) The amplitude of the first Fourier harmonic (F1) of the membrane potential peaked for low spatial frequencies and declined at high frequencies, whereas the mean membrane potential (F0 component) peaked at high frequencies, reaching a peak near ~5–7 cycles $mm^{-1}$ (n = 8 cells). Error bars indicate SEM across cells.

(D) AHP amplitude increased with spatial frequency, reaching a peak near ~5 cycles $mm^{-1}$ (n = 8 cells).

(E) Spike recordings to a drifting or contrast-reversing grating illustrate the relative size of the overall ganglion cell receptive field center and the nonlinear subunits; the subunits represent bipolar cell inputs to the ganglion cell (see Results). The F1 amplitude to a drifting grating is a measure of the overall receptive field center. This amplitude peaks at low frequencies and declines at higher frequencies. The F2 amplitude to a contrast-reversing grating reflects the nonlinear subunit response. The subunit amplitude peaks at high frequencies, similar to the pattern of sensitivity of the F0 membrane potential in (C) and the AHP amplitude in (D) (see also (Demb, Zaghloul, Haarsma et al., 2001)).

For primate diffuse bipolar cells (which synapse onto magnocellular ganglion cells), the receptive field surround strength is 1 to 1.4 times the strength of the receptive field center (D. Dacey et al., 2000). Assuming a similar receptive field profile in guinea pig bipolar cells (presynaptic to the Y-type cell), the surround should reduce each bipolar cell's response to the low spatial frequency, relative to the optimal spatial frequency, to less than 30% of the maximal response (D. Dacey et al., 2000). Thus, the reduced ganglion cell AHP following the low-frequency grating would be explained by the reduced response of each presynaptic bipolar cell. This explanation implies that individual bipolar cells require strong stimulation in order to adapt their release rate and drive the ganglion cell AHP.

We measured grating responses to a total of seven spatial frequencies. As expected, the F1 amplitude peaked at low frequencies and gradually declined at higher frequencies (Figure 2.4C) whereas the AHP amplitude peaked at high frequencies (Figure 2.4D). To put this spatial tuning into context, we made two measurements of the “nonlinear subunit” property of the Y-type cell receptive field, where the subunits apparently represent presynaptic bipolar cells (Demb, Zaghloul, Haarsma et al., 2001; Demb, Zaghloul, & Sterling, 2001; Enroth-Cugell & Freeman, 1987; Enroth-Cugell & Robson, 1966; Hochstein & Shapley, 1976). The first subunit measure is the mean level of depolarization (F0) during the grating, and this showed the same spatial tuning as the AHP (Figure 2.4C). The second measure was the F2 (second harmonic) amplitude to a contrast-reversing grating (spike recordings; Figure 2.4E), and this also showed similar tuning to the

AHP (Figure 2.4E) (Demb, Zaghloul, Haarsma et al., 2001). Thus, the spatial tuning of the AHP matches the tuning of the "nonlinear subunits," suggesting that strong stimulation of bipolar cells is required to evoke the AHP.

### The Afterhyperpolarization Corresponds to a Decreased Inward Current, Consistent with a Bipolar Cell Mechanism

We considered two hypotheses for how bipolar cells could drive a slow AHP in a ganglion cell. First, following the offset of high contrast, bipolar cell glutamate release might be suppressed and recover slowly. Second, bipolar cells might drive inhibitory amacrine cells to release GABA and/or glycine, and this inhibition might require several seconds to subside. To test between these alternatives, we measured membrane currents under voltage clamp during and after high-contrast stimulation. The large cells under study have a low input resistance (37.9 ± 2.1 MΩ, n = 14) (E. D. Cohen, 2001; O'Brien, Isayama, Richardson, & Berson, 2002), and so we initially used holding potentials ($V_h$) close to the resting potential ($V_{rest}$) to minimize errors in the current measurements (n = 8; see Experimental Procedures).

During the high-contrast grating, we measured an inward current with an estimated reversal potential (−23.9 ± 6.7 mV; n = 8) that suggests a mix of excitatory and inhibitory input (Figure 2.5B). Following grating offset, there was an outward "aftercurrent" that recovered slowly back to baseline. This aftercurrent amplitude was larger at $V_h$ of ~−80 mV relative to the amplitude at $V_{rest}$ (~−65 mV); this pattern (negative slope on an I-V plot) suggests that the aftercurrent is driven by a reduced excitatory conductance, rather than an

increased inhibitory conductance (Figure 2.5B). Near $V_{rest}$, we measured similar aftercurrents using pipette solutions that were either $K^+$-based (n = 3) with a weak $Ca^{2+}$ buffer (0.1 mM EGTA; 92.9 ± 11.3 pA) or $Cs^+$-based (n = 5) with a strong $Ca^{2+}$ buffer (10 mM BAPTA; 129.0 ± 14.0 pA; see Experimental Procedures). Thus, the aftercurrent did not depend on $Cs^+$-sensitive $K^+$ channels or a $Ca^{2+}$-dependent mechanism, which is further evidence that the mechanism was not intrinsic to the ganglion cell.

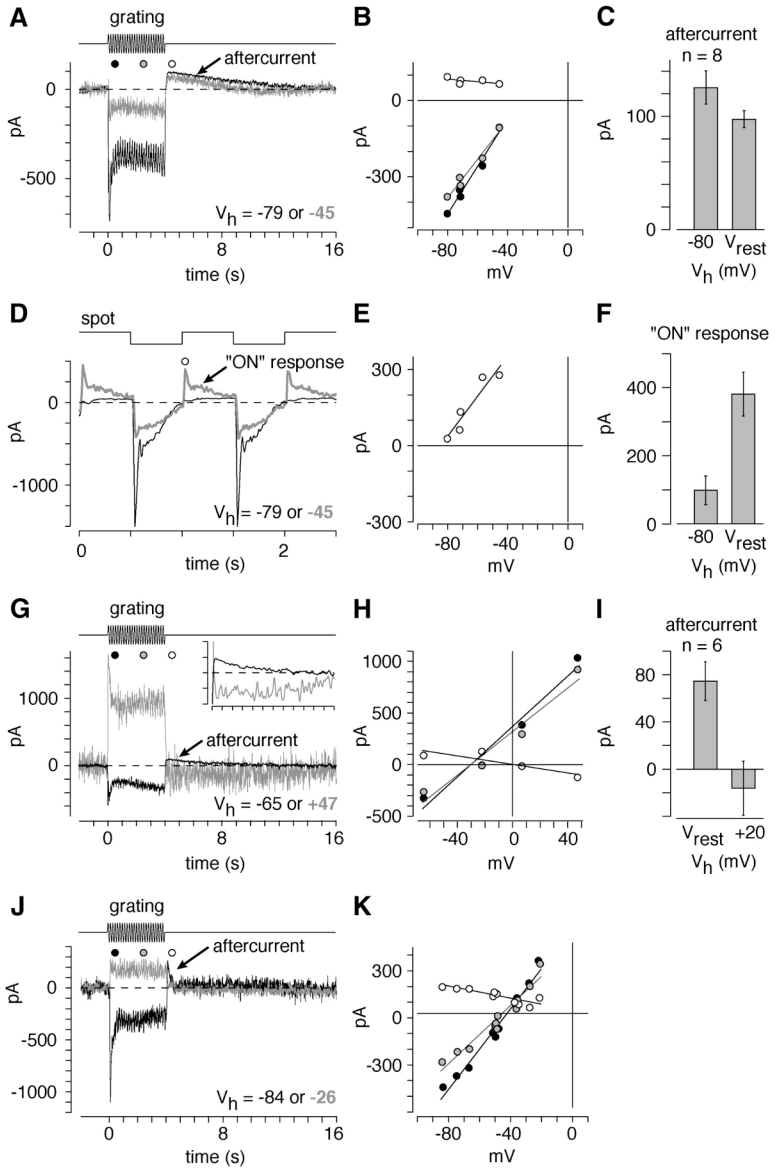


**Figure 2.5. The Afterhyperpolarization Corresponds to a Reduced Excitatory Postsynaptic Current**

(A) An OFF cell was recorded under voltage clamp and stimulated with a 4 s grating (100% contrast; 6.7 cycles $mm^{-1}$; 6 Hz; $K^+$-based solution) at a holding potential ($V_h$) = −45 (gray) or −79 (black). Both the inward current evoked by grating presentation and the outward aftercurrent at grating offset declined at the positive holding potential. Traces are illustrated at 100 Hz sampling. Traces here and below are leak subtracted.

(B) Current-voltage (I-V) plot of transient response (black circles) and sustained response (gray circles) to the grating and the aftercurrent (white circles) from the cell in (A). Grating responses are consistent with a mixed chloride + cation current with estimated reversal potential (transient: −23.8 ± 10.8 mV; sustained: −23.9 ± 6.7 mV; n = 8) between $E_{cation}$ (~0 mV) and $E_{Cl}$ (−73 mV). The aftercurrent response showed a slight decline at positive holding potentials,

consistent with a reduced cation current but inconsistent with a chloride current. Fitted lines here and below show linear regressions.
(C) Outward currents following the grating (aftercurrent) at $V_h$ near $V_{rest}$ (± 5 mV) or near −80 mV (±5 mV). Relative to $V_h = V_{rest}$, $V_h$ = −80 mV increased the aftercurrent. Error bars indicate SEM (n = 8 cells).
(D) The same cell in (A) was stimulated with a spot that reversed contrast (square-wave reversal; 0.6 mm outer diameter, contrast = 100%) at $V_h$ = −45 or −79 mV.
(E) I-V plot of traces in (D) Across cells, outward current during the positive contrast shows an estimated reversal of −86.4 ± 1.4 mV (n = 8 cells), negative to $E_{Cl}$ (−73 mV).
(F) Outward currents during the "ON" response at $V_h$ near $V_{rest}$ (±5 mV) or near −80 mV (±5 mV). The response decreased at $V_h$ of −80 mV relative to the response at $V_h$ of $V_{rest}$. Error bars indicate SEM (n = 8 cells).
(G) Same format as (A) for a second cell probed at positive holding potentials ($Cs^+$-based pipette solution with TEA). The aftercurrent became inward at $V_h$ = +47 mV. Inset shows filtered traces (Gaussian filter, SD = 100 ms); axes represent from 4 to 16 s and from −200 to +200 pA. The time course of the aftercurrent differed at the two holding potentials, probably because of an NMDA receptor component at +47 mV.
(H) Same format as (B), showing a reversal of the aftercurrent near 0 mV.
(I) Same format as (C), showing the average aftercurrent amplitude with $V_h$ = $V_{rest}$ (−65.5 ± 5.6 mV) or ~+20 mV (+19.8 ± 8.3 mV, mean ± SD) across six cells.
(J) An ON cell was recorded under the same conditions as in (A). The aftercurrent was briefer than that in OFF cells but still showed a reduction at the depolarized holding potential.
(K) I-V plot of response to the grating from the cell in (G); same format as in (B).

We performed additional experiments with TEA in the pipette to improve the ability to clamp the dendrites at a positive holding potential (see Experimental Procedures). In the most stable recordings (n = 6), we measured a reversal for the aftercurrent that was +10.3 ± 10.2 mV (Figures 1.5G–5I). This reversal is slightly positive to 0 mV, which is likely explained by an incomplete space clamp of the dendrites (i.e., in which case, an ~+10 mV potential at the soma might correspond to an ~0 mV potential at the dendrite). The aftercurrent showed a more sustained time course at the positive holding potential, relative to the time

course measured near $V_{rest}$ (Figure 2.5G, inset), probably caused by an increased contribution from NMDA-receptor conductances at positive potentials (E. D. Cohen, 2000). Because of a probable NMDA-receptor contribution to the aftercurrent, the linear fits used to estimate reversal potential are approximate.

As a control, we measured an outward current that we did expect to be driven largely by direct inhibition (Demb, Zaghloul, Haarsma et al., 2001; Zaghloul et al., 2003): the OFF cell's "ON" response to a bright spot stimulus (Figures 1.5D–5F). Indeed, this outward current showed an estimated reversal negative to $V_{rest}$, suggesting that it was driven largely by a direct inhibitory conductance and demonstrating that our protocol was adequate to see existing direct inhibitory influences.

Following a grating stimulus, ON-center Y-type cells also showed an aftercurrent, although it was relatively brief (n = 3; Figure 2.5J). This brief period of the aftercurrent explains why spikes were suppressed only transiently in extracellular recordings (see above; Figure 2.1F). An ON cell's aftercurrent corresponded to a reduced inward current, with estimated reversal near 0 mV (Figures 1.5J and 1.5K). Thus, ON-center Y-type cells showed an outward current similar to OFF-center cells, except that the recovery was much faster.

### The Afterhyperpolarization Does Not Require Conductances Driven by GABA or Glycine Receptors, Calcium-Activated Potassium Channels, or Metabotropic Glutamate Receptors

The AHP does not appear to be driven by GABA or glycine release onto the ganglion cell (Figure 2.5); however, GABA or glycine release feeding back

onto the bipolar terminal could play a role in suppressing glutamate release. This seemed unlikely based on a previous experiment with extracellular recording, in which either strychnine (a glycine receptor antagonist) or picrotoxin (a $GABA_{A/C}$ receptor antagonist), when applied *individually*, did not block slow adaptation in spiking (Brown & Masland, 2001). However, this experiment left open the possibility that both GABA and glycine are involved in adaptation, in which case blocking only one class of receptors at a time would not block the total amacrine cell contribution. To follow up this result, we measured the aftercurrent, under voltage clamp, while *simultaneously* blocking glycine and $GABA_{A/B/C}$ receptors (strychnine, 2 μM; bicuculline, 100 μM; CGP35348, 100 μM; TPMPA, 100 μM, respectively).

The receptor antagonists caused, in most cases, spontaneous "bursting" and strongly increased the response to the grating (Figure 2.6A). However, the aftercurrent persisted and in fact the amplitude increased (control: 74.1 ± 13.1 pA; drugs: 219.5 ± 20.9 pA). Furthermore, the antagonists altered the time course of both the grating response and the aftercurrent. The altered time courses probably arise from the extreme change in bipolar release under these conditions, caused by removing all inhibition of the bipolar terminal. Therefore, we do not draw conclusions from these conditions about the normal time course of glutamate release. However, we can conclude that the aftercurrent (and the associated AHP) does not require inhibitory synaptic transmission. This provides further evidence that the AHP arises from reduced bipolar cell glutamate release.

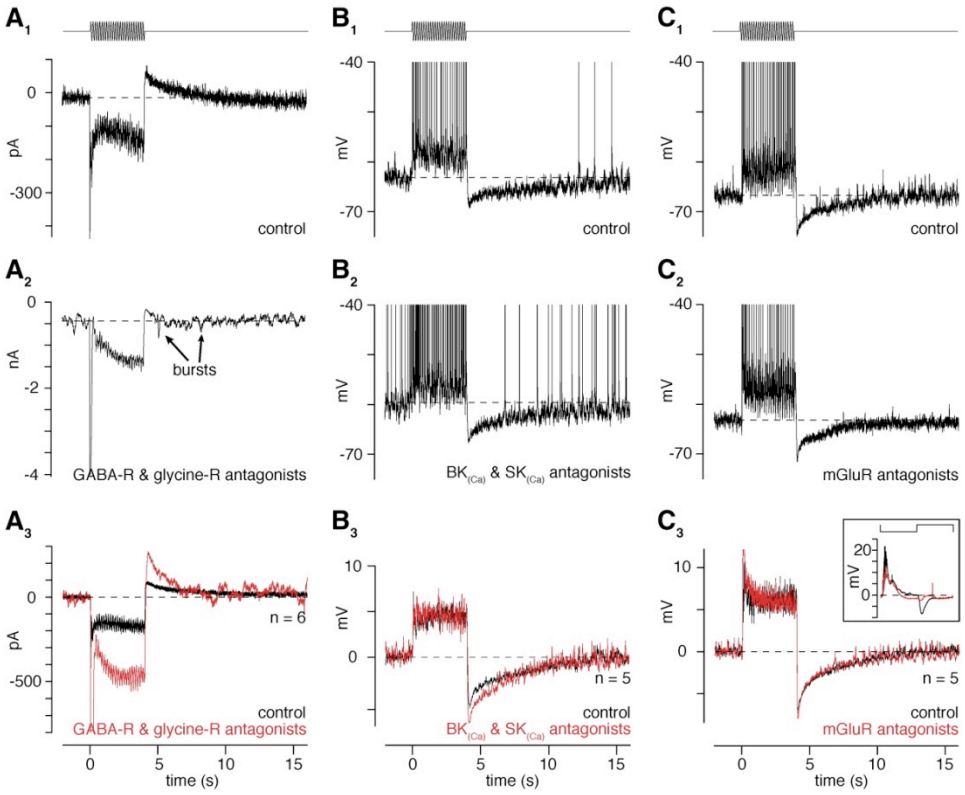


**Figure 2.6. The Afterhyperpolarization Does Not Require Conductances Driven by GABA or Glycine Receptors, $K_{(Ca)}$ Channels, or Metabotropic Glutamate Receptors (mGluRs).**

(A) An OFF cell was stimulated with a 4 s grating (100% contrast; 6.7 cycles $mm^{-1}$; 6 Hz) under voltage clamp ($V_{hold}$ = −75 mV). The grating response was recorded under control conditions ($A_1$) and after adding antagonists to glycine and $GABA_{A/B/C}$ receptors (strychnine, 2 µM; bicuculline, 100 µM; CGP35348, 100 µM; TPMPA, 100 µM) ($A_2$). The receptor antagonists caused a large increase in responsiveness (note the different scales in [$A_1$] and [$A_2$]). However, the aftercurrent, following the stimulus, persisted in the presence of the receptor antagonists ([$A_3$], average traces are leak subtracted). The arrows in ($A_2$) indicate bursts of inward current present during drug application, which probably represents bursts of glutamate caused by blocking all major inhibitory synapses throughout the retina. The initial inward current in the average trace in the presence of the drugs (−1.9 ± 0.53 nA) has been clipped in the figure ($A_3$). Without leak subtraction, the leak current was −50 ± 16 pA in the control condition and −372 ± 41 pA in the drug condition. (B) Same format as (A), except that the cell was recorded in current clamp and we applied antagonists to two types of calcium-activated potassium channels: apamin (1 µM) to block $SK_{(Ca)}$ channels, and charybdotoxin (20 nM) to block $BK_{(Ca)}$ channels. Relative to control ($B_1$), the channel blockers caused bursting of the membrane potential and increased the maintained discharge ($B_2$), but did not block the AHP ($B_3$).

(C) Same format as (B), except that we applied antagonists to all major mGluRs: MCPG (1 mM) to block group I and group II mGluRs, and CPPG (1 mM) to block group III mGluRs. The drugs did not block the AHP following the grating stimulus ($C_2$ and $C_3$). However, during a contrast reversal of a 0.6 mm diameter spot (2 Hz, 10%–20% contrast), the drugs blocked the hyperpolarizing response to light onset in OFF cells ([$C_3$], inset; averaged across five cells; line above indicates time course of the contrast reversal). This was expected, because the hyperpolarizing response to light onset depends on an inhibitory synapse from an ON amacrine cell, and the ON pathway is blocked by CPPG (Awatramani & Slaughter, 2000; Zaghloul et al., 2003).

We checked two putative mechanisms for adaptation in bipolar cell release. Bipolar cells express $Ca^{2+}$-dependent $K^+$ channels [$K_{(Ca)}$] (Sakaba, Ishikane, & Tachibana, 1997), which could contribute to slow adaptation (Llinas & Lopez-Barneo, 1988). We blocked $K_{(Ca)}$ channels throughout the retina (bath applied charybdotoxin, 20 nM; apamin, 1 μM), and this condition caused bursting in the ganglion cell membrane potential and an increased maintained discharge (n = 5; Figure 2.6B). However, the AHP following the grating persisted (control amplitude: −4.7 ± 1.0 mV; drugs: −6.0 ± 0.6 mV). This result also rules out a role for $K_{(Ca)}$ channels in the ganglion cell, consistent with results above showing that the aftercurrent persists under voltage clamp in the presence of high BAPTA (Figure 2.5).

Another possible mechanism for adaptation in bipolar cells is metabotropic glutamate receptors (mGluRs) on the synaptic terminal, which could create a feedback signal and reduce release (Awatramani & Slaughter, 2001). To test this possibility, we blocked group I, II, and III mGluRs simultaneously (MCPG, 1 mM; CPPG, 1 mM) (n = 5; Figure 2.6C). This condition blocked the hyperpolarization at light onset of a spot response, as expected (Zaghloul et al., 2003) (see Figure

2.6$C_3$ inset). However, the AHP following the grating persisted (control amplitude: −6.1 ± 0.9 mV; drugs: −6.8 ± 0.8 mV). This result also rules out a role for mGluRs as a postsynaptic mechanism to generate the AHP in ganglion cells.

### Evidence that Basal Glutamate Release from Bipolar Cells Affects the Afterhyperpolarization

During the course of the experiments, we varied the mean luminance (see Experimental Procedures). At lower mean luminance, we observed in OFF Y-type ganglion cells two effects: a depolarized resting potential (low, −63.4 ± 1.3 mV; high, −68.0 ± 1.1 mV; $p < 0.05$; $n = 6$) and increased voltage noise (low, 1.9 ± 0.4 mV; high, 0.7 ± 0.1 mV; $p < 0.05$) (Figure 2.7). This pattern implies that glutamate release from OFF bipolar cells increased at the lower mean, presumably driven by increased glutamate release from cones (Demb, Sterling, & Freed, 2004). We hypothesized that the AHP in the ganglion cell would be related to the level of basal glutamate release from bipolar cells: higher basal release (at low mean luminance), when suppressed, would produce a relatively larger AHP in the ganglion cell.

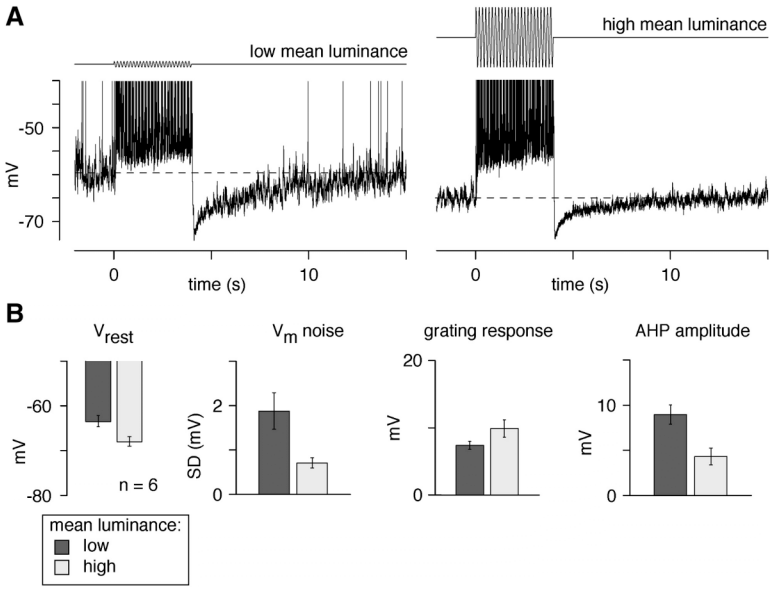


**Figure 2.7. At Low Mean Luminance, an OFF Cell Shows a Depolarized Membrane Potential, Increased Membrane Noise, and an Enhanced Afterhyperpolarization.**
(A) An OFF cell was stimulated with a 4 s grating stimulus (100% contrast; 6.7 cycles $mm^{-1}$; 6 Hz). The response was recorded at two different levels of mean luminance differing by a factor of ten (see Experimental Procedures). The low mean luminance caused a depolarized $V_{rest}$ and increased membrane noise, suggesting increased presynaptic glutamate release. Low mean luminance also increased the amplitude of the AHP from −7.1 to −12.8 mV.
(B) Across cells, reducing mean luminance by a factor of ten had multiple effects: depolarization of $V_{rest}$, increased synaptic noise (SD of $V_m$ measured over 2 s, before stimulus onset), and increased AHP amplitude. However, the response to the grating was similar under the two conditions. Error bars indicate SEM across cells (n = 6).

We tested the effect of mean luminance on AHP size, presenting the same cell with the 4 s drifting grating (100% contrast; 6.7 cycles $mm^{-1}$; 6 Hz) at two levels of mean luminance, differing by a factor of ten (Figure 2.7). At the two levels of mean luminance, the response to the grating was similar (low, 7.4 ± 0.6 mV; high, 9.9 ± 1.3 mV; $p > 0.10$; n = 6). However, the AHP was about twice as large at low mean luminance (low, −9.0 ± 1.1 mV; high, −4.3 ± 0.9 mV; $p < 0.05$).

Thus, increasing the apparent basal glutamate release onto the ganglion cell, by reducing the mean luminance, increased the AHP.

## Discussion

We have demonstrated a slow form of contrast adaptation in the subthreshold membrane potential of mammalian ganglion cells in vitro. Following a period of high contrast, spike rate was suppressed and required several seconds to recover; we observed suppressed spiking with both extracellular and whole-cell recordings (Figure 2.1). The recovery of the spike rate corresponded to a period of membrane hyperpolarization (Figure 2.1), and this afterhyperpolarization (AHP) depended on the period of prior visual stimulation (Figure 2.2). Spiking was neither necessary nor sufficient to generate the full visually evoked AHP (1. 3 and Figure 2.4). However, spiking was sufficient to generate at least a minor component of the visually evoked AHP (Figure 2.3). The AHP was strongest following high spatial frequency stimuli, tuned to presynaptic bipolar cells (Figure 2.4). Voltage-clamp analysis showed that the AHP corresponded to a reduced inward current, consistent with suppressed bipolar cell glutamate release (Figure 2.5). Pharmacology experiments ruled out a role for amacrine cell GABAergic or glycinergic synapses or for calcium-activated $K^+$ channels or metabotropic glutamate receptors in the bipolar cell (or elsewhere; Figure 2.6). Lowering mean luminance apparently increased basal glutamate release from OFF bipolar cells (Figure 2.7). At the lower mean

luminance, the AHP increased, suggesting a link between basal release and the size of the AHP (Figure 2.7).

### Retinal Model for Slow Adaptation following a Period of High Contrast

Our results support a model where, at the offset of high contrast, bipolar cell glutamate release drops below the basal rate, and this drop in release hyperpolarizes the ganglion cell, causing the observed AHP and suppressed spiking. Glutamate release apparently requires several seconds to return to the basal level, resulting in gradual membrane depolarization of the ganglion cell back to its resting potential (Figure 2.8). In this model, bipolar cells require strong stimulation in order to suppress their release. So, for example, when a low spatial frequency grating is presented and stimulates a bipolar cell weakly (due to the influence of the receptive field surround; (D. Dacey et al., 2000), there would be no suppression at stimulus offset, and the ganglion cell AHP would be weak or absent (Figure 2.4).

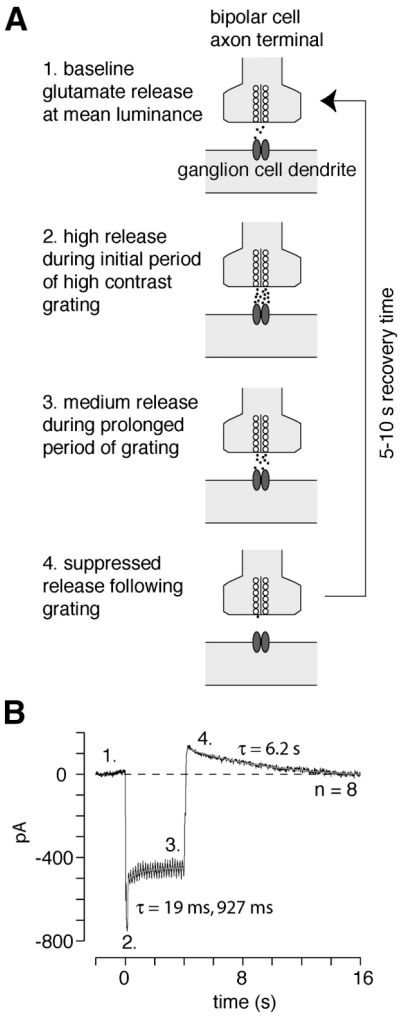


**Figure 2.8. Working Model for the Mechanism of Slow Contrast Adaptation**
(A) Glutamate release increases during periods of high contrast to a high level initially and then to a medium level for the duration of the stimulus. Following the offset of high contrast, glutamate release declines sharply. The release rate takes several seconds to recover to the initial baseline level.
(B) Time course of adaptation during and following high-contrast stimulation. Trace shows the average response, under voltage clamp, of eight cells, where $V_{hold}$ was near $E_{Cl}$ (trace is leak subtracted; 100 Hz sampling). The inward current is suppressed soon after grating onset causing a decrease in the inward current; gray line shows a double exponential fit with time constants of 19 and 927 ms. This decline in the inward current could reflect multiple mechanisms, including a drop in glutamate release during high contrast (see [A], stages 2 and 3) as well as possible postsynaptic receptor desensitization caused by the high glutamate release (see Discussion). At stimulus offset, there is an outward aftercurrent that slowly recovers back to baseline (dashed line); the gray line shows a single exponential fit with time constant of 6.2 s. This aftercurrent presumably reflects suppressed glutamate release that requires several seconds to recover (see [A], stages 4 and 1).

Our synaptic model for slow adaptation in ganglion cells is consistent with the conclusion reached in a previous study, based on extracellular recording (Brown & Masland, 2001). However, we also found a minor contribution to slow adaptation from an intrinsic property of the ganglion cell: current injection evoked a depolarization and spiking, followed by an AHP with an integral that was, at most, about 25% of the visually evoked AHP integral (Figure 2.3). However, relative to the visual stimulus, the current injection typically evoked greater depolarization and more spikes. Thus, taking into account the relatively smaller response to the visual stimulus, the intrinsic mechanism for adaptation in the ganglion cell probably contributes less than 25% of the visually evoked AHP.

**Retinal Model for Slow Adaptation during a Period of High Contrast**

Here, we have focused on the slowly recovering AHP following a grating stimulus, but we could also measure adaptation during the presentation of the grating itself. This side of adaptation was reflected by an initially high spike rate that declined during prolonged contrast stimulation (Figure 2.1 and Figure 2.3). This adaptation *during* the stimulus seemed to depend on two components. First, there was an excitatory synaptic component driving the response, which is apparent in voltage-clamp recordings near $E_{Cl}$ (Figure 2.5 and Figure 2.8): inward currents were initially large and then declined during continued grating presentation. This decline could occur due to a decreasing glutamate release rate during the grating or postsynaptic mechanisms of receptor desensitization

caused by the high release (von Gersdorff & Borst, 2002). Possible presynaptic mechanisms for a decline in release during high contrast include vesicle depletion or auto-feedback at the bipolar terminal (DeVries, 2001; Palmer, Hull, Vigh, & von Gersdorff, 2003; Palmer, Taschenberger, Hull, Tremere, & von Gersdorff, 2003; Singer & Diamond, 2006). A second component driving adaptation during the grating was a spike-frequency adaptation. This adaptation was apparent during direct current injection, which caused a high rate of spiking that then declined (Figure 2.3). Spike frequency adaptation seems to be a general property of many types of ganglion cells and at least partially reflects the effect of sodium channel inactivation (Kim & Rieke, 2001, 2003; O'Brien et al., 2002). Furthermore, this spike frequency adaptation mechanism may explain why some cortical cells show a decline in spike rate during a stimulus with no subsequent recovery period following the stimulus (Sanchez-Vives et al., 2000b).

We examined, for excitatory synaptic currents, the relationship between the time course of adaptation *during* a high-contrast stimulus and the subsequent recovery period *following* the stimulus (Figure 2.8B). The onset of adaptation, during the grating, was well fit by two exponentials, with time constants of 19 ms (87%) and 927 ms (13%). The aftercurrent, following the grating, was well fit by a single exponential with a time constant of 6.2 s. Thus, the decline of the inward current during the stimulus is apparently ~10–100 times faster than the recovery time. There are two explanations for this asymmetry in time course between these two sides of adaptation. First, as described above, the period during the grating alone could involve mechanisms of synaptic depression that relate

specifically to periods of high transmitter release (e.g., postsynaptic receptor desensitization; (von Gersdorff & Borst, 2002), and these mechanisms could shorten the time constant for this period of adaptation relative to the time constant for the aftercurrent. Second, even without the involvement of postsynaptic mechanisms, such as receptor desensitization, there appears to be an asymmetry between the onset and recovery from depression of presynaptic release. For example, suppressed release from the rod bipolar cell shows fast onset (<1 s) with a slow recovery time (~10 s; (Singer & Diamond, 2006). A similar asymmetry exists at the calyx of Held, where depression can be induced in <1 s but requires several seconds to recover (von Gersdorff, Schneggenburger, Weis, & Neher, 1997; Wang & Kaczmarek, 1998). Furthermore, a similar rapid onset with slow recovery exists, on a different time scale, for sodium channel inactivation (Colbert, Magee, Hoffman, & Johnston, 1997).

### Comparison between Guinea Pig and Primate Retina

A recent study based on extracellular recordings in vivo suggested that the suppressed spiking following high contrast arises from a postsynaptic mechanism in the ganglion cell (Solomon et al., 2004). That conclusion was based on an experiment in which a stationary, contrast-reversing grating was positioned so as to evoke no response in the ganglion cell (because the border between grating bars was centered over the cell's receptive field, in a “null” phase). Following this stimulus, the ganglion cell responses were not

suppressed, which suggests that the ganglion cell must necessarily be stimulated in order to evoke an adaptive effect. This result would be consistent with an intrinsic mechanism in the ganglion cell for adaptation, rather than a network mechanism involving bipolar cells. There are several explanations for the discrepancy between these findings in primate and ours. Two explanations relate to the different recording conditions (in vivo versus in vitro) and the different species (primate versus guinea pig). For example, the intrinsic mechanism for adaptation in the in vitro guinea pig cells was a minor component of adaptation under our conditions (Figure 2.3), but this component might be more prominent in the in vivo primate cells. Even within primate experiments, there are differences in slow adaptation between in vitro and in vivo conditions (Chander & Chichilnisky, 2001; Solomon et al., 2004). Another example of a difference between the guinea pig and primate studies relates to adaptation in ON and OFF cells. The primate study found adaptation in both ON and OFF magnocellular cells, whereas we found strong adaptation in OFF cells but only weak effects in ON cells; presently we cannot explain this discrepancy (Solomon et al., 2004).

We offer one further explanation for the lack of adaptation following the "null" stimulus in the primate study (Solomon et al., 2004). Magnocellular ganglion cells in the previous study were recorded at 5°–25° eccentricity, which should have dendritic tree diameters of ~40–140 μm (Croner & Kaplan, 1995; Perry, Oehler, & Cowey, 1984). These ganglion cells probably collect from up to ~30 bipolar cells (Calkins, 1999; Jacoby, Wiechmann, Amara, Leighton, & Marshak, 2000), which would correspond to ~6 cells across the width of the

dendritic tree. We also assume that each bipolar cell receptive field width is ~90–100 μm (D. Dacey et al., 2000). Furthermore, the central-most bipolar cells contribute the largest number of synapses onto the ganglion cell (Kier, Buchsbaum, & Sterling, 1995). Thus, based on this pattern of convergence, it is likely that the “null” stimulus for the ganglion cell was also largely ineffective at strongly driving the central-most bipolar cells. Given this weak stimulation, these central-most bipolar cells would not show an adaptive effect after the stimulus was removed, and this might explain the lack of adaptation in the ganglion cell. However, intracellular studies of magnocellular ganglion cells are clearly required to fully resolve this issue.

## Conclusion

Nonspiking cells exist in many sensory systems, and these cells may also express mechanisms of slow adaptation. At present, the most likely mechanism in bipolar cells is an activity-dependent suppression of glutamate release. This mechanism apparently does not involve inhibitory synaptic feedback, $K_{(Ca)}$ channels in the bipolar cell, or mGluRs at the bipolar terminal (Figure 2.6; (Awatramani & Slaughter, 2001; Sakaba et al., 1997). Furthermore, voltage recordings from salamander retina suggest that the AHP in ganglion cells exists in the absence of an AHP in presynaptic bipolar cells (Baccus & Meister, 2002; Rieke, 2001). Thus, the most likely mechanism for the ganglion cell AHP is a depressed bipolar cell glutamate release that is not reflected by a hyperpolarization of the bipolar cell membrane potential. Further studies will be

required to elucidate the mechanism for depressed bipolar cell glutamate release, as it relates to contrast adaptation. This would apparently require a novel preparation in mammalian retina: the ability to record from pairs of *cone* bipolar cells and postsynaptic neurons (amacrine or ganglion cell) where the bipolar voltage can be controlled while its release is read out directly by the postsynaptic neuron. Presently, such paired recordings, which require routine identification of synaptically connected cells, have only been accomplished in the rod pathway (Singer & Diamond, 2006; Singer, Lassova, Vardi, & Diamond, 2004).

## Experimental Procedures

### Recordings

In each experimental session, a guinea pig was anesthetized with ketamine (100 mg $kg^{-1}$) and xylazine (10 mg $kg^{-1}$) and decapitated, and both eyes were removed. All procedures conformed to NIH and University of Michigan guidelines. The back of the eye (retina, pigment epithelium, choroids, and sclera) was mounted flat in a chamber on a microscope stage. The retina was superfused (~6 ml $min^{-1}$) with oxygenated (95% $O_2$ and 5% $CO_2$) Ames medium (Sigma, St. Louis, MO) at 33°C–35°C. The retina and electrode were visualized using a cooled CCD camera (Retiga 1300C, Qcapture software; Qimaging corporation, Burnaby, British Columbia). The largest cell bodies in the ganglion cell layer (20–25 μm diameter) were targeted for recording. A glass electrode (tip resistance, 2–6 MΩ) was filled with Ames' solution for extracellular recording, or

intracellular recording solution. Intracellular solutions included $K^+$-based solution (solution 1; in mM: K-methylsulfate, 140; NaCl, 8; HEPES, 10; EGTA, 0.1; ATP-$Mg^{2+}$, 2; GTP-$Na^+$, 0.3; titrated to pH = 7.3); $K^+$-based solution with QX-314 (solution 2), where NaCl was reduced to 3 mM and QX-314-Br was added (5 mM); or $Cs^+$-based solution (solution 3) where Cs-methane sulfonate (120 mM) replaced K-methylsulfate and BAPTA (10 mM) replaced EGTA; $Cs^+$-based solution with TEA (solution 4), where TEA-Cl (5 mM) and Lucifer Yellow (0.1%) were added and QX-314-Br was reduced to 2 mM. The chloride reversal potential ($E_{Cl}$) indicates the reversal of the synaptic response to GABA or glycine and includes a contribution from bromide; the calculated reversal was ~−73 mV for solutions 1 through 3 and ~−67 mV for solution 4. All chemicals were purchased from Sigma-Aldrich (St. Louis, MO) except for BAPTA (Invitrogen; Eugene, OR), Strychnine (Fisher Scientific; Pittsburgh, PA), and (RS)-MCPG and CPPG (Tocris, Bristol, UK).

Membrane potential was amplified, continuously sampled at 10 kHz, and stored on computer using a MultiClamp 700A amplifier and pClamp 9 software (Axon Instruments, Foster City, CA; Zaghloul et al., 2005). Junction potential was corrected in all cases. We wrote programs in Matlab (The Mathworks, Natick, MA) to analyze responses in the spike rate, subthreshold membrane potential, or membrane currents. For current-clamp recordings, we balanced the bridge every few minutes in cases where we injected current. For voltage-clamp recordings, we corrected for an error in the holding potential introduced by the series resistance. The corrected holding potential ($V_{h\_corr}$) was determined by the

formula $V_{h\_corr} = V_h - (I_{leak} \times R_s \times (1 - R_{s\_correct}))$, where $V_h$ is the apparent holding potential before the stimulus (in mV), $I_{leak}$ is the leak current (in nA), $R_s$ is the series resistance (18.2 ± 0.3 MΩ; n = 14) and $R_{s\_correct}$ is the series resistance compensation (typically 0.4–0.5). For positive holding potentials (Figure 2.5B), we allowed an outward current, unblocked by $Cs^+$ or 5 mM TEA, to inactivate (~30–60 s) before recording the visual response. Results are from 80 cells: 16 ON cells and 64 OFF cells. The resting potential ($V_{rest}$) of OFF cells was similar between experimental conditions ($K^+$-based solution, −66.0 ± 1.5 mV, n = 20; $K^+$-based solution with QX-314 solution, −65.6 ± 1.5 mV, n = 10; $Cs^+$-based solution, −64.8 ± 0.7 mV, n = 5; $Cs^+$-based solution with TEA, −64.2 ± 2.2 mV, n = 6).

## Visual Stimuli

The stimulus was displayed on a miniature monochrome computer monitor (Lucivid MR1-103; Microbrightfield, Colchester, VT) projected through the top port of the microscope through a 4× objective and focused on the photoreceptors (mean luminance, ~$10^3$–$10^4$ isomerizations $cone^{-1}$ $s^{-1}$; resolution, 640 × 480 pixels; 60 Hz vertical refresh). The relationship between gun voltage and monitor intensity was linearized in software with a lookup table. Stimuli were programmed in Matlab as described previously (Brainard, 1997; Demb et al., 1999; Pelli, 1997). Cell type was determined using methods described previously (Zaghloul, Boahen, & Demb, 2005), and cell health was ascertained by repeated measurements of the responses to spots, annuli, and gratings.

The grating was either windowed in a circular patch (0.75 mm diameter; in most experiments) or presented over a 3 × 3 mm field (Figure 2.4). The gratings drifted at 6 Hz and in most cases had a spatial frequency of 5–7 cycles $mm^{-1}$ and contrast of 100%. All stimuli were centered on the cell body. In some cases, a neutral density filter was inserted in the light path to change the mean luminance by a factor of ten.

## Analysis

Except where noted, we measured AHP or aftercurrent amplitude by averaging over 100 ms centered at times noted in the text. Recovery time of the AHP was determined by fitting a polynomial function to the AHP and determining the time required for the fit to return 90% back to the baseline response level. We used standard fitting routines in Matlab. To determine the AHP integral, we normalized the trace by subtracting $V_{rest}$ and measured the integral of the trace, over an 8 s period, starting at grating offset. Spike poststimulus time histograms are binned at 500 ms, except where noted. Average membrane potential traces are shown with the resting potential subtracted. Data are reported as mean ± SEM.

## Acknowledgments

We thank Jeff Diamond, Peter Sterling, and Howard Gritton for comments on the manuscript. Our research was supported by a Research to Prevent Blindness Career Development Award (J.B.D.), an Alfred P. Sloan Foundation

Fellowship (J.B.D.), and the NIH (EY14454 and EY07003; T32-DC005341 and T32-EY13934, support to M.B.M.).

## Chapter 3

## Disinhibition Combines with Excitation to Extend the Operating Range of the OFF Visual Pathway in Daylight

### Summary

Cone signals divide into parallel ON and OFF bipolar cell pathways, which respond to objects brighter or darker than the background and release glutamate onto the corresponding type of ganglion cell. It is assumed that ganglion cell excitatory responses are driven by these bipolar cell synapses. Here, we report an additional mechanism: OFF ganglion cells were driven in part by the removal of synaptic inhibition (disinhibition). The disinhibition played a relatively large role in driving responses at low contrasts. The disinhibition persisted in the presence of CNQX and D-AP-5. Furthermore, the CNQX/D-AP-5-resistant response was blocked by L-AP-4, meclofenamic acid, quinine, or strychnine but not by bicuculline. Thus, the disinhibition circuit was driven by the ON pathway and required gap junctions and glycine receptors but not ionotropic glutamate or $GABA_A$ receptors. These properties implicate the AII amacrine cell, better known for its role in rod vision, as a critical circuit element through the following pathway: cone → ON cone bipolar cell → AII cell → OFF ganglion cell. Rods could also drive this circuit through their gap junctions with cones. Thus, to light decrement, AII cells, driven by electrical synapses with ON cone bipolar cells, would hyperpolarize and reduce glycine release to excite OFF ganglion cells. To light

increment, the AII circuit would directly inhibit OFF ganglion cells. These results show a new role for disinhibition in the retina and suggest a new role for the AII amacrine cell in daylight vision.

## Introduction

The retina encodes increments and decrements in light intensity using parallel ON and OFF pathways (Schiller, 1992; Werblin & Dowling, 1969). ON and OFF ganglion cells dedicate their output range for encoding only half the input range, and thus the split into two pathways apparently doubles the operating range of the visual system (Sterling, 2004). Under cone-driven conditions, the excitatory circuitry for these pathways is well understood. Cones release glutamate onto ON and OFF bipolar cells, which express distinct glutamate receptors at their dendrites [metabotropic glutamate receptor subtype 6 (mGluR6) vs AMPA/kainate] and consequently show opposite responses to both cone glutamate release and light (DeVries, 2000; Nakajima et al., 1993; Nomura et al., 1994; Slaughter & Miller, 1981) (see Figure 3.1B). ON and OFF cone bipolar cells release glutamate onto ionotropic receptors to excite the corresponding ON or OFF ganglion cell type (Chen & Diamond, 2002; E. D. Cohen, Zhou, & Fain, 1994; Diamond & Copenhagen, 1993) (see Figure 3.1B).

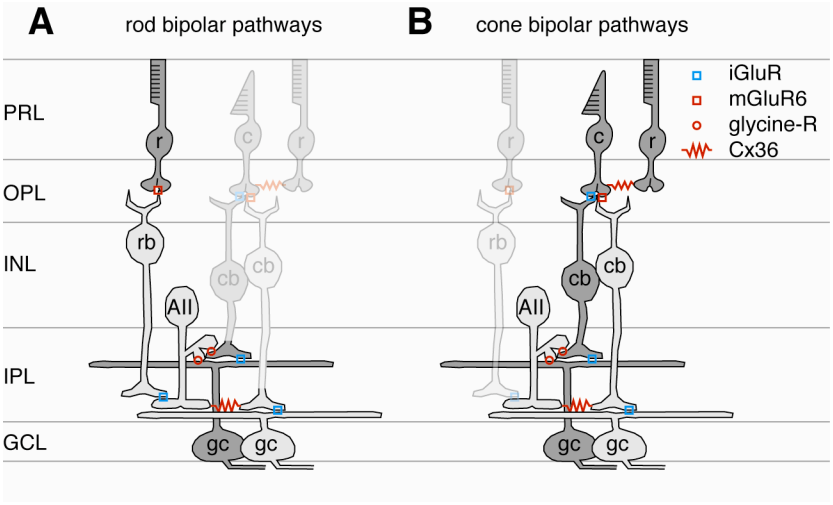


**Figure 3.1.** Rod and cone pathways of mammalian retina. ***A***, The rod (r) synapses with an ON-type rod bipolar cell (rb), which in turn excites the AII amacrine cell (AII). The AII excites the ON cone bipolar (cb) terminal and inhibits the OFF cone bipolar terminal and OFF ganglion cell (gc) dendrite. PRL, photoreceptor layer; OPL, outer plexiform layer. OFF cells (i.e., those that depolarize to light decrement) are shaded dark gray, whereas ON cells (i.e., those that depolarize to light increment) are shaded light gray. ***B***, The cone synapses with OFF and ON cone bipolar cells using different glutamate receptors; rods influence the cone response via gap junctions. Each cone bipolar synapses onto the same type of ganglion cell. The ON cone bipolar cell also excites the AII through the gap junction; the AII releases glycine onto the OFF cone bipolar terminal and OFF ganglion cell dendrite. A light decrement would hyperpolarize the ON cone bipolar cell, which would hyperpolarize the AII and reduce its glycine release onto the OFF cone bipolar and ganglion cells, causing disinhibition. This AII pathway does not require an iGluR to relay cone signals to the OFF ganglion cell.

In addition to these "vertical glutamate pathways," ganglion cell responses are modulated by synaptic inhibition. For example, under cone-driven conditions, OFF ganglion cells receive inhibitory synaptic input at light onset; the inhibition is driven by an amacrine cell, which is in turn driven by ON bipolar cells (Roska, Molnar, & Werblin, 2006; Zaghloul et al., 2003). Thus, OFF-pathway excitation and ON-pathway inhibition drive the OFF ganglion cell membrane potential in opposite directions to dark and light, respectively. Here, we reveal an additional,

unexpected function of this ON-pathway inhibition and probe the underlying amacrine cell circuit.

In experiments below, we show that OFF ganglion cell responses to negative contrast (i.e., light decrement) were driven in part by excitatory synapses, as expected. However, these responses were also driven in part by the removal of inhibition (i.e., disinhibition); the disinhibition played a relatively large role at low contrast. Thus, tonic inhibition at steady mean luminance could be increased or decreased depending on contrast sign. A strong candidate for the source of inhibition is the well studied AII amacrine cell: a bistratified interneuron that interacts with both ON and OFF pathways (Famiglietti & Kolb, 1975). The AII cell is widely studied for its prominent role in rod vision (Bloomfield & Dacheux, 2001; Singer, 2007) (see Figure 3.1A). It has been proposed that these cells might be functionally removed from the circuit in bright light (Mills & Massey, 1995; Smith, Freed, & Sterling, 1986), but AII cells, in fact, respond in bright light (D. M. Dacey, 1999; Pang et al., 2007; Xin & Bloomfield, 1999). Furthermore, OFF ganglion cells respond, in bright light, after blocking ionotropic glutamate receptors (iGluRs) (E. D. Cohen, 1998; E. D. Cohen & Miller, 1999); the only known circuit to explain these responses is the following: cone →ON cone bipolar cell →AII cell →OFF ganglion cell (Murphy & Rieke, 2006; Pang et al., 2007; Trexler, Li, & Massey, 2005) (see Figure 3.1*B*). Below, we provide evidence that this AII circuit explains OFF ganglion cell disinhibition. These results show a new role for disinhibition in the retina and suggest a function for the AII amacrine cell in daylight vision.

## Results

### Targeting and identification of Y-type/α ganglion cells

We recorded from ganglion cells in an *in vitro* preparation of the guinea pig retina (Demb et al., 1999; Demb, Zaghloul, & Sterling, 2001) (see Experimental Procedures). We targeted ON and OFF Y-type/α ganglion cells by recording from the largest cell bodies (20–25 μm diameter) in the GCL. In several cases, we filled the cells to reveal the morphology and confirm the cell type. We report on the morphological features of cells both from the present study (*n* = 9 cells) and those from a wider series of studies from our laboratory (*n* = 42 cells in total). The cells that had the characteristic physiological features of Y-type/α cells as defined by previous studies (i.e., brisk-transient responses; center-surround receptive fields; nonlinear spatial summation) (Demb, Zaghloul, Haarsma et al., 2001; Enroth-Cugell & Robson, 1966; Hochstein & Shapley, 1976) had wide dendritic trees and a characteristic position of their dendrites in the IPL. The OFF Y-type/α cells (*n* = 24) had dendritic tree diameters of 535 ± 72 μm (mean ± SEM) and stratified at 70 ± 3% depth in the IPL; this position is on the vitreal side of the nearby OFF ChAT band (76 ± 3%; *n* = 42) (see Experimental Procedures) (Figure 3.2*C*). The ON Y-type/α cells (*n* = 11) had dendritic tree diameters of 652 ± 109 μm and stratified at 28 ± 3%; this position is on the vitreal side of the nearby ON ChAT band (42 ± 3%; *n* = 42) (Figure 3.2*C*). Thus, ON or OFF Y-type/α cells in the guinea pig stratified on the vitreal side of the nearby ON or OFF ChAT band,

similar to the dendrite positions of $\alpha$ cells in the rabbit retina (J. Zhang, Li, Hoshi, Mills, & Massey, 2005).

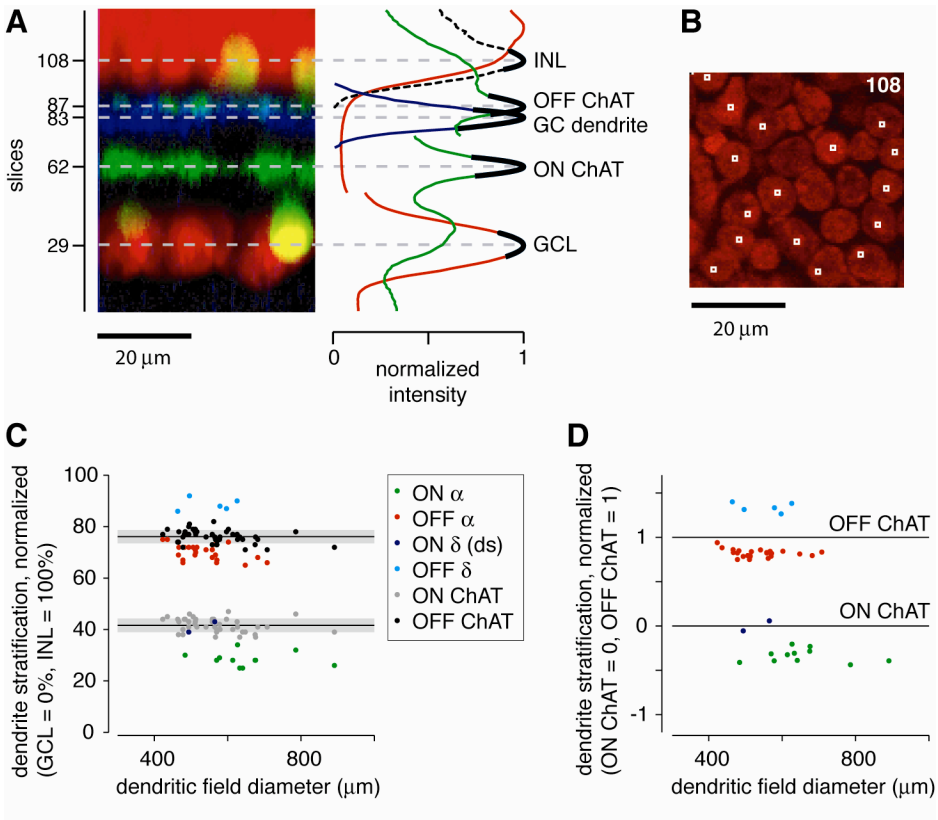


**Figure 3.2.** Morphological properties of ganglion cells with large somas in guinea pig retina. ***A***, Vertical projection of a stack of confocal images, showing the level of ganglion cell (GC) dendrites, nuclear layer boundaries (INL and GCL), and starburst amacrine cell dendrites (ON and OFF ChAT bands). The plot at right shows the normalized intensity for the GC dendrite (blue), the nuclear dye (red), and the ChAT labeling (green). The ganglion cell layer and inner nuclear layer peaks were normalized separately, resulting in two discontinuous red lines. The two ChAT band peaks were normalized separately, resulting in two discontinuous green lines. The dashed black line plots ToPro-3 intensity within the boxed regions shown in ***B***. Solid black lines are polynomial fits used to define the fluorescent intensity peaks. Plotted at these peak positions are the horizontal dashed gray lines, which indicate the position of the ganglion cell layer (slice 29), the ON (inner) ChAT band (slice 62), the OFF (outer) ChAT band (slice 87), and an OFF α cell dendrite (slice 83). ***B***, Confocal image of slice 108 showing ToPro-3-labeled nuclei. The small boxes overlie selected central regions of nuclei in the inner most layer of the INL. ***C***, The dendritic stratification depths within the IPL of ON α cells, OFF α cells, OFF δ cells, ON δ (direction-selective) cells, and the corresponding position of ChAT bands in the same tissues (black or gray dots). Ganglion cell dendrite and ChAT band depths are plotted as a function of ganglion cell dendritic field diameter. Solid lines show the mean of each ChAT band; gray boxes show ± 1 SD of these bands. ***D***, Normalized dendrite position of cells in ***C***. The stratification in ***C*** was normalized relative to the ChAT bands

measured in the same tissue (ON ChAT band, 0; OFF ChAT band, 1).

When targeting large cell bodies, two other cell types were occasionally recorded but could be distinguished from the Y-type/α cells. One type was an OFF cell (*n* = 5), with a wide dendritic tree diameter (552 ± 69 μm) that stratified between the OFF ChAT band and the INL at 89 ± 2% (Figure 3.2*C*). A second type was the ON direction-selective (DS) cell (*n* = 2) (Amthor, Takahashi, & Oyster, 1989), which had a diameter of ~530 μm and costratified with the ON ChAT band (Figure 3.2*C*). For all cells, we also plotted the anatomical data in a second normalized coordinate system, in which dendrite positions are shown relative to the two ChAT band positions measured in the same tissues (Figure 3.2*D*). Here, it is evident that there are four clusters distinguished by their dendritic stratification level relative to the ChAT bands. These four cell types in guinea pig resemble those four cell types with large cell bodies in the rat retina: ON and OFF Y-type/α and ON and OFF δ ganglion cells (in which the ON δ cell is presumably the ON DS cell) (Peichl, 1989). The OFF α cell was also reported in the mouse retina and had similar properties to the guinea pig OFF δ cell: a large soma and dendritic tree diameter, with dendrite stratification near the INL (Margolis & Detwiler, 2007; Tagawa, Sawai, Ueda, Tauchi, & Nakanishi, 1999). Other features of the Y-type/α cells were consistent with previous measurements with sharp electrodes (Zaghloul et al., 2003) and allowed us to distinguish OFF α and δ cells based on the physiology alone. We measured *I–V* plots to full-contrast step responses of a spot (0.6 mm diameter). At a holding potential near –50 mV, the ON Y-type/α cell showed a transient inward current at light onset and an

outward current at light offset (Figure 3.3). The responses to light onset and offset both reversed between $E_{cation}$ (0 mV) and $E_{Cl}$ (–67 mV) (see Experimental Procedures). Thus, the ON cell response arose from the modulation of a pair of excitatory and inhibitory conductances that were increased or decreased in parallel (Zaghloul et al., 2003). The OFF Y-type/$\alpha$ cell showed a different pattern: a transient inward current ($V_{hold}$ of approximately –50 mV) at light offset that reversed near 0 mV with a transient outward current at light onset that reversed near –80 mV (Figure 3.3). Thus, the OFF cell response arose primarily from excitation at light offset and inhibition at light onset (Zaghloul et al., 2003). These conductances are analyzed in more detail at multiple contrast levels in the remainder of the paper.

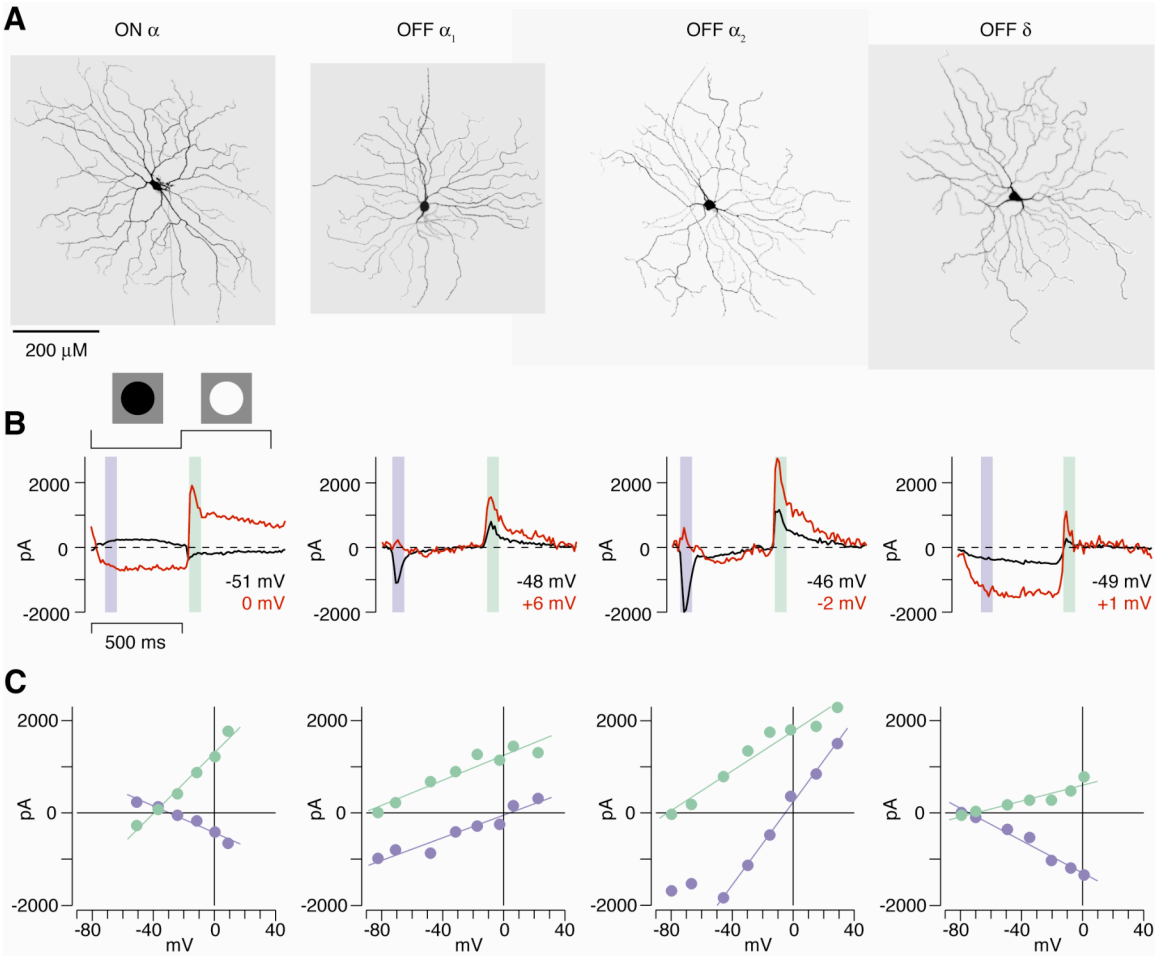


**Figure 3.3.** Physiological properties of ganglion cells with large somas in guinea pig retina. ***A***, Filled cell body and dendritic tree for one ON α cell, two OFF α cells, and one OFF δ cell. Dendritic field diameters (left to right) were 570, 512, 541, and 626 µm. Dendrite stratifications for the same cells were 30, 71, 71, and 90%. ***B***, Spot responses at different holding potentials ($V_{hold}$) for cells in ***A***. ***C***, *I–V* relationship for the cells in ***B***. The ON-α/Y-cell response to the dark spot reversed at –30 mV (left; reversal to light spot, –40 mV). Both OFF-α/Y-cell responses to the dark spot reversed near the excitatory reversal ($E_{excitation}$, ~0 mV), but one cell (OFF $\alpha_1$) showed a relatively linear conductance, whereas the other (OFF $\alpha_2$) showed a pronounced J-shaped conductance. In the OFF δ cell, responses to both light and dark spots reversed near $E_{Cl}$ (–70 and –74 mV, respectively), suggesting that contrast processing arises primarily from modulation of an inhibitory synapse.

In the *I–V* plot for the light offset response, some OFF Y-type/$\alpha$ cells showed a relatively linear relationship (Figure 3.3, OFF $\alpha_1$), whereas others showed a more nonlinear relationship (Figure 3.3, OFF $\alpha_2$): a J-shaped pattern that indicated a contribution from NMDA receptors (Chen & Diamond, 2002; E. D. Cohen, 1998; Sagdullaev, McCall, & Lukasiewicz, 2006). However, cells with or without the J-shaped *I–V* plot showed a similar time course of their step response (Figure 3.3), and their dendrites stratified in similar positions in the IPL (Figure 3.2*C*,*D*). Thus, we consider these two patterns in the *I–V* plot to represent diversity within the OFF Y-type/$\alpha$ cell population. At present, it is unclear why the apparent NMDA contribution varied across cells.

The OFF $\delta$ cell showed a distinct pattern from the OFF Y-type/$\alpha$ cells: a more sustained response to light offset with a negative slope conductance in the *I–V* plot (Figure 3.3), and thus the OFF $\delta$ cell could be distinguished from the OFF Y-type/$\alpha$ cell based on its physiology alone. The focus in the remainder of the study is on the ON and OFF Y-type/$\alpha$ cells, which we refer to simply as ON and OFF cells.

### Ganglion cell membrane current responses at low and high contrast

The above step response measurements were acquired using a contrast-reversing spot stimulus that changed its contrast polarity above and below the mean luminance. In most of the following experiments, we instead measured responses to a 200 ms spot stimulus, in which spot contrast was 2.5, 5, 10, or 80% and defined as an increment or decrement in intensity relative to a steady

mean luminance. The contrast was matched to the sign of the center: decrement stimuli for OFF cells and increment stimuli for ON cells.

Contrast responses were measured while holding voltage near the resting potential. In all cells, the spot evoked an excitatory inward current followed by a "rebound" outward current (Figure 3.4*A*). Below we focus on the excitatory inward current. The size of the inward current increased with contrast (Figure 3.4). OFF cells showed a wider response range than ON cells, as indicated by a larger response amplitude at 80% contrast (OFF cells, 790 ± 74 pA, $n$ = 38 cells; ON cells, 219 ± 50 pA, $n$ = 11 cells; $p < 0.01$, unpaired $t$ test) (Figure 3.4*B*). Notably, there were measurable responses, in both OFF and ON cells, at low contrast levels (2.5–10%). Below, we analyze responses at several contrast levels to reveal the underlying synaptic conductances and to understand how these conductances change with contrast level.

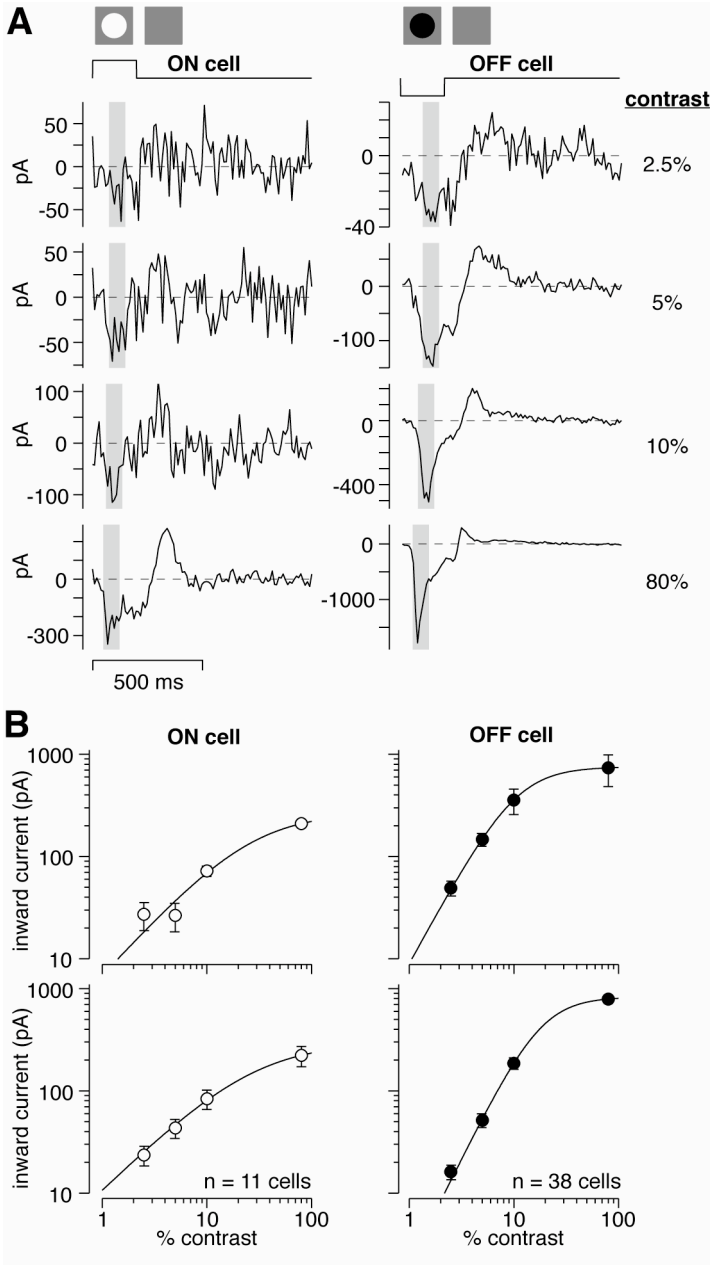


**Figure 3.4.** Membrane current responses at low and high contrast. ***A***, An OFF or ON cell was stimulated with a 200 ms spot (0.6 mm diameter) over the receptive field center at 2.5, 5, 10, or 80% contrast. Contrast is defined as an increment (ON cells) or decrement (OFF cells) in the mean luminance. Voltage was held near the resting potential ($V_{rest}$) (see Experimental Procedures). Shaded area shows the sampling window for measuring current amplitude in ***B***. Traces show an average across 6–12 cycles. ***B***, Top row, Contrast–response functions for the cells in ***A***. Points show average inward current at each contrast ($V_{hold}$ near $V_{rest}$). Error bars show SEM of response across cycles. Line is a fit to the data (see Experimental Procedures). ON cell parameters: $R_{max}$, 170; $c_{50}$, 9.3; $n$, 1.0. OFF cell parameters: $R_{max}$, 750; $c_{50}$, 11; $n$, 1.9. Bottom row, Average inward current as

a function of contrast across cells. Error bars show SEM across cells. Population ON cell parameters: $R_{max}$, 330; $c_{50}$, 29; $n$, 1.0. Population OFF cell parameters: $R_{max}$, 830; $c_{50}$, 18; $n$, 2.1.

**Disinhibition contributes to OFF cell responses**

In ON cells ($n$ = 11), both low- and high-contrast responses showed an increased conductance (2.5%, 1.1 ± 0.2 nS; 5%, 2.1 ± 0.3 nS; 10%, 4.4 ± 0.7 nS; 80%, 12.2 ± 1.9 nS) with a reversal potential that implied a mix of excitation and feedforward inhibition (Figure 3.5*B*) (see Experimental Procedures). Furthermore, the reversal potential was similar at low contrast (2.5%, –35 ± 5 mV; 5%, –38 ± 3 mV; 10%, –36 ± 2 mV) and high contrast (80%, –39 ± 2 mV), suggesting that the relative weight of excitation and inhibition was fixed and independent of contrast level.

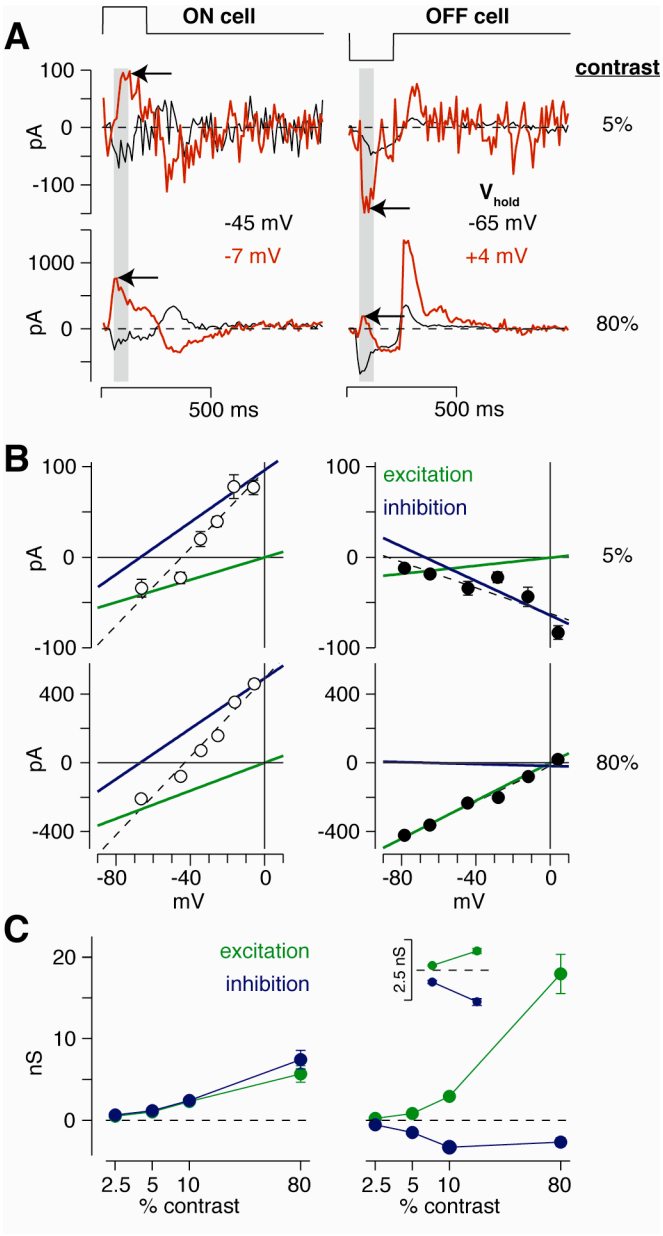


**Figure 3.5.** OFF cell contrast responses are driven in part by disinhibition. ***A***, Flash responses at different holding potentials ($V_{hold}$). In the ON cell, low- and high-contrast flashes both elicited an inward current near rest and an outward current near the excitatory reversal (red; $E_{excitation}$, ~0 mV; arrows). In the OFF cell, low- and high-contrast flashes both elicited an inward current near the resting potential. Holding the cell near $E_{excitation}$ elicited an inward current at low contrast but an outward current at high contrast (arrows). ***B***, *I–V* relationship for the cells in ***A***. The ON cell responses to low (5%) and high contrast (80%) had similar reversals (low contrast, –44 mV; high contrast, –43 mV) and proportional increases in excitatory and inhibitory conductance (green and blue lines, respectively). Dashed lines are linear fits to the data. The low-contrast response in the OFF cell reversed at –90 mV and predominantly comprised removal of an

inhibitory conductance and a minor excitatory conductance. The opposite was true at high contrast, at which the response reversed at +4 mV and was primarily caused by an excitatory conductance. ***C***, Comparison of excitatory and inhibitory conductances. For ON cells, excitation and inhibition increased in parallel with increasing contrast (*n* = 11). For OFF cell low-contrast responses (2.5–10%), disinhibition contributed substantially (*n* = 38), whereas for high-contrast responses, excitation dominated (*n* = 21); inset shows conductances for the 2.5 and 5% contrast responses on an expanded scale.

OFF cells showed a different pattern of results. At low contrast, OFF cell responses showed a negative slope on the *I–V* plot (Figure 3.5*B*), and thus these responses were driven primarily by a decreased conductance (2.5%, –0.32 ± 0.05 nS; 5%, –0.66 ± 0.14 nS; 10%, –0.4 ± 0.4 nS; *n* = 38 cells). In raw traces, this result was reflected by an increased inward current at positive holding potentials, which is opposite to the pattern of the response in ON cells (Figure 3.5*A*, arrows). At high contrast (80%; *n* = 21), there was an increased conductance (15.3 ± 2.7 nS) with a reversal potential that was, on average, positive to 0 mV (+16 ± 9 mV). The positive value of the reversal potential indicates a response driven primarily by glutamate release from bipolar cells in parallel with a net decrease in inhibition relative to a baseline level (see Experimental Procedures). However, there was variability in the degree to which the reversal was positive to 0 mV; in some cases, the reversal was close to 0 mV (Figure 3.5*B*).

To quantify further the above results, we fit each *I–V* plot with the sum of two underlying conductances reversing at 0 and –67 mV (see Experimental Procedures). This conductance analysis calculates the relative contribution from excitatory and inhibitory synapses. The conductance analysis showed that ON

cells received increased excitation and inhibition, in parallel, at all contrasts (Figure 3.5*C*). OFF cells received increased excitation in parallel with decreased inhibition (i.e., disinhibition) at all contrasts. However, disinhibition played a relatively prominent role at low contrasts (Figure 3.5*C*). For example, at 2.5% contrast, the decreased inhibitory conductance was –0.55 ± 0.06 nS, which was greater in magnitude than the increased excitatory conductance of 0.23 ± 0.03 nS (difference of 0.32 ± 0.05 nS; $n = 38$; $p < 0.001$). Similarly, at 5% contrast, the decreased inhibitory conductance was –1.50 ± 0.16 nS, which was greater in magnitude than the increased excitatory conductance of 0.84 ± 0.12 nS (difference of 0.66 ± 0.14 nS; $n = 38$; $p < 0.001$). At 10% contrast, the decreased inhibitory conductance (–3.3 ± 0.3 nS) and the increased excitatory conductance (2.9 ± 0.4 nS) were of similar magnitude (difference of 0.4 ± 0.4 nS; $n = 38$; $p > 0.2$). In Discussion, we consider how these two conductances would contribute to low-contrast voltage responses, given the expected resting potential and reversal potentials for excitation and inhibition *in situ*.

OFF cell responses to high contrast (80%) were dominated by an increased excitatory conductance. Some cells showed a linear conductance (Figures 5*B*, 6*D*), whereas others showed a nonlinear, J-shaped conductance, indicating an NMDA receptor contribution (Figure 3.7*A*,*C*) (see also Figure 3.3*C*). To estimate the full AMPA plus NMDA conductance, we performed the conductance analysis on data collected for $V_{hold}$ values positive to –40 mV, at which the nonlinearity associated with NMDA receptors has minimal effect (see Experimental Procedures). At 80% contrast, the magnitude of the decreased

inhibitory conductance was relatively small (–2.7 ± 0.6 nS) compared with the excitatory conductance (17.9 ± 2.4 nS; *n* = 21).

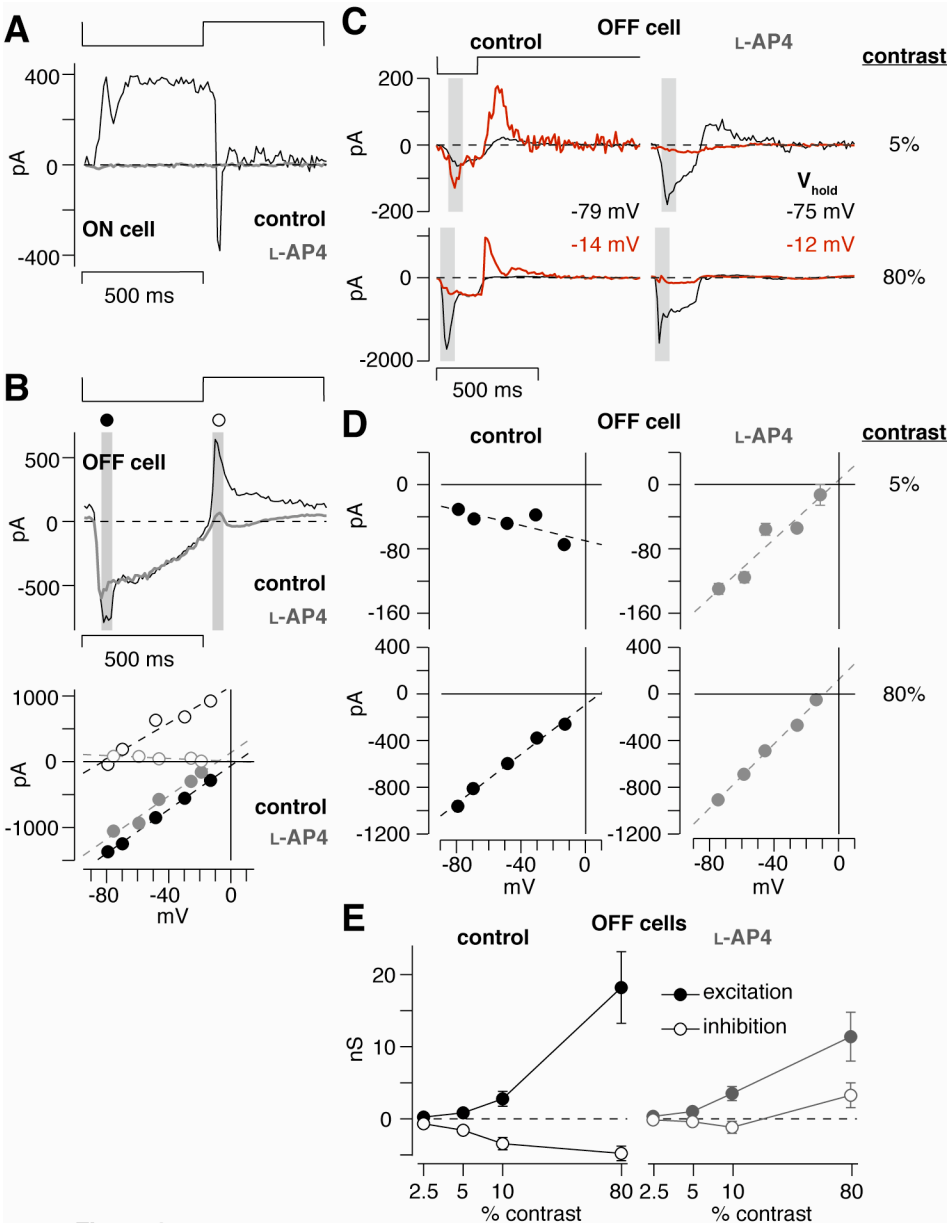


**Figure 3.6.** The ON pathway mediates disinhibition in OFF cells. ***A***, An ON cell was stimulated with a contrast-reversing spot (100% contrast, 1 Hz). Under control conditions (black; $V_{hold}$ of –45 mV), the cell responded to dark with an outward current and to light with a transient inward current. Bath-applied 50 μM L-AP-4 blocked the response (gray; $V_{hold}$ of –60 mV). ***B***, An OFF cell was stimulated with the spot described in ***A***. The cell responded to dark with an inward current and to light with an outward current; 50 μM L-AP-4 blocked the outward current (top; control, $V_{hold}$ of –69 mV; L-AP-4, $V_{hold}$ of –59 mV). The *I–V* plot (bottom) shows a positive conductance after the dark spot (filled circles) during control (black; reversal potential, +4 mV) and L-AP-4 conditions (gray; reversal potential, –8 mV). The light spot (white circles) elicited a large inhibitory

conductance under control conditions (reversal potential, –82 mV) and a small withdrawal of an excitatory conductance in the presence of L-AP-4 (gray; reversal potential, +3 mV). ***C***, Flash responses in an OFF cell at different holding potentials under control conditions and in the presence of l-AP-4. ***D***, *I–V* plots for the cell in ***C***. At 5% contrast, there was a negative conductance under control conditions that reversed to a positive conductance in the presence of L-AP-4. Adding L-AP-4 had minimal effect on the 80% contrast conductance. ***E***, Summary of the results in ***D*** across OFF cells. Excitation slightly increased in the presence of L-AP-4 (gray circles) versus control conditions (black circles), but the inhibitory components of the response decreased in the presence of L-AP-4 (white circles; $n$ = 10 cells for 2.5–10% contrast). At 80% contrast, there was an increased inhibitory conductance in the presence of L-AP-4, suggesting an unmasked feedforward inhibition ($n$ = 8 cells).

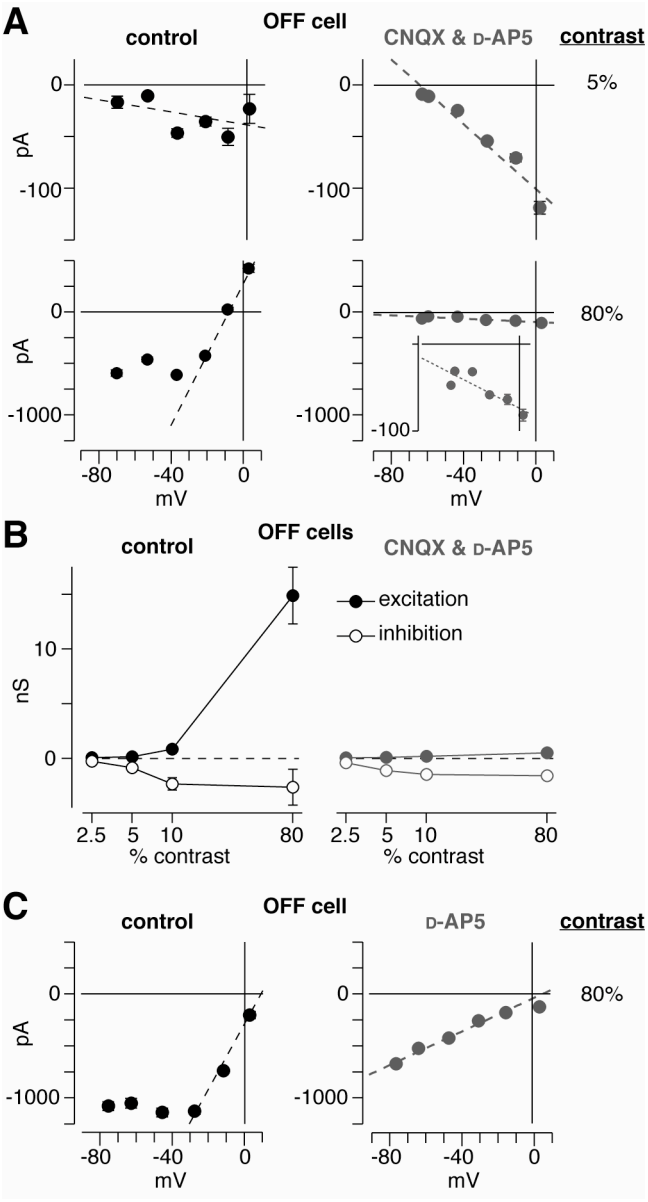


**Figure 3.7.** Disinhibition of OFF ganglion cells does not require ionotropic glutamate receptors. ***A***, *I–V* plot for low- and high-contrast responses in an OFF cell (same conventions as for Figure 3.5*B*). Under control conditions, there was a negative conductance at 5% contrast and a positive conductance at 80% contrast with an apparent NMDA component, resulting in a J-shaped function. In the presence of CNQX and D-AP-5 (100 μM each), the 5% response persisted, whereas the 80% response was primarily blocked. Inset, The persisting response at 80% contrast had a negative slope, similar to the 5% response. ***B***, Conductance analysis under control conditions and in the presence of CNQX plus D-AP-5 (same conventions as for Figure 3.5*C*). The drugs primarily blocked the excitatory component, leaving disinhibition intact. ***C***, Same format as in ***A*** for an OFF cell, in which D-AP-5 was applied alone.

**The OFF cell disinhibition circuit is driven by the ON pathway**

The above results suggest that contrast responses in an OFF ganglion cell are driven partly by removing synaptic inhibition (i.e., disinhibition). It follows that the disinhibition would be driven by the ON pathway: light decrement would hyperpolarize ON bipolar cells and consequently hyperpolarize downstream inhibitory amacrine cells that synapse on the OFF ganglion cell. To test this idea, we suppressed the ON pathway using the mGluR6 agonist L-AP-4, which continually activates the ON bipolar cell mGluR6 cascade resulting in cation channel closure and hyperpolarization (Nakajima et al., 1993; Slaughter & Miller, 1981). At 50 μM, L-AP-4 completely suppressed the response of an ON ganglion cell to a high-contrast reversing spot ($n$ = 2 cells) (same stimulus used in Figure 3.3), suggesting that the presynaptic ON bipolar cells were completely inhibited at this concentration (Figure 3.6*A*). In OFF ganglion cells, L-AP-4 did not suppress the inward current to the dark phase of the reversing spot (100% contrast), which is presumably driven primarily by OFF bipolar cells, but did suppress the outward current to the light phase (control, 357 ± 75 pA; L-AP-4, 0.6 ± 22.2 pA; $n$ = 10 cells; $p < 0.001$; average ± SD $V_{hold}$, –54 ± 5 mV) (Figure 3.6*B*). This confirms previous work showing that, for OFF ganglion cells, the ON pathway drives an inhibitory conductance at light onset (E. D. Cohen, 1998; Murphy & Rieke, 2006; Pang, Gao, & Wu, 2003; Roska et al., 2006; Wassle, Schafer-Trenkler, & Voigt, 1986; Zaghloul et al., 2003).

We next tested whether the ON pathway drives OFF cell low-contrast responses to light offset, using the 200 ms decrement stimulus (Figure 3.6*C*). At low contrast, there was a decreased conductance, as indicated by negative slopes on the *I–V* plots (Figure 3.6*D*). In the presence of L-AP-4, these negative slopes became positive, suggesting that the disinhibition pathway was blocked. At high contrast (80%), there were positive slopes in both control and L-AP-4 conditions (Figure 3.6*D*). We performed a conductance analysis, as described above. L-AP-4 significantly reduced the magnitude of the decreased inhibitory conductance ($p < 0.05$ at each contrast) but did not block the increased excitatory conductance (Figure 3.6*E*). These data suggest that disinhibition of OFF cells is driven by ON-pathway amacrine cell synapses.

In addition to blocking the decreased inhibitory conductance, L-AP-4 revealed an increased inhibitory conductance at 80% contrast (Figure 3.6*E*). Across cells, this conductance was 3.4 ± 1.8 nS ($n = 8$). This inhibitory conductance may be present at high contrast under control conditions but masked by the decreased inhibitory conductance. This suggests that a feedforward inhibitory synapse, driven by the OFF pathway, acts in parallel with OFF bipolar cell excitation. However, this putative feedforward inhibition requires additional characterization. For example, our conclusion depends on a slight shift in the reversal potential (Figure 3.6*D*). Furthermore, in the presence of L-AP-4, inhibition of the OFF bipolar terminal is presumably reduced, and thus the output of OFF bipolar cells would increase, potentially altering the degree of feedforward inhibition present under natural conditions.

**The disinhibition circuit does not require ionotropic glutamate receptors**

Virtually every circuit, from photoreceptors to amacrine or ganglion cells in the inner retina, requires at least one synapse mediated by an iGluR (Dumitrescu, Protti, Majumdar, Zeilhofer, & Wassle, 2006; Kalloniatis et al., 2004; Marc, 1999a, 1999b). The one known exception is the following circuit: cone → ON cone bipolar cell → AII amacrine cell → OFF ganglion cell (see Introduction); rods could also drive this circuit through their gap junctions with cones. The cone → ON cone bipolar synapse uses an mGluR6 receptor (Nakajima et al., 1993; Nomura et al., 1994); the ON cone bipolar → AII amacrine cell synapse uses a connexin (cx) 36 gap junction or a cx36/cx45 gap junction (Deans, Volgyi, Goodenough, Bloomfield, & Paul, 2002; Feigenspan, Teubner, Willecke, & Weiler, 2001; Han & Massey, 2005; Lin, Jakobs, & Masland, 2005; Mills, O'Brien, Li, O'Brien, & Massey, 2001); the AII amacrine cell → OFF ganglion cell synapse uses a glycine receptor (Muller, Wassle, & Voigt, 1988; Murphy & Rieke, 2006; Sassoe-Pognetto, Wassle, & Grunert, 1994). Thus, if this circuit explains ON pathway disinhibition of OFF ganglion cells, then it should persist in the presence of iGluR antagonists.

To test the above possibility, we measured responses while blocking both AMPA/kainate and NMDA receptors with CNQX (100 μM) and D-AP-5 (100 μM) (E. D. Cohen, 1998; E. D. Cohen & Miller, 1999; E. D. Cohen et al., 1994). In the presence of these antagonists, low-contrast responses persisted, and these responses were driven primarily by disinhibition (Figure 3.7*B*). However, high-

contrast responses were suppressed; the inward current decreased from –399 ± 37 pA under control conditions to –59 ± 16 pA in the presence of the antagonists (decrease of 86 ± 3%, $p < 0.001$; $n = 6$ cells; $V_{hold}$ near the $V_{rest}$). Furthermore, in the presence of the antagonists, the conductance at high contrast showed a negative slope, similar to the low-contrast conductance (Figure 3.7*A*). Blocking NMDA receptors alone with D-AP-5 (50 μM) made the J-shaped *I*–*V* plot more linear but did not completely block excitatory currents at high contrast (Figure 3.7*C*). Thus, we conclude that disinhibition of OFF cells, at low and high contrast, could originate in the above described AII amacrine cell pathway.

The above response cannot, however, be driven by two of the rod pathways. Rods release glutamate onto OFF cone bipolar cell dendrites, but these dendrites express iGluRs (Hack, Peichl, & Brandstatter, 1999; Li, Keung, & Massey, 2004; Soucy, Wang, Nirenberg, Nathans, & Meister, 1998; Tsukamoto, Morigiwa, Ueda, & Sterling, 2001). Furthermore, the rod pathway illustrated in Figure 3.1*A* uses an iGluR at the rod bipolar → AII cell synapse (Boos, Schneider, & Wassle, 1993; Singer & Diamond, 2003). Rods can signal cones directly, through gap junctions (Bloomfield & Dacheux, 2001; DeVries & Baylor, 1995). These rod signals could reach ganglion cells through cone synapses with ON cone bipolar cells and then through the AII circuit (i.e., rod → cone → ON cone bipolar → AII cell → ganglion cell). However, rod signals could not reach ganglion cells through cone synapses with OFF cone bipolar cells, because the cones release onto iGluRs on the bipolar cell (Figure 3.1*B*).

### Evidence that the disinhibition circuit includes the AII amacrine cell

To test the role of the above AII circuit in OFF ganglion cell disinhibition, we performed several experiments designed to disrupt each synapse in the circuit. We first isolated the putative circuit by blocking iGluRs with D-AP-5 (200 μM) and CNQX (200 μM) (Figure 3.8*A*) and then measured the 10% contrast response before and after adding additional drugs ($V_{hold}$ of –35 to –25 mV) (Figure 3.8*A*). In one experiment, we added L-AP-4, to confirm that the response was driven by the ON pathway (cone →ON cone bipolar synapse), as suggested by the results in Figure 3.6 (Figure 3.8$A_1$). The inward current in the presence of CNQX and D-AP-5 (–37.0 ± 17.3 pA) was significantly reduced by adding L-AP-4 (+1.6 ± 2.0 pA; $p < 0.05$; $n = 6$). During a washout of all drugs, the response partially recovered to –23 ± 9 pA (compared with an initial response of –57 ± 27 pA; $n = 4$).

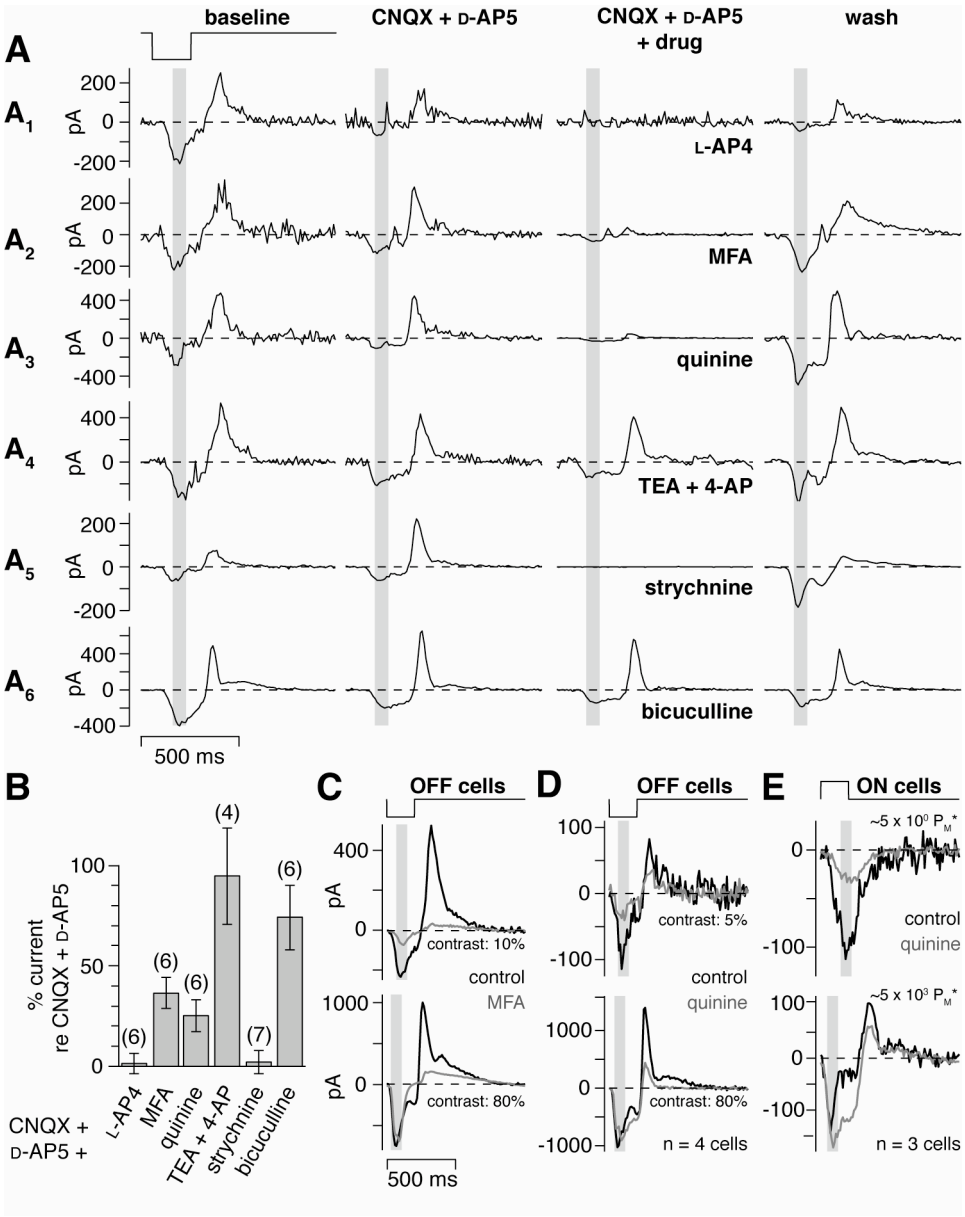


**Figure 3.8.** Evidence that the disinhibition circuit uses the AII amacrine cell. ***A***, Six OFF cells were stimulated with repeating dark flashes (contrast, 10%; $V_{hold}$, approximately –35 to –25 mV) under baseline conditions, with bath-applied drugs, and after washing out the drugs. Adding L-AP-4 (***A₁***, 100 μM), MFA (***A₂***, 200 μM), quinine (***A₃***, 200 μM), or strychnine (***A₅***, 2 μM) to CNQX (200 μM) and D-AP-5 (200 μM) sharply reduced the current responses to the flash, whereas adding bicuculline (***A₆***, 100 μM) or TEA and 4-AP (***A₄***, 1 mM each) had little effect. ***B***, Results for the experiment in ***A*** across multiple cells (number of cells in parentheses). The bars show the inward current elicited by the 10% contrast flash in each drug condition (CNQX and D-AP-5, plus the drug on the *x*-axis) relative to the inward current in the presence of CNQX and D-AP-5 alone. Adding L-AP-4, meclofenamic acid, quinine, or strychnine decreased the inward current to a small percentage of the original current. Adding bicuculline or TEA and 4-AP

had little effect (see Results). Error bars indicate SEM across cells. ***C***, Meclofenamic acid (200 μM) applied alone reduced the 10% contrast response and also reduced the outward current at the offset of 80% contrast. The inward current at high contrast was unaffected, suggesting no general depression of OFF bipolar cells. Traces show the average response of five to six cells. ***D***, Quinine (200 μM) applied alone produced results similar to ***C***, reducing the 5% contrast response and also reducing the outward current at the offset of 80% contrast. The inward current at high contrast was unaffected. Traces show the average of recordings from four cells. ***E***, ON cells were stimulated with repeating bright flashes (contrast, 100%; 20 repeats; $V_{hold}$, approximately –63 mV) at two levels of mean luminance. Quinine suppressed the inward current only under rod-bipolar-driven conditions (~5 x $10^0$ $P_M$*). Traces show the average of recordings from three cells.

We next tested a role for a gap junction at the ON cone bipolar→AII amacrine cell synapse (Deans et al., 2002; Feigenspan et al., 2001; Han & Massey, 2005; Lee, Kim et al., 2003; Mills et al., 2001). To test this, we applied meclofenamic acid (MFA) (200 μM), which blocks tracer coupling between AII cells and ON cone bipolar cells (Pan, Mills, & Massey, 2007). The inward current in the presence of CNQX and D-AP-5 (–127 ± 9 pA) was significantly reduced by adding MFA (–46 ± 11 pA; $p < 0.01$; $n = 6$). We measured a recovery, after washing out all drugs, in two cases; one is shown in Figure 3.8*A*$_2$. In another set of experiments, we applied quinine (200 μM), which blocks cx36 gap junctions (Schubert et al., 2005; Srinivas, Hopperstad, & Spray, 2001). The inward current in the presence of CNQX and D-AP-5 (–52.2 ± 13.9 pA) was significantly reduced by adding quinine (–12.9 ± 3.4 pA; $p < 0.05$; $n = 6$). The response partially recovered after washing out all drugs to –39 ± 22 pA (compared with initial response of –50 ± 16 pA; $n = 4$) (Figure 3.8*A*$_3$). Quinine can also block potassium channels, and so as a control we repeated the above experiment but applied potassium channel blockers (1 mM TEA and 1 mM 4-AP) in place of quinine

(Imai, Suzuki, Sato, & Tokimasa, 1999). The inward current in the presence of CNQX and D-AP-5 (–134 ± 35 pA) was not blocked by adding TEA and 4-AP (–113 ± 31 pA; $p > 0.10$; $n = 4$), suggesting that quinine did not act by blocking potassium channels (Figure 3.8*A*$_4$). Additional control experiments for MFA and quinine are described in a separate section below.

We next tested roles for glycine and GABA. Glycine receptors were blocked with strychnine (2 μM). The inward current in the presence of CNQX and D-AP-5 (–31.9 ± 4.2 pA) was completely blocked by adding strychnine (–0.1 ± 1.4 pA; $p < 0.05$; $n = 7$). In general, it was difficult to measure recovery after strychnine application, although we were able to measure partial recovery in two cells; one is shown in Figure 3.8*A*$_5$. In separate experiments, we blocked $GABA_A$ receptors with bicuculline (100 μM). The response in the presence of CNQX and D-AP-5 (–93.0 ± 19.2 pA) was only slightly suppressed by adding bicuculline (–69.5 ± 18.8 pA; $n = 6$) (Figure 3.8*A*$_6$).

The above results are summarized in Figure 3.8*B*. The inward current response at 10% contrast showed, relative to the recording in the presence of D-AP-5 and CNQX, a significant percent reduction after adding L-AP-4 (99 ± 5%; $p < 0.001$), MFA (64 ± 8%; $p < 0.01$), quinine (75 ± 8%; $p < 0.001$), or strychnine (98 ± 6%; $p < 0.001$) but not after adding TEA and 4-AP (5 ± 24%; $p > 0.10$) or bicuculline (26 ± 16%; $p > 0.05$). The small effect of bicuculline could be explained by nonspecific effects of bicuculline on glycine receptors (Wang and Slaughter, 2005). These results suggest that the disinhibition circuit for OFF ganglion cells depends on mGluR6 receptors, gap junctions, and glycine receptors. These

results can be explained most parsimoniously by the above-described circuit: (rod →) cone → ON cone bipolar cell → AII amacrine cell → OFF ganglion cell (Figure 3.1*B*).

## Control experiments further suggest that MFA and quinine block the gap junction between AII cells and ON cone bipolar cells

We performed additional experiments to test whether MFA or quinine had unexpected, nonspecific effects on retinal processing, similar to other gap junction blockers (Xia & Nawy, 2003). In OFF cells ($n$ = 6; $V_{hold}$, –20 to –35 mV), applying MFA in isolation did not affect the inward current at 80% contrast (control, –591 ± 88 pA; MFA, –601 ± 126 pA; $p > 0.4$) but did reduce the outward rebound current (control, +629 ± 131 pA; MFA, +72 ± 32 pA) by 557 ± 128 pA ($p < 0.01$) (Figure 3.8*C*). Furthermore, MFA reduced the inward current at 10% contrast (control, –209 ± 23 pA; MFA, –47 ± 18 pA) by 162 ± 34 pA ($p < 0.01$) (Figure 3.8*C*). In additional experiments on OFF cells ($n$ = 4; $V_{hold}$, –29 to –36 mV), applying quinine in isolation did not affect the inward current at 80% contrast (control, –804 ± 97 pA; quinine, –775 ± 156 pA; $p > 0.4$) but did reduce the outward rebound current (control, +747 ± 83 pA; quinine, +140 ± 20 pA) by 606 ± 97 pA ($p < 0.01$) (Figure 3.8*D*). Furthermore, quinine reduced the inward current at 5% contrast (control, –77 ± 15 pA; quinine, –29 ± 8 pA) by 48 ± 9 pA ($p < 0.05$) (Figure 3.8*D*). The above results suggest that MFA and quinine interrupt the cone → ON cone bipolar → AII amacrine cell → OFF ganglion cell circuit, presumably by blocking the ON bipolar → AII cell synapse. The rebound current at high

contrast would be driven, at light onset (i.e., dark spot offset), by stimulating the AII circuit (Figure 3.6*B*). The inward current at low contrast would be driven in large part by disinhibition from the AII circuit, as described above.

We performed additional control experiments in ON cells ($n = 3$; $V_{hold}$, –63 to –64 mV). If quinine blocks the ON cone bipolar cell → AII cell gap junction, then ON ganglion cell responses should decrease under conditions that depend heavily on the rod bipolar pathway but persist under conditions driven by the cone bipolar pathway (Figure 3.1). Under rod-driven conditions, the inward current to the flash decreased from –126 ± 49 pA (control) to –29 ± 13 pA in the presence of quinine (a difference of 97 ± 37 pA; $p < 0.10$). At cone-driven levels, however, the inward current was similar across conditions (control, –103 ± 31 pA; quinine, –109 ± 34 pA; $p > 0.4$) (Figure 3.8*E*). This result suggests that quinine inhibits the ON cone bipolar → AII cell synapse. There were other effects of quinine that we cannot explain, such as the more sustained inward current for ON cells at high mean luminance (Figure 3.8*E*). Gap junctions exist at several sites in the retina, including the rod → cone gap junction (Deans et al., 2002; Lee, Han et al., 2003) and ganglion cell → amacrine cell gap junctions (Schubert et al., 2005; Volgyi, Abrams, Paul, & Bloomfield, 2005); thus, some effects of quinine could be explained by actions at these alternative sites. However, these control experiments are generally consistent with an effect of MFA or quinine at the ON cone bipolar → AII cell synapse.

**Disinhibition from the putative AII amacrine cell circuit drives OFF ganglion cell responses under conditions driven by both cone and rod bipolar cells**

Above, we assumed that AII cells synapse directly onto OFF ganglion cell dendrites. To test this, we measured responses at lower levels of mean luminance (Figure 3.9). At all light levels, the rods should be active (i.e., not saturated) (Yin, Smith, Sterling, & Brainard, 2006). At the higher levels, rods would contribute primarily through their gap junctions with cones, whereas at the lowest levels, the rod bipolar cell should be active and the AII circuit should become a dominant mechanism for light responses (Bloomfield & Dacheux, 2001; Deans et al., 2002; Kolb & Famiglietti, 1974) (Figure 3.1*A*). Thus, at the lower levels of mean luminance, the conductance analysis should reflect the switch to the AII circuit. We measured *I*–*V* plots for 100% contrast responses at four levels of mean luminance ($n$ = 3 OFF cells). At high mean luminance (~5 x $10^3$ $P_M$*) (see Experimental Procedures), the initial response to the flash showed an increased conductance with a J-shaped *I*–*V* plot, indicating a mixed AMPA/NMDA-mediated response (~5 x $10^2$ $P_M$*: excitation, 33 ± 3 nS, inhibition, –1.9 ± 0.7 nS; ~5 x $10^3$ $P_M$*: excitation, 37 ± 7 nS; inhibition, 1.7 ± 0.8 nS). At lower mean luminance, however, the response to the flash showed a decreased conductance, consistent with a removal of inhibition from the AII circuit (Figure 3.9*B*) (~5 x $10^0$ $P_M$*: excitation, 1.7 ± 0.4 nS; inhibition, –6.1 ± 0.2 nS; ~5 x $10^1$ $P_M$*: excitation, 3.2 ± 0.4 nS; inhibition, –7.6 ± 0.4 nS). Thus, this putative AII circuit dominated the response at ~5 x $10^0$–$10^1$ $P_M$*, which was the apparent level of rod-dominated responses measured previously (Yin et al., 2006).

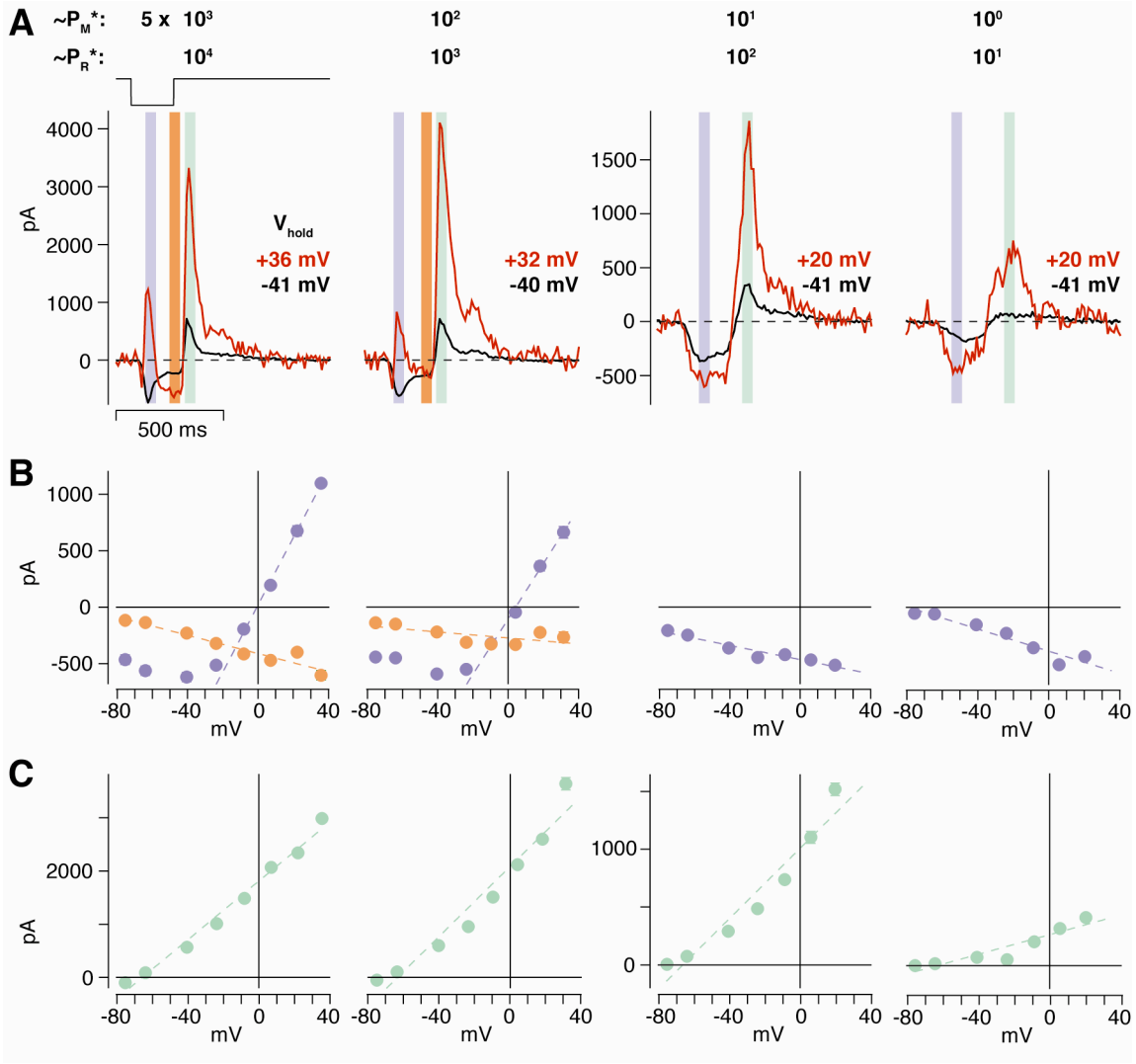


**Figure 3.9.** The AII circuit can be driven by either rod- or cone-bipolar pathways. ***A***, An OFF cell was stimulated with 100% contrast, dark flashes at several levels of mean luminance (~5 x $10^0$–$10^3$ $P_M$*; $10^1$–$10^4$ $P_R$*). At high mean luminances (~5 x $10^2$–$10^3$ $P_M$*), the transient inward current (blue strip) reversed to outward at positive $V_{hold}$, whereas at low mean luminances (~5 x $10^0$-$10^1$ $P_M$*), this current became more negative at positive $V_{hold}$. At high mean luminance, a sustained response (orange strip) showed a pattern that resembled the low mean luminance response: increased inward current at positive $V_{hold}$. At each mean luminance, a rebound outward current (green strip) followed flash offset. Traces show the average of 10–20 repeats. ***B***, *I–V* relationships for the cell in ***A***. The transient response (blue circles) at high mean luminances showed a J-shaped conductance, indicating a response driven by excitatory (AMPA plus NMDA) synapses. The sustained response (orange) showed a negative conductance,

indicating substantial disinhibition. Responses at low mean luminances were driven by a negative conductance, indicating disinhibition. Dashed lines are linear fits to the data (see Experimental Procedures). ***C***, Current–voltage relationship for the outward rebound current in ***A***. Conductances at all luminance levels were positive and reversed near $E_{Cl}$.

The sustained response to the 100% contrast flash at high mean luminance was also apparently driven by a distinct mechanism from the transient response (Figure 3.9*A*) (see also Figure 3.5*A*). The sustained response also included disinhibition (~5 x $10^2$ $P_M$*: excitation, 8.4 ± 1.8 nS; inhibition, –4.9 ± 0.2 nS; ~5 x $10^3$ $P_M$*; excitation, 6.1 ± 1.7 nS; inhibition, –5.2 ± 0.7 nS), similar to the low-contrast response at high mean luminance (Figures 5–7) and the high-contrast response at low mean luminance (Figure 3.9*B*). Thus, at high mean luminance, the sustained high-contrast response, after the initial excitatory response attenuates, also apparently depends on the AII circuit.

At light onset (i.e., dark spot offset), there was an outward rebound current at each level of mean luminance that reversed near $E_{Cl}$ (Figure 3.9*C*). This rebound current is presumably caused, at least in part, by activating the AII circuit (see Discussion), and the circuit makes a similar contribution at all light levels. The inhibitory conductance at the two brighter levels (~5 x $10^2$ $P_M$*: excitation, 0.2 ± 0.7 nS; inhibition, 30 ± 4 nS; ~5 x $10^3$ $P_M$*; excitation, 0.7 ± 0.7 nS; inhibition, 31 ± 6 nS) was larger than that at the two dimmer levels (~5 x $10^0$ $P_M$*: excitation, 0.1 ± 0.1 nS; inhibition, 5 ± 2 nS; ~5 x $10^1$ $P_M$*: excitation, 0 ± 0.14 nS; inhibition, 14 ± 1 nS). Still, it was remarkable that, across a ~1000-fold change in mean luminance, the inhibitory conductance varied by only ~6-fold.

## Discussion

Figure 3.1*B* illustrates our circuit model for contrast processing in the OFF ganglion cell under conditions driven by cone bipolar pathways. Responses are driven by a combination of excitation mediated by the OFF pathway and disinhibition mediated by the ON pathway. The disinhibition arises because a light decrement hyperpolarizes ON bipolar cells and electrically coupled AII amacrine cells; this latter hyperpolarization decreases glycine release onto the OFF ganglion cell. At low contrast, disinhibition plays a relatively large role, leading to an inward current at $V_{rest}$ associated with a negative conductance (Figures 5–7, 9). At high contrast, disinhibition plays a smaller role, leading to an inward current at $V_{rest}$ associated with a positive conductance (Figures 5–7, 9). At light onset (or dark offset), an inhibitory conductance is observed under conditions driven by either rod or cone bipolar pathways (Figures 6B, 8, 9). This inhibition would arise from stimulating the AII circuit, which in turn inhibits the OFF ganglion cell. Thus, the AII circuit could explain crossover inhibition from ON to OFF pathways described previously (Zaghloul et al., 2003).

### Support for the circuit model for disinhibition of the OFF pathway

The disinhibition circuit for OFF cells seems unconventional. Thus, it is worth reviewing evidence for each step in the pathway. First, ON bipolar cell responses should not be strongly rectifying, so they could signal either light increments or decrements to AII cells. Evidence for nonrectifying responses in

ON bipolar cells comes from studies of ON ganglion cells. ON ganglion cells show excitatory responses that increase or decrease from a baseline level (Demb, Zaghloul, Haarsma et al., 2001; Murphy & Rieke, 2006; Zaghloul et al., 2003) (Figure 3.3). Thus, ON bipolar cells apparently rest near the middle of their operating range and neither their voltage responses nor their glutamate release strongly rectify. Direct bipolar cell recordings support this interpretation (D. Dacey et al., 2000).

At the next step, current would flow from ON bipolar cells to AII cells. Depolarizing an ON bipolar cell causes depolarization of a coupled AII cell (Trexler et al., 2005; Veruki & Hartveit, 2002). Furthermore, AII cells responded to light under cone-driven conditions (Bloomfield & Dacheux, 2001; D. M. Dacey, 1999; Pang et al., 2007; Xin & Bloomfield, 1999). The apparent pathway mediating the cone-driven response is the following: cone → ON cone bipolar → AII cell. In support of this, AII light responses persist in the presence of an iGluR antagonist, which blocks the synaptic output of rod bipolar cells (Pang et al., 2007; Trexler et al., 2005; Xin & Bloomfield, 1999).

At the final step, the AII cell would directly synapse onto the OFF ganglion cell. Electron micrographs (EM) suggested that AII glycinergic outputs contact both OFF ganglion cell dendrites and their presynaptic OFF bipolar terminals (Dacheux & Raviola, 1986; Famiglietti & Kolb, 1975; Kolb, 1979). The relative number of these synapses has been estimated by serial section EM. In rat, at least 33% of chemical synaptic output from putative AII cells is onto ganglion cell dendrites (Chun, Han, Chung, & Wassle, 1993). However, in rabbit, only 4% of

output is onto ganglion cell dendrites (Strettoi, Raviola, & Dacheux, 1992). Recordings in mouse implied a strong output of AII cells onto OFF ganglion cell dendrites. At light levels at which rod bipolar cells are the primary conveyor of rod signals to the inner retina (~2 $P_R$*), an OFF $\alpha$ ganglion cell was driven primarily by an inhibitory glycinergic synapse (Murphy & Rieke, 2006); this glycinergic input is explained by the AII circuit (Murphy & Rieke, 2008). Thus, the dominant output of the mouse AII cell (driven by the rod bipolar cell) is onto the OFF ganglion cell dendrite. Our recordings at ~10 $P_R$* support this interpretation; the OFF ganglion cell response was primarily modulated by an inhibitory conductance (Figure 3.9*C*). Furthermore, from the perspective of the OFF $\alpha$ ganglion cell (cat), the direct AII synapses are substantial: they are approximately equal in number to those from the OFF cone bipolar cells (Kolb & Nelson, 1993). Thus, there is strong evidence for a substantial input from AII cells to OFF ganglion cell dendrites in several species. The main exception is the EM study in rabbit, and this could reflect a species difference.

Our model suggests that disinhibition of an OFF ganglion cell is driven exclusively by AII cells. However, we cannot rule out a contribution from other narrow-field glycinergic amacrine cell types that could act in parallel with the AII cell (Menger, Pow, & Wassle, 1998). These other amacrine cell types would have to share certain features with the AII cell: excitation from ON bipolar cells and inhibitory synapses with the OFF $\alpha$ cell. However, the CNQX/D-AP-5-resistant response in the OFF ganglion cell is almost certainly explained exclusively by the AII circuit, because this is the only known pathway that can be driven by ON

bipolar cells through gap junctions and thus does not require an iGluR in the circuit (E. Cohen & Sterling, 1990; Kolb, 1979). Because this CNQX/D-AP-5-resistant response explains the bulk of disinhibition (Figures 7, 8), the AII circuit is likely the primary conveyor of disinhibition to the OFF ganglion cell.

### Rod and cone inputs to the AII circuit

At the highest light level tested, responses are driven in approximately equal combination by rods and cones (Yin et al., 2006). At this level (~5 x $10^3$ $P_M$*, ~$10^4$ $P_R$*), rods likely act primarily through their electrical synapses with cones, assuming that the rod → rod bipolar pathway is saturated. We have not measured the level at which the rod bipolar saturates in guinea pig, but several lines of evidence suggest that cone bipolar pathways dominate at ~$10^4$ $P_R$*. First, the excitatory response of OFF ganglion cells persists in the presence of L-AP-4, which would block the (ON-type) rod bipolar cell (Figure 3.6*B*) (Zaghloul et al., 2003). Furthermore, inhibitory light responses in OFF ganglion cells persist in the presence of iGluR antagonists (Figures 7, 8), and these must not depend on rod bipolar synapses (Figure 3.1*A*). Thus, at ~$10^4$ $P_R$*, rods apparently drive the proposed AII circuit that converges on the OFF ganglion cell, but this contribution must arise through their gap junctions with cones.

At the lowest light level tested here (~10 $P_R$*; ~5 $P_M$*), the response is driven exclusively by rods (Yin et al., 2006). At this level, the OFF ganglion cell response to light offset (at high contrast) modulated an inhibitory conductance almost exclusively (Figure 3.9). This response can be explained by the pathway:

rod → rod bipolar → AII cell → ganglion cell. The other route (rod → cone → cone bipolar → ganglion cell) must be relatively inactive under this condition. Thus, rods drive the AII circuit at all light levels, but as light level decreases, the pathway for their drive switches between the cone bipolar circuit to the rod bipolar circuit (Xin and Bloomfield, 1999; Trexler et al., 2005; Pang et al., 2007).

### OFF bipolar input to the AII cell

We have not considered here an additional synaptic pathway to the AII cell. OFF bipolar cells synapse onto AII cells, suggesting that OFF bipolar cells can excite the AII, in addition to receiving inhibition from the AII (Chun et al., 1993; Strettoi et al., 1992; Xin & Bloomfield, 1999). Under most conditions, the AII cell depolarizes at light onset, suggesting that ON bipolar excitation dominates the light response. However, under certain conditions, the AII shows an excitatory response at light offset (Xin & Bloomfield, 1999). How does this synapse fit into our model? Some feedforward inhibition onto the OFF ganglion cell (Figure 3.6*E*) could possibly be explained by this synaptic pathway (cone → OFF cone bipolar → AII cell → OFF ganglion cell). However, at present, we cannot distinguish this from other types of amacrine cell that could play the same role (Kolb & Nelson, 1993).

### Impact of the disinhibition pathway for OFF ganglion cells *in situ*

For OFF cells at the lowest contrast level tested (2.5%), the negative conductance associated with disinhibition was approximately twice the magnitude

of the positive conductance associated with excitation (Figure 3.5). Here, we set $E_{Cl}$ to be –67 mV, but *in situ* we expect it to be more negative, approximately –80 mV (Murphy & Rieke, 2006); we expect $E_{cation}$ to be ~0 mV. Furthermore, OFF ganglion cells rest between –60 and –65 mV (Manookin & Demb, 2006; Zaghloul et al., 2003). Thus, the driving force on excitation is three to four times larger than the driving force on inhibition. Taking into account the conductances and driving forces, disinhibition should generate approximately two-thirds of the inward current compared with excitation for threshold responses at $V_{rest}$ (Figure 3.10). As the cell depolarizes from rest, the impact of disinhibition would increase. This analysis probably underestimates the complete drive from the AII circuit, which could also contribute by disinhibiting the OFF bipolar terminal to drive the excitatory conductance of the ganglion cell (Molnar & Werblin, 2007). Thus, under daylight conditions, the AII circuit contributes substantially to low-contrast responses through disinhibition of the OFF pathway.

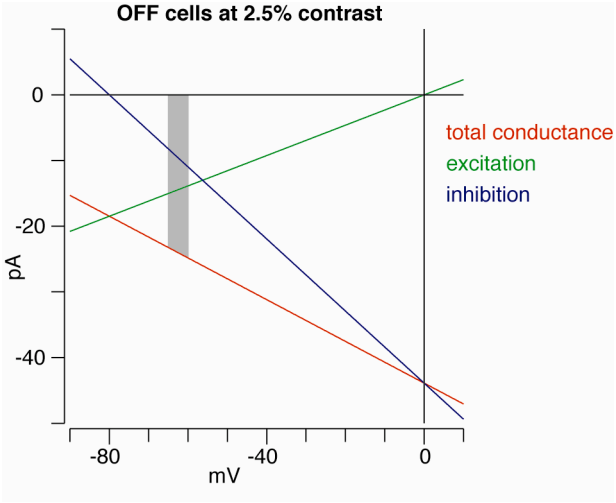


**Figure 3.10.** Disinhibition contributes substantially to low-contrast responses in OFF ganglion cells. Red line shows the total conductance measured from 38 OFF cells at the lowest contrast tested (2.5%), which is near the threshold for responding. $E_{Cl}$ was shifted to –80 mV, the expected reversal potential for inhibition *in situ* (see Discussion). The underlying excitatory and inhibitory conductances are shown in green and blue, respectively. The expected resting potential for OFF cells *in situ* is between –60 and –65 mV (gray strip). Within this range, disinhibition provides approximately two-thirds the current as excitation.

## Experimental Procedures

### Tissue preparation and electrophysiology

Hartley guinea pigs were housed in a 12 h light/dark cycle. On the day of an experiment, an animal was brought to a room illuminated with red light and anesthetized with ketamine (100 mg/kg) and xylazine (10 mg/kg). The animal was then decapitated, and both eyes were removed. All procedures conformed to National Institutes of Health and University of Michigan guidelines for use and care of animals in research. The retina was hemisected under dim white light, and the vitreous, lens, and cornea were removed and discarded. The back of the eye, including the retina, pigment epithelium, choroid, and sclera, was either maintained as a single piece or cut along the vertical midline into two pieces

(nasal and temporal halves). Slits were made in each piece of tissue so that the retina would lie flat (Demb et al., 1999), and the tissue was mounted on filter paper with two to three small holes (0.5 mm diameter) punched out. The retina was mounted so that the hole positions were aligned with the dorsal retina. Those areas of retina over the holes could be later visualized using transmitted infrared light. The pieces of retina were stored at room temperature in oxygenated (95% $O_2$ and 5% $CO_2$) Ames medium (Sigma, St. Louis, MO) in a light-tight container until the time of recording (storage time, 30 min to 5 h). At the time of recording, the filter paper, with retina attached, was placed in a chamber on a microscope stage and superfused (~6 ml/min) with oxygenated (95% $O_2$ and 5% $CO_2$) Ames medium heated to 33–35°C with an in-line heater (TC-344B; Warner Instruments, Hamden, CT).

The retina and electrode were visualized using a cooled CCD camera (Retiga 1300C, Qcapture software; Qimaging, Burnaby, British Columbia, Columbia) mounted on an Olympus (Center Valley, PA) BX51WI microscope. We targeted Y-type/$\alpha$ ganglion cells by recording from the largest cell bodies in the ganglion cell layer (diameter, 20–25 μm). Cell type was confirmed by measuring light responses and in some cases by analyzing the dendritic tree, as described below (see Results). A glass electrode (tip resistance, 2–6 MΩ) was filled with recording solution [120 mM cesium-methanesulfonate, 5 mM tetraethylammonium (TEA)-Cl, 10 mM HEPES, 3 mM NaCl, 10 mM BAPTA, 2 mM QX-314-Cl, 2 mM ATP-$Mg^{2+}$, 0.3 mM GTP-$Na^{+}$, and 0.10% Lucifer yellow, titrated to pH 7.3]. All chemicals were purchased from Sigma (St. Louis, MO)

except for BAPTA (Invitrogen, Carlsbad, CA), strychnine (Fisher Scientific, Pittsburgh, PA), and the glutamate-receptor drugs (CNQX, D-AP-5, and L-AP-4; Tocris Bioscience, Bristol, UK).

Membrane current was amplified, continuously sampled at 10 kHz, and stored on a computer using a MultiClamp 700A amplifier, Digidata 1322A analog-to-digital board, and pClamp 9 software (Molecular Devices, Sunnyvale, CA). Junction potential (–9 mV) was corrected in all cases. We wrote programs in Matlab (version 7; MathWorks, Natick, MA) to analyze light responses. We corrected for an error in the holding potential introduced by the series resistance. The corrected holding potential ($V_h$) was determined by the formula $V_h = V_{h\_uncorr} – (I_{leak} \times R_S \times (1 – R_{S\_correct}))$, where $V_{h\_uncorr}$ is the apparent (uncorrected) holding potential before the stimulus (in millivolts), $I_{leak}$ is the leak current (in nanoamperes), $R_S$ is the series resistance (mean ± SD, 18 ± 6 MΩ; $n$ = 109 cells), and $R_{S\_correct}$ is the series resistance compensation (typically 0.4). $R_S$ was stable over the recording period (15–57 min). Across cells, $R_S$ increased from 16 ± 4 to 21 ± 8 MΩ (mean ± SD) between the first and last recording used in the analysis ($n$ = 109). We generally excluded cells from the analysis with $R_S$ > 35 MΩ.

Results are from 109 cells: 18 ON cells and 91 OFF cells. The zero-current potential, at which no current was required to clamp voltage, was –43.1 ± 0.9 mV for ON cells (mean ± SEM; $n$ = 11) or –65.3 ± 0.4 mV for OFF cells (n = 38). The zero-current potential for a cell was determined from the $x$-intercept of the current–voltage ($I$–$V$) plot for the leak current. Below we refer to the zero-current

potential as the resting potential ($V_{rest}$), although this potential is determined partly by the composition of the pipette solution. For example, with sharp microelectrodes the resting potential of ON cells was approximately –59 mV (Zaghloul et al., 2003), whereas with the present pipette solution the zero-current potential for ON cells was more depolarized by ~16 mV; this was probably caused in part by the potassium channel blockers in the pipette solution.

## Visual stimuli

The stimulus was displayed on a miniature monochrome computer monitor (Lucivid MR1–103; MicroBrightField, Colchester, VT) projected through the top port of the microscope through a 4x objective and focused on the photoreceptors (resolution, 640 x 480 pixels; 60 Hz vertical refresh). The relationship between gun voltage and monitor intensity was linearized in software with a lookup table. Stimuli were programmed in Matlab as described previously (Brainard, 1997; Demb et al., 1999; Pelli, 1997). All stimuli were centered on the cell body.

Cells were recorded in the superior retina, in which the cone distribution is ~95% M-cones and ~5% S-cones (Rohlich, van Veen, & Szel, 1994; Yin et al., 2006). During recording, the cell was exposed to stimuli that fluctuated around a constant mean luminance. Light level is described as the isomerization rate per photopigment molecule (Rhodopsin, M-cone opsin, and S-cone opsin) $s^{-1}$: $P_R$*, $P_M$*, and $P_S$*. Photoisomerization rates were calculated based on the spectral output of the monitor, the intensity of the monitor ($W/mm^{-2}$) at the plane of the retina, and the photoreceptor properties described by Yin et al. (2006). The

typical mean luminance evoked ~$10^4$ $P_R$*, ~5 x $10^3$ $P_M$*, and ~5 x $10^2$ $P_S$*. Under these conditions, M-cones and rods contribute approximately equally to the light response, whereas S-cones contribute minimally (Yin et al., 2006). At this light level, rod contributions presumably arise through their gap junctions with cones (Bloomfield & Dacheux, 2001). In some cases, we decreased the light level by 10-, 100-, or 1000-fold. At the two dimmest light levels (~5 x $10^1$ or ~5 x $10^0$ $P_M$*; ~$10^2$ or ~$10^1$ $P_R$*), responses are driven by rods (Yin et al., 2006).

The main protocol consisted of a spot (0.6 mm diameter) presented for 200 ms alternating with 800 ms at mean luminance (i.e., 1 Hz presentation rate). Spot contrast was an increment (for ON cells) or decrement (for OFF cells) of 2.5, 5, 10, or 80% of the mean luminance. In most conditions, responses were averaged over 12 repeats at 2.5 and 5% contrast and over six repeats at 10 and 80% contrast. In the presence of CNQX, D-AP-5, and either strychnine or bicuculline, there were typically oscillations in the response, uncorrelated with the light stimulus, that were not blocked by further adding the nicotinic acetylcholine receptor antagonist D-tubocurarine (100 μM; n = 2 cells); thus, the oscillations apparently arose from residual glutamate responses or from inhibition. Under these conditions, 10% contrast spot responses were averaged over 300 repeats. These were compared with responses averaged over 100 repeats in the other conditions.

**Analysis**

We measured the inward current to a flash by averaging over 80 ms centered on the maximal response. Data are reported as mean ± SEM. Statistical

significance was determined using a paired *t* test unless otherwise indicated. Current responses to contrast flashes (see Figure 3.4B) were fit with the following equation (least-squares fit):

$$R(c) = R_{max} \frac{c^n}{c_{50}^n + c^n}$$

where $R(c)$ is the response at a given contrast level, $c$ is stimulus contrast, $R_{max}$ is an asymptotic scale factor, $n$ is the steepest slope of the contrast–response function, and $c_{50}$ is the contrast gain (contrast that evokes the half-maximal current response) (Albrecht & Hamilton, 1982).

For the conductance analysis, we analyzed the I–V plot for responses evoked at multiple holding potentials. The current responses at each contrast were fit with a line, and these data were then used to determine the excitatory and inhibitory conductances ($g_{excitation}$ and $g_{inhibition}$, respectively) according to the following equations (Borg-Graham, 2001; Taylor & Vaney, 2002):

$$g_{excitation} = \frac{g_{total}(E_{total} - E_{inhibition})}{E_{excitation} - E_{inhibition}},$$

$$g_{inhibition} = \frac{g_{total}(E_{total} - E_{excitation})}{E_{inhibition} - E_{excitation}},$$

where $E_{total}$ is the reversal potential of the light-evoked response (*x*-intercept of the linear fit), $g_{total}$ is the total conductance (slope of the linear fit), and $E_{excitation}$ and $E_{inhibition}$ are the excitatory and inhibitory reversal potentials, respectively.

The reversal potential for inhibitory synapses ($E_{inhibition}$; i.e., $Cl^-$ reversal) was calculated as –67 mV. To test this calculation, we blocked synaptic transmission with $CoCl_2$ (3 or 6 μM) and measured the reversal potential of the conductance evoked by adding the $GABA_A$ agonist muscimol (10 or 100 μM; Tocris Bioscience) to the bath. Before and after adding muscimol, we measured currents after stepping to several holding potentials around $V_{rest}$; the muscimol-evoked conductance was measured by subtracting the two sets of current measurements. In some cases, TEA-Cl (10 mM) was added to the bath solution to block $K^+$ channels. Adding $CoCl_2$ and TEA-Cl to the Ames medium increased osmolarity by up to ~10% and shifted $E_{Cl}$ slightly negative to that calculated for Ames medium alone. However, the reversal potential of the muscimol-evoked conductance was –2 ± 2 mV from the calculated $E_{Cl}$ ($n$ = 5 OFF cells, 1 ON cell), suggesting that the calculated $E_{Cl}$ is appropriate for the conductance analysis used in this study.

The conductance analysis also assumed that the I–V plots could be well fit by a straight line. At high contrast, however, many OFF cells showed a J-shaped *I–V* curve, suggesting the contribution of an NMDA conductance. For these responses, we analyzed conductance in the subset of cells in which there were at least three current measurements with $V_{hold}$ positive to –40 mV, in which the nonlinearity associated with NMDA conductances would have minimal effect.

### Interpretation of I–V plots for light-evoked responses

To measure synaptic conductance, ganglion cell responses were measured at a series of holding potentials ($V_{hold}$ values). Leak-subtracted response amplitude was plotted versus $V_{hold}$ in an *I–V* plot, in which the slope indicates the total conductance evoked by the spot and the *x*-intercept indicates the associated reversal potential. In this case, the conductance and reversal potential for the spot response are likely to reflect not a single neurotransmitter conductance but rather the sum of two or more conductances in parallel. For example, if the response were mediated by a glutamate synapse in parallel with a "feedforward" inhibitory synapse (GABA or glycine), there would be an increase in two conductances (and a positive slope on the I–V plot) with a reversal potential between the reversals for the excitatory cation channels (0 mV) and the inhibitory receptor channels (–67 mV; see above). Thus, a reversal between 0 and –67 mV is consistent with an increase in two conductances. If the response is instead mediated by a glutamate synapse in parallel with the withdrawal of an inhibitory synapse, there would be an increase in an excitatory conductance plus a decrease in an inhibitory conductance (disinhibition). The sum of these two influences would generate one of three possible patterns. First, if the magnitude of the excitation is greater than the magnitude of the disinhibition, the summed conductance would be positive and the reversal potential would be >0 mV. Second, if the magnitudes of the excitation and disinhibition are equal, the summed conductance would have a slope of zero with no reversal. Third, if the magnitude of the excitation is less than the magnitude of the disinhibition, the summed conductance would be negative with a reversal less than –67 mV.

## Cell labeling and tissue fixation

In a subset of cells from this study (*n* = 9), we analyzed dendritic morphology and stratification. These cells were combined with others recorded in related studies from our laboratory (*n* = 33). During whole-cell recording, Lucifer yellow in the pipette solution filled the dendritic tree of the cell. After recording, the tissue was fixed for 1 h in 4% paraformaldehyde (Electron Microscopy Sciences, Hatfield, PA) in 0.1 M PBS (Sigma) at room temperature and then stored in 0.1 M PBS at 2–8°C.

## Immunocytochemistry

A purpose of filling ganglion cells was to determine their dendritic stratification in the inner plexiform layer (IPL) (Figure 3.1). The tissue was thus reacted with an antibody against Lucifer yellow to amplify the fluorescence in the dendritic tree. The retina was further stained with a nuclear dye to label cell bodies in the ganglion cell layer (GCL) and inner nuclear layer (INL); these cell layers define the boundaries of the IPL. Two IPL strata, corresponding to the dendrites of ON and OFF cholinergic (starburst) amacrine cells, were also labeled with an antibody against choline acetyltransferase (ChAT) to mark standard positions in the IPL (Yamada, Bordt, & Marshak, 2005; J. Zhang et al., 2005).

The fixed tissue was incubated for 1 h in 6% normal donkey serum (NDS) (Jackson ImmunoResearch, West Grove, PA) and 1% Triton X-100 (Sigma) in

0.05 M Tris-buffered saline (TBS) (Sigma) to permeabilize the tissue and block nonspecific immunolabeling. The tissue was rinsed for 5 min in 0.05 M TBS and then incubated overnight at 4°C in blocking buffer (2% NDS, 0.2% Triton X-100 in 0.05 M TBS) plus goat anti-ChAT antibody (1:200 dilution; Millipore Bioscience Research Reagents, Temecula, CA) and rabbit anti-Lucifer yellow antibody (1:2000 dilution; Invitrogen). Next, the tissue was rinsed for 30 min in 0.05 M TBS and then incubated for 45 min in secondary antibody: donkey anti-goat bound to cyanine 3 (Cy3) (1:200 dilution; Jackson ImmunoResearch) and donkey anti-rabbit bound to FITC (1:400 dilution; Jackson ImmunoResearch) in blocking buffer. The tissue was rinsed for 30 min in 0.05 M TBS and incubated for 30 min in 0.2% ToPro-3 iodide (Invitrogen) in 0.1 M PBS. The tissue was rinsed for 30 min (0.1 M PBS) and subsequently mounted with Vectashield (Vector Laboratories, Burlingame, CA) and coverslipped. Glass spacers, made from coverslips (0.13–0.17 mm thick; Fisherbrand; Fisher Scientific, Hampton, NH), were inserted between the coverslip and slide, on opposite sides of the tissue, to prevent tissue compression.

### Confocal microscopy

The retina was imaged with an Olympus FluoView 300 confocal microscope, and images were captured with FluoView software (Olympus). The dendritic field of a filled ganglion cell was captured with a through focal series (*z*-stack) at 2 μm intervals with a 40x oil objective [numerical aperture (NA) 1.3] and projected onto a single plane. The dendritic field was larger than the field of view,

and so multiple projection images were assembled in Photoshop (Adobe Systems, San Jose, CA). In addition, one or two *z*-stacks were taken using a 60x oil objective (NA 1.4) at 0.5 µm intervals starting at the inner (vitreal) side of the GCL and ending within the middle of the INL. These *z*-stacks were used to determine dendrite position within the IPL.

### Morphological analysis

A ganglion cell dendritic field diameter was measured by outlining the dendritic tree using Adobe Photoshop and software written in Matlab. We report dendritic tree diameter as the diameter of a circle with area equivalent to the polygon.

Confocal *z*-stacks were analyzed with programs written in Matlab. FluoView software generated a *z*-stack for each fluorescent signal, the dimensions of which were 512 x 512 pixels (236 x 236 µm) in the *x*–*y* image plane and typically comprised 120–160 slices (60–80 µm) in the *z* dimension. The *z*-stacks were loaded into Matlab, and a projection of each fluorescent signal was displayed by averaging the stacks across the *z*-dimension for FITC (ganglion cell morphology) and Cy3 signals (ChAT labeling). We used custom Matlab programs to measure these signals, but other commercial software could be used instead (Yamada et al., 2005). For display purposes, the "levels" were adjusted in Adobe Photoshop to reduce noise; quantitative analysis, however, is based on raw data.

When inspecting the *z*-stacks, it was evident that the tissue was often warped. However, by analyzing a smaller area in the *x*–*y* dimension (100 x 100 pixels; 46 x 46 μm), the effect of this distortion was minimized (Figure 3.2A). The user selected three to nine such small areas for analysis, and measurements were averaged over the analyses from these individual areas. Areas were selected over distal regions of the ganglion cell dendritic tree at which point the dendrites were well stratified. Within each region, the slices of interest were identified as follows. To identify slices centered on ChAT bands and ganglion cell dendrites, the fluorescent signals were plotted as a function of slice number (Figure 3.2*A*), and the user selected the approximate peaks of the Cy3 fluorescence (ChAT bands) and the FITC fluorescence (ganglion cell dendrite). To identify slices at the IPL borders, the user viewed a *z*-stack of the Cy5 fluorescences (ToPro-3-labeled nuclei) and selected the slice near the middle of the GCL and the slice at the IPL/INL border.

Additional analysis localized the IPL/INL boundary more precisely. The user selected the *x*–*y* position of the central point of multiple cell bodies within the slice containing the initial cells on the vitreal (inner) side of the INL (Figure 3.2*B*). These central points included the nucleolus of a cell, which was typically the brightest region in the image. At each of these points, a 3 x 3 pixel (1.4 x 1.4 μm) region of interest ("boxed regions") was used to compute fluorescent ToPro-3 signal as a function of slice number. These boxed regions encompassed an intense area of fluorescence in the most proximal (vitreal) layer of cells (by design) but only occasionally contained such a signal (by chance) in more distal

cell bodies. Thus, by summing the fluorescence across boxed regions, a sharp peak in fluorescence was generated at the first layer of cell bodies in the INL, i.e., those at the IPL/INL border (Figure 3.2*A*, dashed black line).

The peak of each fluorescent signal was used to determine the percentage depths of dendrites within the IPL. Third-order polynomials were fitted (using standard fitting routines in Matlab) around the estimated fluorescent peaks associated with the GCL, ChAT bands, ganglion cell dendrites, and INL (Figure 3.2*A*). Fits were made to six to eight points (3–4 μm) around the peak. The peak of the fitted line was used to define a given cellular or dendritic layer. The IPL width was calculated as the distance between the GCL and the INL peaks. Given the IPL width and GCL and INL positions, the positions of the ChAT bands and ganglion cell dendrites were expressed as a percentage depth through the IPL from 0% at the GCL/IPL border to 100% at the IPL/INL border. The IPL thickness was 38 ± 4 μm (mean ± SD; $n$ = 42). Measured positions of ChAT bands showed variability (SD) across tissues of ~3% (see Results), which corresponds to ~1.2 μm.

**Acknowledgements**

This work was supported by National Institutes of Health Grants T32-EY13934, EY14454, and EY07003 (Core Grant). J.B.D. is the recipient of a Research to Prevent Blindness Career Development Award and an Alfred P. Sloan Research Fellowship. We thank Drs. Daniel Green, Gabe Murphy, Fred

Rieke, Josh Singer, and Peter Sterling for comments and suggestions on this manuscript.

## Chapter 4

## Multiple roles for NMDA receptors in early visual processing


### Summary

AMPA- and NMDA-type glutamate receptors play unique and well-studied roles in brain areas involved with learning and memory, but their roles in sensory processing remain poorly understood. Here, we investigated how AMPA and NMDA receptors contribute to visual processing in mammalian retinal ganglion cells under physiological conditions, *in vitro*. NMDA-mediated responses were present in multiple ganglion cell types but absent in one type, the ON Alpha cell. OFF Alpha and Delta cells used NMDA receptors for encoding different contrast ranges: the full range (Alpha), including near-threshold responses, versus a high range (Delta). The Delta cell expressed the NR2B subunit, consistent with an extra-synaptic NMDA receptor location that is stimulated by glutamate spillover during high contrast. The contrast-independent role for NMDA receptors in OFF Alpha cells correlated with two circuit properties: high contrast sensitivity and low presynaptic basal glutamate release.


### Introduction

Excitatory synaptic transmission in the CNS is mediated primarily by glutamate neurotransmission. Glutamate is released from a presynaptic axon

terminal onto receptors on a postsynaptic dendrite. Postsynaptic ionotropic glutamate receptors (iGluRs) can be divided primarily into two classes, AMPA and NMDA, which differ on a number of fundamental properties (for review, see (Dingledine et al., 1999; Erreger et al., 2004)). For example, AMPA receptors have fast kinetics (deactivation time of <3 ms), whereas NMDA receptors have slower kinetics (deactivation time of >30 ms). Most types of AMPA receptor (i.e., depending on subunit composition) have low $Ca^{2+}$ permeability, whereas NMDA receptors have high permeability. Finally, the AMPA receptor mediates a voltage-independent cation conductance (over the physiological range), whereas the NMDA receptor mediates a voltage-dependent conductance that is blocked near the resting potential ($V_{rest}$) by extracellular $Mg^{2+}$.

AMPA and NMDA receptors are typically expressed by the same neuron where they play complementary roles in information processing. For example, a hippocampal neuron's AMPA and NMDA receptors together establish long-term changes in synaptic function. Glutamate release evokes AMPA receptor-mediated depolarization which, following relief of $Mg^{2+}$ block, allows $Ca^{2+}$ to flow through NMDA receptors and mediate long-term changes in synaptic efficacy (Malenka & Bear, 2004). AMPA and NMDA receptors are also expressed in sensory neurons (Kwon, Nelson, Toth, & Sur, 1992; Myme, Sugino, Turrigiano, & Nelson, 2003; Nelson & Sur, 1992). However, long-term changes in synaptic efficacy are not desirable in sensory circuits suggesting that NMDA receptors play some other role in information processing.

To investigate the roles of AMPA and NMDA receptors in sensory processing, we studied retinal ganglion cells, the output neurons of the retina. There are ~15 discrete types of ganglion cell that each collect inputs selectively from a subset of glutamatergic bipolar cells and other inhibitory and excitatory interneurons (amacrine cells) (Field & Chichilnisky, 2007; Masland, 2001; Wassle, 2004). We studied here the role of NMDA receptors in visual processing by combining whole-cell recording of identified ganglion cell types in an intact mammalian retina under physiological conditions with synaptic inhibition intact. We developed a method to describe light-evoked conductances as the weighted sum of the underlying ligand-gated receptor conductances in order to characterize the NMDA receptor contribution to natural sensory stimulation.

Many types of ganglion cell express NMDA receptors (E. D. Cohen, 2000; E. D. Cohen & Miller, 1994; Diamond & Copenhagen, 1993; Kalbaugh, Zhang, & Diamond, 2009; Manookin et al., 2008; Massey & Miller, 1990; Miller, 2008; Mittman, Taylor, & Copenhagen, 1990; Sagdullaev et al., 2006; J. Zhang & Diamond, 2009). However, we report here that at least one type lacks the NMDA receptor; this lack of expression correlated with a high rate of presynaptic glutamate release. In two other cell types, NMDA receptors were used to encode either the full range of visual contrast or only the high end of this range. This difference in contrast coding corresponded to a difference in NR2B subunit expression and a difference in contrast sensitivity in the firing rate. Thus, NMDA receptors play multiple functional roles in the retina, and the expression of the

receptor and specific subunits varies with specialized properties of the presynaptic circuitry.

## Results

We measured responses to visual stimuli and NMDA application in a whole-mount preparation of the intact, *in vitro* guinea pig retina (see Experimental Procedures). Ganglion cells (n = 197) were recorded with patch electrodes (~3-5 MΩ). Targeting large cell bodies led to recordings of three ganglion cell types: ON Alpha, OFF Alpha and OFF Delta. These types differ in their light-evoked conductance and in their dendritic tree stratification, as described previously (Manookin et al., 2008). Input resistance was 19±5 MΩ (mean±SD) (ON Alpha; n = 11), 26 ± 6 MΩ (OFF Alpha; n = 68) and 37±11 MΩ (OFF Delta; n = 29); series resistance across all recordings was 15±4 MΩ (n = 171; compensated typically by 40%; see Experimental Procedures). We also recorded from a few other types of ganglion cell with smaller cell bodies. In most cases, the morphology of these cells was analyzed as described previously to characterize dendritic tree stratification and diameter (Manookin et al., 2008). Results below are reported as mean±SEM.

### NMDA receptor-mediated conductance is present in multiple ganglion cell types but not in the ON Alpha cell

We tested for the presence of NMDA receptors by recording the response to NMDA puffed directly onto ganglion cells. The first goal was to test whether NMDA receptors were expressed by the three major cell types studied here. The

second goal was to characterize the NMDA receptor current-voltage (I-V) relationship in intact cells so that we could later determine how these channels contributed to visual responses using a fitting procedure described below.

Following an initial characterization of cell type, based on extracellular and/or whole-cell light-evoked responses (see Experimental Procedures), we recorded the NMDA puff response with synaptic transmission blocked or strongly attenuated. To block synaptic transmission, we bath-applied the $Ca^{2+}$ channel blocker $Co^{2+}$ (6 mM) along with the NMDA receptor co-agonist glycine (6 mM) (Miller, 2008). In another case, we made an extracellular ringer that included $Cd^{2+}$ (1 mM) plus the co-agonists D-serine (200 μM) and glycine (6 mM; see Experimental Procedures) (Gustafson, Stevens, Wolosker, & Miller, 2007; Kalbaugh et al., 2009). In a third case, we applied the L-type $Ca^{2+}$ channel blocker isradipine (30 uM) plus D-serine (200 μM), glycine (6 mM) and antagonists to glycine receptors (strychnine, 2 μM), $GABA_A$ receptors (bicuculline, 100 μM) and AMPA/kainate receptors (DNQX, 50 μM). In all three conditions, we tested for the presence of NMDA responses. However, the quantitative analysis of NMDA responses was based on the third condition (isradipine plus receptor antagonists) because $Co^{2+}$ and $Cd^{2+}$ attenuate the NMDA response and $Co^{2+}$ does so in a voltage-dependent manner (Ascher & Nowak, 1988).

NMDA always evoked a response (i.e., current at $V_{hold}$ = -40 ± 5 mV) in OFF Alpha cells (-256 ± 30 pA; n = 29) and OFF Delta cells (-121 ± 15 pA; n= 14), and the I-V relationship showed the characteristic voltage-dependent 'J-

shaped' conductance (Mayer, Westbrook, & Guthrie, 1984; Nowak, Bregestovski, Ascher, Herbet, & Prochiantz, 1984) (Figure 4.1A, B). However, the ON Alpha cell showed no response to NMDA (-0.06 ± 1.9 pA; n = 6) (Figure 4.1C). In separate recordings, we confirmed that ON Alpha cells responded to puffs of glycine or the $GABA_A$ agonist muscimol (data not shown), and thus it was possible to elicit puff-evoked agonist responses from these cells. We conclude that ON Alpha cells do not express NMDA receptors.

Previous work suggested that virtually all ganglion cells, including various ON cell types, express NMDA receptors (Sagdullaev et al., 2006; J. Zhang & Diamond, 2009), and so we tested further the presence of these receptors in other types of ON or ON-OFF cells. In a sample of 10 cells with small cell bodies (10-20 μm diameter), every cell showed an NMDA-mediated response with the characteristic J-shaped conductance (-154 ± 49 pA at $V_{hold}$ = -40 ± 5 mV). Data from one example cell (an ON direction-selective cell; (Manookin et al., 2008)) are shown in Figure 4.1D. While we have not tested exhaustively for the presence of NMDA receptors in all ~15 ganglion cell types, the collected results suggest multiple types express NMDA receptors but that at least one type does not.

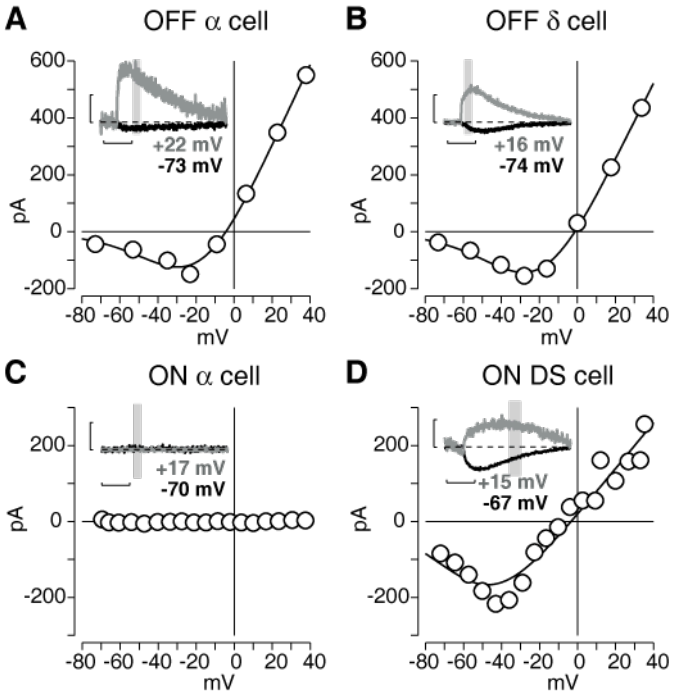


**Figure 4.1. Most ganglion cell types express NMDA receptors.** Puff-evoked application of NMDA generated a response in OFF Alpha (A), OFF Delta (B) and an ON direction-selective (DS) cell (D) but not in an ON Alpha cell (C). Insets show responses at two $V_{holds}$ (horizontal scale, 2 sec; vertical scale, 200 pA). Here and below $V_{holds}$ of the traces are indicated within the figure. Gray bar indicates sampling area.

## Population analysis generates robust ligand-gated receptor basis functions for evaluating light-evoked conductances

A major goal of this work is to describe light-evoked responses as the weighted sum of the underlying ligand-gated receptor conductances. This method was applied previously but only in cases where the total conductance was relatively linear and hence a major NMDA-component was not evident (Murphy & Rieke, 2006; Roska & Werblin, 2001; Taylor & Vaney, 2002; van Wyk, Taylor, & Vaney, 2006). The ganglion cell AMPA receptor conductance is approximately linear and reverses at ~0 mV (Beaudoin, Manookin, & Demb, 2008). Below, we established similar conductance 'basis functions' for the other

major receptor classes: the inhibitory (GABA/glycine) receptors and the NMDA receptor.

To measure the inhibitory receptor basis function, we blocked synaptic transmission with $Co^{2+}$ (6 mM) and puffed glycine (200 μM) or muscimol (1 mM). These agonists evoked large outward currents as the membrane was stepped positive to $E_{Cl}$ (-67 mV) (Figure 4.2A). However, upon return to the original $V_{hold}$, there was typically both an inward leak current and an inward agonist-evoked current (i.e., reversed in sign from the original response) (Figure 4.2B). These results suggest a substantial change in the intracellular $Cl^-$ concentration during the $V_{holds}$ positive to $E_{Cl}$. We thus took a second approach to measure the inhibitory receptor basis function.

We recorded the response to a brief negative contrast flash in an OFF cell in the presence of the NMDA receptor antagonist D-AP5 (100 μM). Thus, the response was driven by a combination of AMPA and GABA/glycine receptors. Following the excitatory response to the flash, there was a 'rebound' response that comprised an inhibitory current plus the suppression of a basal excitatory current (i.e., an active resting AMPA conductance that was suppressed during the rebound); the sum of these two conductances results in a reversal potential negative to $E_{Cl}$. With this protocol, responses at the beginning and upon the return to the original $V_{hold}$ were relatively stable (Figure 4.2C). We therefore used these measurements to characterize the inhibitory receptor basis function. To do so, we subtracted from the rebound response a negative AMPA conductance and derived a GABA/glycine-mediated conductance (Figure 4.2D).

We performed a population analysis on the normalized inhibitory receptor conductance. The conductance at each $V_{hold}$ was determined by dividing the current amplitude by the driving force on chloride; measurements at $V_{hold}$'s within 10 mV of $E_{Cl}$ were excluded, as these produced spurious results. The conductance-voltage (g-V) relationship was fit with an exponential function (see Experimental Procedures; Figure 4.2E). The resulting fit was converted back to currents to generate the population I-V basis function for inhibitory receptors (Figure 4.2F). The same procedure was used to generate the I-V basis function for inhibitory receptors of OFF Delta cells (Figure 4.2G).

A similar procedure was used to generate the NMDA receptor basis function. The puff-evoked NMDA responses described above (isradipine + receptor antagonists condition) generated I-V plots that typically reversed negative to 0 mV (OFF Alpha: -8.9 ± 1.9 mV, n = 14 cells; OFF Delta: -7.9 ± 1.5 mV, n = 14 cells). We assumed that the negative reversal was due to an unblocked feed-forward inhibition onto the cells. [The reversal potential in the $Co^{2+}$ or $Cd^{2+}$ conditions, where synaptic transmission was blocked more completely, reversed closer to zero, at -5.3 ± 1.3 mV (n = 7 cells) and -1.2 ± 1.3 mV (n = 8 cells), respectively.] We thus subtracted the inhibitory receptor basis function described above to generate the NMDA response in each cell (Figure 4.2H). These were converted to conductance as described above and the population was fit (see Experimental Procedures; Figure 4.2I). Conductance was converted back to current to generate the population I-V basis functions for the NMDA response of both OFF Alpha and Delta cells (Figure 4.2J, K).

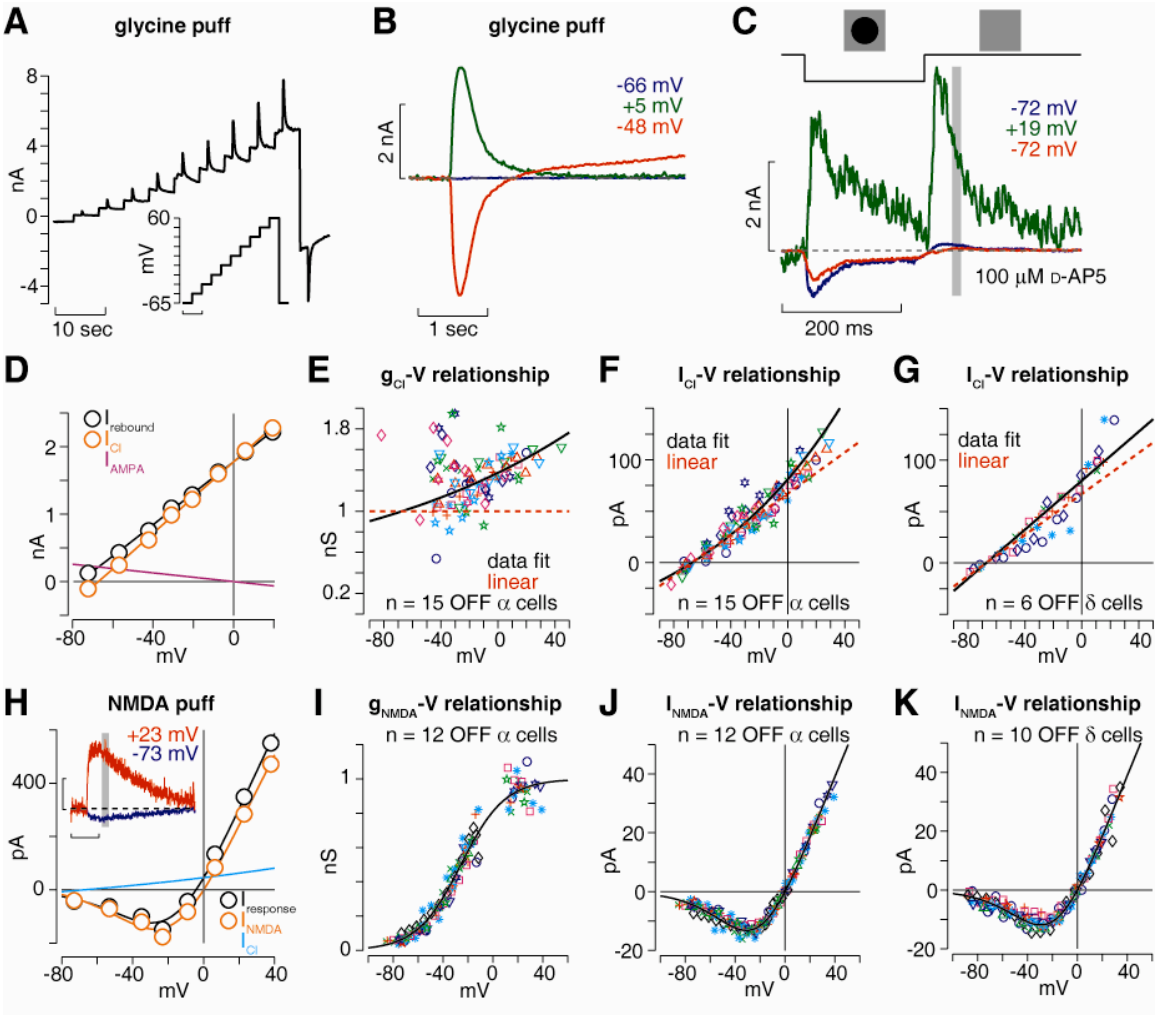


**Figure 4.2. Generating robust basis functions for ligand-gated conductances.**

**A**, An OFF Alpha cell was stimulated with a glycine puff at several $V_{holds}$. Command voltages (inset) ranged from -65 to +60 mV (horizontal scale, 10 sec).

**B**, Leak-subtracted traces from A at three $V_{holds}$. The blue and red traces were recorded at identical command voltages at the beginning (blue) and end (red) of the voltage steps. The difference in actual $V_{hold}$ reflects the correction for the series resistance (see Experimental Procedures).

**C**, An OFF Alpha cell was stimulated with a 100%-contrast dark flash with NMDA receptors blocked (D-AP5, 100 µM). The response was measured 50 ms after the peak rebound current (window size, 20 ms).

**D**, Current-voltage plot of the responses in **C**. A putative negative conductance was subtracted (magenta) to force the chloride current through the calculated $E_{Cl}$.

**E**, The conductance was calculated as a function of $V_{hold}$ for 15 OFF Alpha cells. Each symbol represents the conductance of a cell.

**F**, The current-voltage relationship for the same cells generally showed mild rectification that deviated from a linear conductance. A function was fit to the data and was used as the GABA/glycine basis function (black solid line).
**G**, Same format at F. for OFF Delta cells (n = 6).
**H**, NMDA was puffed onto an OFF Alpha cell at several $V_{holds}$. The puff evoked an NMDA conductance (black). A putative inhibitory conductance (green) was subtracted to force the NMDA current through $E_{cation}$ (orange).
**I**, The conductance-voltage relationship was calculated from the puffing data and normalized to a 1-nS peak conductance. The responses were fitted with a function (black line).
**J**, The current-voltage relationship in the same cells (n = 12 OFF alpha cells). The fitted line (black) was calculated using the function in **I**.
**K**, Same as J. for OFF Delta cells.

## Light-evoked responses can be modeled with three ligand-gated receptor basis functions under physiological conditions

To characterize the role of NMDA receptors in light-evoked responses, we fit I-V plots with the weighted sum of three ligand-gated receptor basis functions (Figure 4.3C). A cell was presented with a 200-ms decrement from the mean luminance (contrast, -50%; spot diameter, 0.2 mm; Figure 4.3$A_1$). The I-V relationship for the excitatory portion of the response showed a J-shaped conductance (Figure 4.3$B_1$), which was well fit by the weighted sum of the three basis functions (Figure 4.3C). We tested the validity of the fit by recording the same response with NMDA receptors blocked (D-AP5, 100 μM) (Figure 4.3A2). Under this condition, the I-V relationship became more linear (Figure 4.3B2), and consequently the fitted NMDA component declined (Figure 4.3D). The drug no doubt had effects throughout the retinal network, and so it is not surprising that the AMPA and GABA/glycine components changed somewhat as well.

We performed additional validation experiments, using D-AP5, across multiple cells and contrast conditions (Figure 4.3E, F). In both OFF Alpha and Delta cells, and across three contrasts, D-AP5 suppressed the NMDA component with good selectivity. NMDA receptors contributed to OFF Alpha cell responses at each contrast (Figure $4.3E_1$), and the NMDA-receptor component was suppressed by D-AP5 (Figure $4.3E_2$; 25%, control: 2.8 ±0.7 nS, D-AP5: -0.1 ± 0.3 nS; 50%, control: 3.8 ± 1.0 nS, D-AP5: -0.3 ± 0.2 nS; 100%, control: 4.4 ± 1.3 nS, D-AP5: -0.5 ± 0.3 nS; $p < 0.005$ in all cases, paired *t*-test; n =10 cells). OFF Delta cells displayed a negligible NMDA-receptor conductance to the -25% contrast flash (conductance, 0.14 ± 0.24 nS; $p > 0.3$; n = 5 cells; Figure $4.3F_1$). However, an NMDA-receptor component was observed at the two highest contrasts, and this conductance was suppressed in the presence of D-AP5 (-50%, control: 0.8 ± 0.4 nS, D-AP5: 0.2 ± 0.4 nS; -100%, control: 1.8 ± 0.3 nS, D-AP5: 0.2 ± 0.3 nS; $p < 0.05$ for both contrasts; n = 5 cells; Figure 4.3F). These contrast-dependent conductances are analyzed further below in a larger population of cells. Here and below, the reported NMDA conductance for light responses represents the conductance at -62 mV, near $V_{rest}$ for OFF Alpha and Delta cells; the NMDA conductance increases substantially at more depolarized potentials (Figure 4.2I).

The response to NMDA puffing suggested that ON Alpha cells lack NMDA receptors, and light-evoked responses supported this conclusion. The ON cell's I-V relationship for the excitatory response to positive contrasts was relatively linear (Figure 4.3G), and the fit lacked an NMDA component across several

contrasts (Figure 4.3H). For negative contrasts, ON Alpha cells showed a negative AMPA component, consistent with a high tonic level of AMPA receptor activity that can decrease substantially to negative contrast (Manookin et al., 2008; Murphy & Rieke, 2006; Pang et al., 2003; Trong & Rieke, 2008; Zaghloul et al., 2003). Thus, the lack of an NMDA component in the ON Alpha cell's light response correlated with an apparently high basal rate of glutamate release.

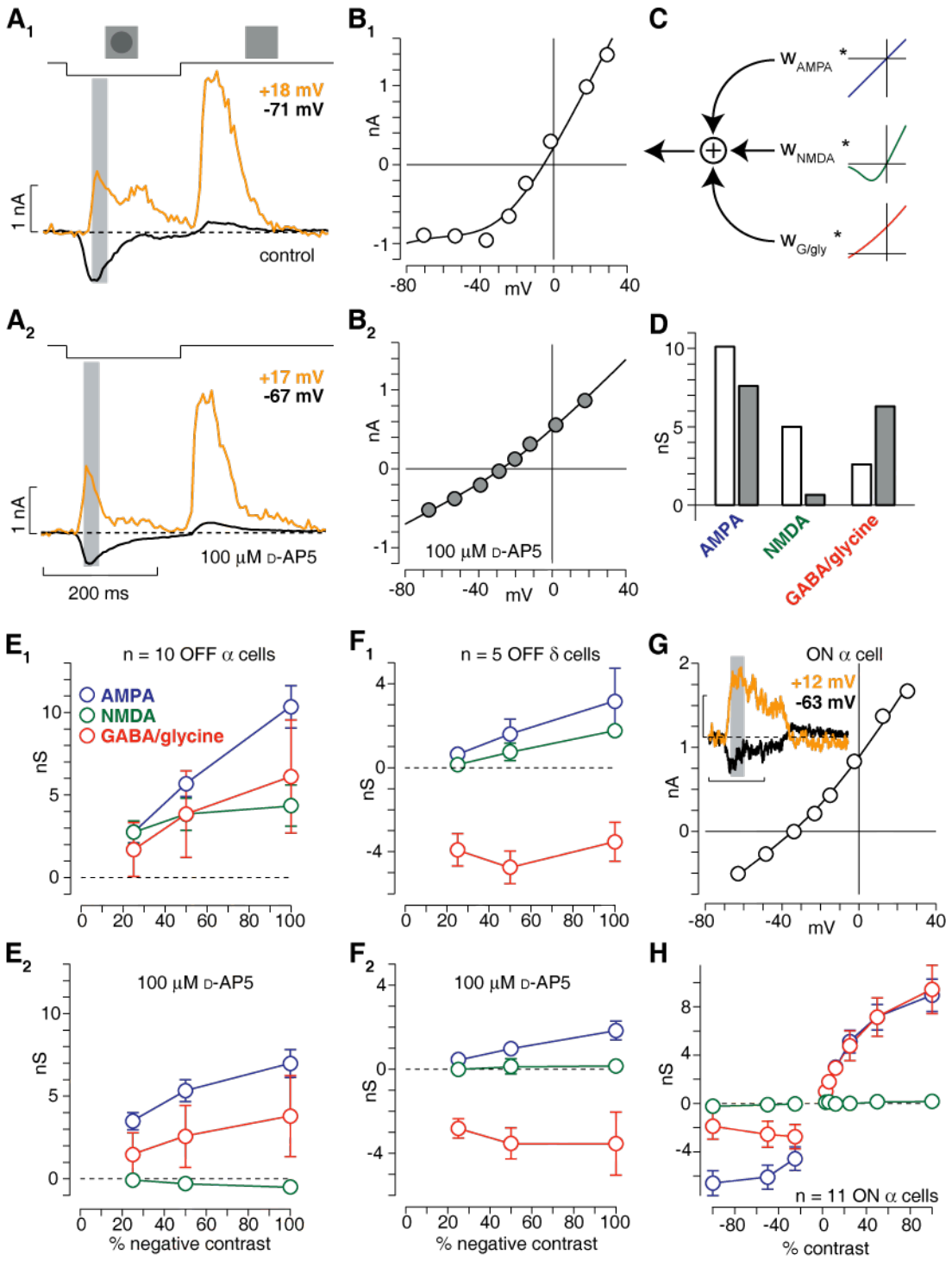


**Figure 4.3**.
**A**, In an OFF Alpha cell, a dark flash (contrast, -50%) evoked large current responses under control conditions (A1) and with NMDA receptors blocked (A2). **B**, Current-voltage plots for the cell in A. The I-V plot was J-shaped under control conditions (B1) but became linear in the presence of the NMDA-receptor antagonist (B2).

**C**, Visual responses were modeled as the sum of three ligand-gated conductances.
**D**, The model estimated the conductances in **B** (control, white bars; D-AP5, gray bars).
**E**, The three ligand-gated conductances as a function of contrast (n = 10 OFF $\alpha$ cells). The NMDA-receptor conductance (green; E1) was suppressed in the presence of D-AP5 (E2).
**F**, Same as E. for OFF Delta cells.
**G**, An ON Alpha cell was presented a bright flash (inset; contrast, +100%; diameter, 0.5 mm; horizontal scale, 200 ms; vertical scale, 1 nA). The I-V plot was relatively linear.
**H**, ON Alpha cell conductance was explained by an AMPA conductance plus feedforward inhibition, with effectively no NMDA component (n = 11 cells).

**NMDA receptors contribute to low-contrast responses in OFF Alpha cells**

Results in Figure 4.3 (parts E1, F1) suggested that OFF Alpha cells but not Delta cells have a prominent NMDA receptor contribution to responses at 25% contrast. We tested further the contrast sensitivity of the NMDA conductance in a larger set of cells and expanded the analysis to a lower contrast range. To achieve good signal-to-noise without evoking excessively large responses (i.e., to prevent errors in $V_{hold}$; see Experimental Procedures), spot diameter was either 0.2 mm (25-100% contrast) or 0.4 mm (3-12% contrast).

At low contrast, OFF Alpha cells showed a J-shaped I-V relationship that reversed positive to 0 mV (Figure 4.4A1). The response could be modeled as a combination of a mixed AMPA/NMDA conductance and the removal of inhibition (or 'disinhibition'; Manookin et al., 2008). The disinhibition was smaller than in previous measurements using a larger spot size (0.6-mm diameter; Manookin et al., 2008). At higher contrast levels, there was again a mixed AMPA/NMDA conductance but the inhibitory conductance became positive (Figure 4.4B1). The

total inhibition onto the OFF Alpha cell comprises a mix of disinhibition, which we previously showed was glycinergic (Manookin et al., 2008), and a feed-forward inhibition, which we show below is GABAergic. The relative weight of these two sources of inhibition depended on the spot size (as well as contrast). Specifically, the feed-forward inhibition became relatively large with small spot stimuli; however, we did not quantify this size-dependence further. The NMDA component persisted at all contrast levels, including the lowest level (contrast, 3%) (Figure 4.4A2). This contrast approximates the threshold for OFF Alpha cells, suggesting that NMDA receptors contribute to minimal levels of excitatory stimulation (Dhingra et al., 2003).

A similar analysis in OFF Delta cells suggested that NMDA receptors do not contribute at ~25% contrast or below (Figure 4.4C2, D2). Rather, the response at lower contrasts combined AMPA and disinhibitory conductances (Figure 4.4C, D). At high contrast, the mix of three conductances resulted in a 'U-shaped' I-V relationship (Figure 4.4D1), whereas at low contrast, there was a relatively linear negative conductance (Figure 4.4C1). We conclude that OFF Alpha and Delta cells use NMDA receptors over different contrast ranges: the full range (Alpha) versus a high range (Delta).

To investigate the time-course of the three conductances, we fitted data over time and averaged across cells (Figure 4.4E-H; see Experimental Procedures). For the OFF Alpha cells at all contrasts, and for the OFF Delta cells at high contrast, the time course of the AMPA and NMDA conductances were similar. Thus, it was not the case that the AMPA and NMDA components

served separate transient versus sustained components of the response, as in salamander ganglion cells (recorded with inhibition blocked) (Diamond & Copenhagen, 1993; Mittman et al., 1990; Taylor, Chen, & Copenhagen, 1995).

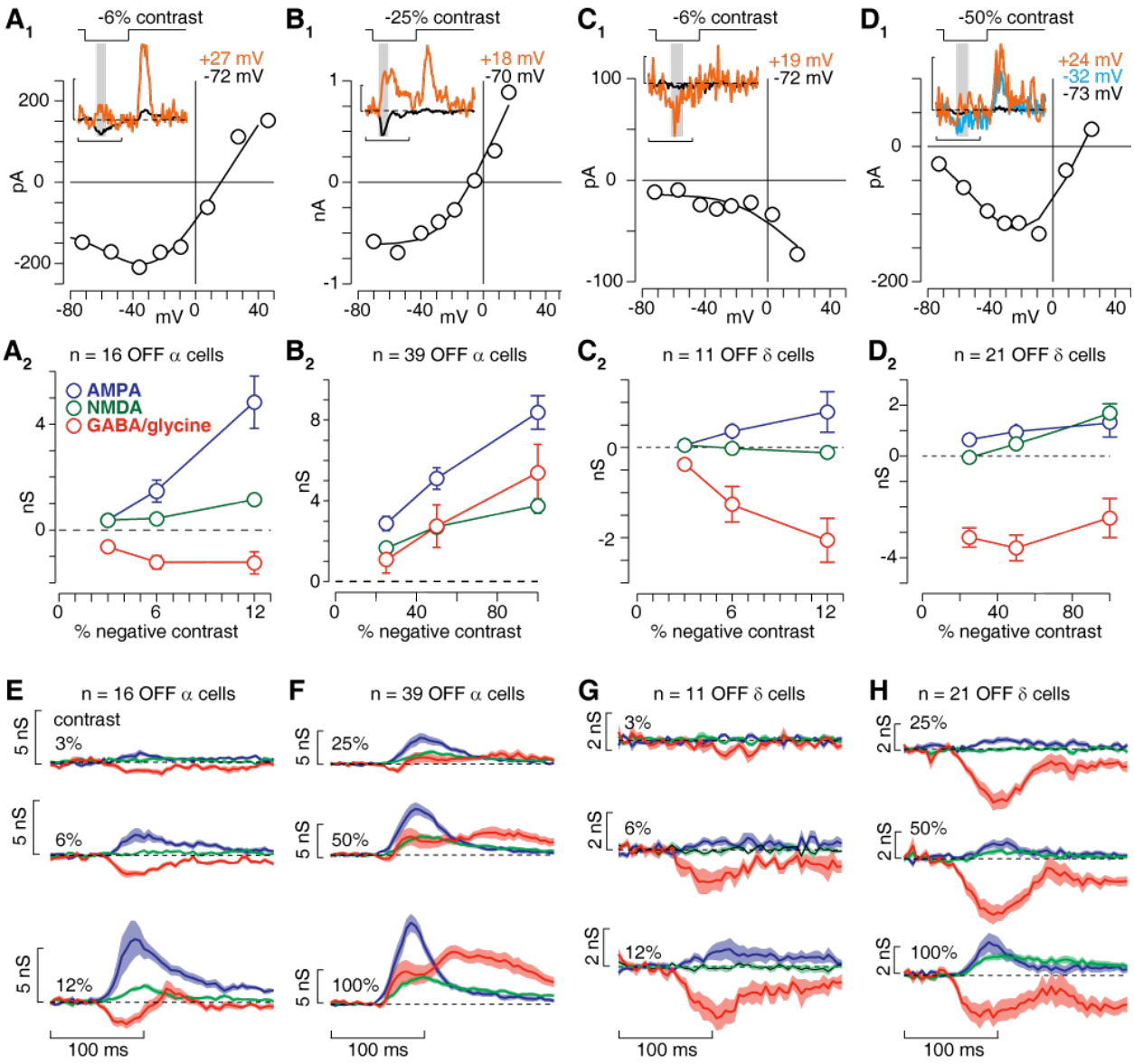


**Figure 4.4. NMDA receptors contribute to different ranges of contrast coding in two OFF ganglion cell types.**

**A1-D1,** Contrast responses at stated $V_{holds}$ and I-V plots for OFF Alpha (A1, B1) and OFF Delta cells (C1, D1). Lines show fitted response based on basis functions. (Insets, horizontal scale: 200ms. Vertical scale: 1 nA for A1 and B1; 100 pA for C1; 500 pA for D1.) Spot size was 0.4-mm dia. for low contrast (A1, C1) and 0.2-mm dia. for high contrast (B1, D1).

**A2-D2**, Fitted conductances as a function of contrast.

**E-H**, Time course of fitted conductances at each contrast for the two cell types.

## NMDA receptors in OFF Alpha cells are driven by minimal spatial stimulation

The 3% contrast responses in OFF Alpha cells suggested a role for NMDA receptors in encoding minimal excitatory stimulation. We tested this further using a minimal spatial stimulus: a small square (25 x 25 μm) about the size of a presynaptic bipolar cell's dendritic tree. These trees are ~30-50 μm diameter, although the receptive field size is larger: ~50-100 μm diameter (Berntson & Taylor, 2000; D. Dacey et al., 2000; Wassle, Puller, Muller, & Haverkamp, 2009; A. J. Zhang & Wu, 2009). Thus, the stimulus should excite one or a small number of bipolar cells. Generating responses with adequate signal-to-noise, even after averaging (14 repeats at each $V_{hold}$), required a high contrast (-100%).

An OFF Alpha cell's response to the square stimulus is shown in Figure 4.5A. The response at each $V_{hold}$ differed significantly from zero ($p < 0.05$, paired t-test) for all but the one $V_{hold}$ (-15 mV) near the reversal potential for the response. In 10 out of 22 cells, flash responses were significantly different from zero for at least six of eight $V_{holds}$, and in these cells the stimulus evoked significant ($p < 0.05$) AMPA, NMDA and GABA/glycine receptor conductances (Figure 4.5B). Because the response was relatively noisy, we performed a control analysis of a later period (700 ms following stimulus presentation); this control response yielded small conductances close to zero (<0.1 nS) (Figure 4.5C). We conclude that NMDA receptors are recruited by minimal spatial stimulation in OFF Alpha cells suggesting that activity at a small number of synapses activates these receptors.

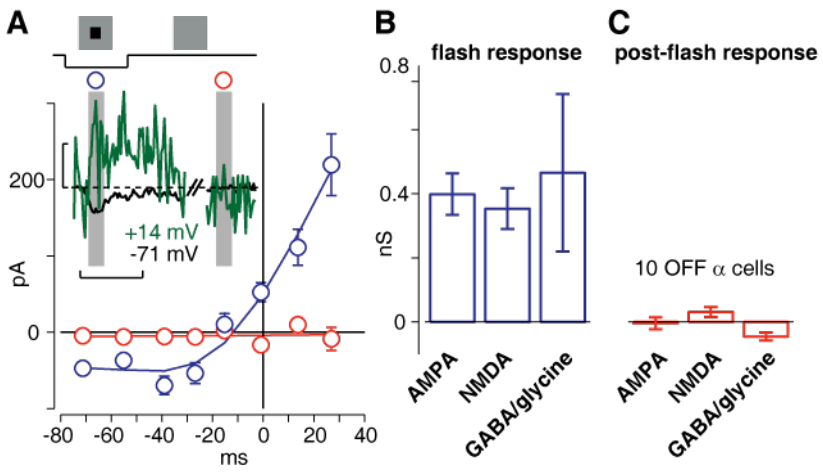


**Figure 4.5**. NMDA receptors are activated in OFF Alpha cells by minimal spatial stimulation.
**A.** A 25 x 25 um square at high contrast (-100%) evoked an excitatory response with an NMDA component. I-V plot shows response during peak excitation and during a later control time interval (700 ms after stimulus onset). Inset; horizontal scale, 200 ms; vertical scale, 100 pA).
**B**, The average response comprised three ligand-gated conductances.
**C**, The response in the control interval was minimal.

## Blocking inhibition increases presynaptic basal glutamate release and obscures the NMDA component of the contrast response.

Studies in salamander demonstrated both an AMPA and NMDA component to the light response after blocking synaptic inhibition (Diamond & Copenhagen, 1993; Mittman et al., 1990; Taylor, Mittman, & Copenhagen, 1996). We recorded under similar conditions here in OFF Alpha cells to study excitatory receptors in relative isolation. A major source of inhibition onto OFF Alpha cells comes from the AII amacrine cell, a glycinergic interneuron that plays a role in both dark- and light-adapted conditions (Bloomfield & Dacheux, 2001; Manookin et al., 2008; Murphy & Rieke, 2008; van Wyk, Wassle, & Taylor, 2009). The AII

cell is driven by the ON pathway, and ON bipolar cells hyperpolarize in the presence of L-AP4, an agonist of the mGluR6 receptor which resides on ON bipolar dendrites and causes cation channel closure (Nakajima et al., 1993; Slaughter & Miller, 1981). We thus applied L-AP4 (50 μM) plus the $GABA_A$ antagonist bicuculline (100 μM) to block much of the direct inhibition onto the ganglion cell (Fletcher, Koulen, & Wassle, 1998; Koulen et al., 1997; Wassle, Koulen, Brandstatter, Fletcher, & Becker, 1998).

The combination of L-AP4 and bicuculline affected both the spontaneous and light-evoked synaptic conductances. During recordings at the mean luminance, the inward leak current at $E_{Cl}$ increased from -85 ± 32 pA to -366 ± 59 pA ($n = 6$; $p < 0.005$; paired *t*-test). Furthermore, the drugs blocked both the feed-forward inhibitory current at stimulus onset (contrast: -50%) and the subsequent inhibitory rebound (Figure 4.6A1, B1). The feed-forward inhibition is not blocked by L-AP-4 alone (Manookin et al., 2008), suggesting that here it was blocked by bicuculline and is therefore mediated by $GABA_A$ receptors.

Across several contrasts, the drugs suppressed the fitted inhibitory component of the I-V plot ($p < 0.05$ at each contrast level). Unexpectedly, the drugs also suppressed the NMDA component ($p < 0.05$ at each contrast level) (Figure 4.6A2, B2). We reasoned that, in the presence of the drugs, the increased excitatory leak current resulted from a substantial increase in basal glutamate release. To estimate the change in basal release, we measured under control conditions the outward current at $E_{Cl}$ during the 'rebound' response when glutamate release is temporarily suppressed (+180 ± 64 pA, $n = 6$). The

difference between this value and the leak under control conditions suggests that the inward current due to basal release was ~265 pA. The increased leak current during the drug condition was about double this value, ~546 pA, suggesting that basal release increased roughly two-fold in the presence of the drugs. It is possible that under these conditions, the NMDA receptors become continuously active, because their long time constant would not allow recovery between release events resulting in a continual stimulation at baseline (see Discussion).

To test this idea, we suppressed glutamate release onto the OFF ganglion cell by presenting a light flash (+100% contrast). In some cells, there was a clear inverted J-shaped function (Figure 4.6C1) indicating the block of baseline NMDA-receptor activity. Across cells, the light flash caused a negative AMPA and NMDA conductance combined with an inhibitory conductance that reflects inhibition that was not completely blocked under this drug condition (Figure 4.6C2). We conclude that suppressing synaptic inhibition with drugs alters the NMDA component of the light response by increasing the basal release of glutamate; this increase results in apparent saturation of the NMDA receptor and thereby attenuates the NMDA component of the excitatory contrast response (see Discussion).

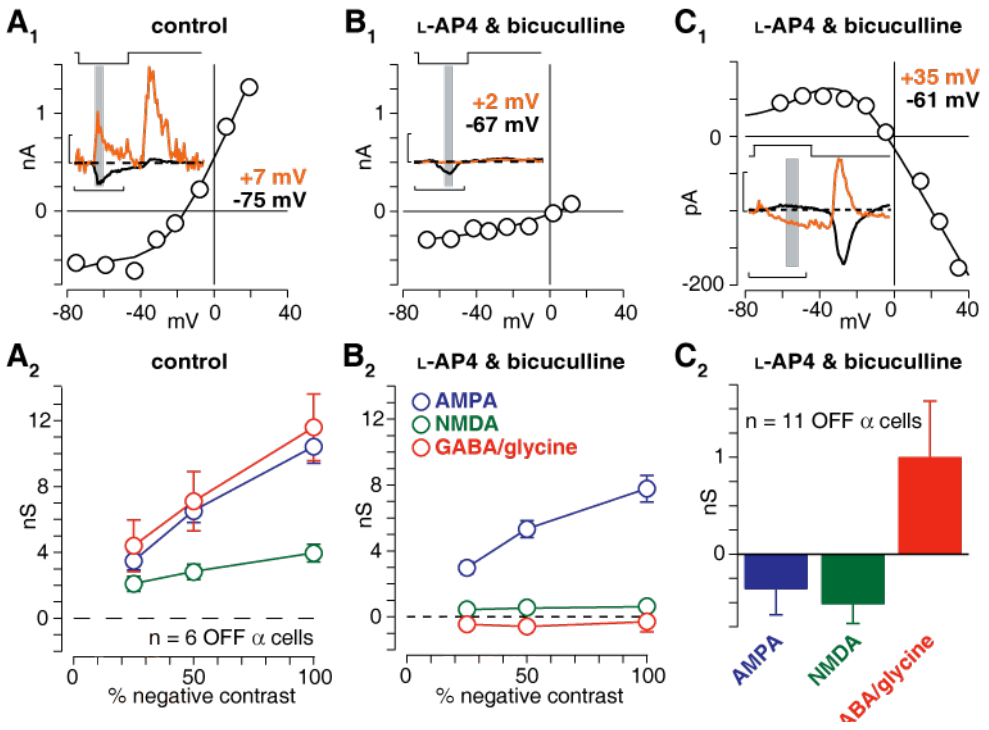


**Figure 4.6**. Increasing presynaptic glutamate release suppressed evoked NMDA-receptor responses.
**A**, An OFF Alpha cell was presented with dark flash (contrast, -50%). The flash evoked an inward current near the chloride reversal and an outward current positive to zero mV (A1, inset; horizontal scale, 200 ms; vertical scale, 1000 pA). The flash caused a J-shaped conductance (A1). Flashes of three different contrasts were presented to OFF Alpha cells (A2; n = 6 cells). The flashes produced a large NMDA-receptor conductance and a net feed-forward inhibition (*x*-axis, flash contrast; *y*-axis, conductance).
**B**, In the same cell (**A**), we presented the stimulus in the presence of bath-applied L-AP4 and bicuculline. Current responses were suppressed and the overall conductance because linear (B1). Across cells, both the NMDA-receptor-mediated and inhibitory conductances were strongly suppressed (B2).
**C**, An OFF Alpha cell was presented with a bright flash (contrast, +100%; duration, 200 ms; diameter, 0.2 mm) in the presence of L-AP4 and bicuculline. The current responses were outward at -61 mV and inward at +35 mV (C1, inset; horizontal scale, 200 ms; vertical scale, 500 pA). The evoked conductance had an inverted J-shape, indicating a removal of excitation (C1). Across cells, the flash induced a removal of an AMPA-receptor and NMDA-receptor conductance and an increased inhibitory conductance (C2; n = 11 cells).

**OFF Delta cells express NMDA receptors comprised of the NR2B subunit**

The NMDA receptor is a heterotetramer comprised of two NR1 subunits and two other subunits (NR2 and/or NR3). Four subtypes of NR2 subunits exist (A, B, C, and D) and each of these subtypes confers distinct properties (Erreger et al., 2004; Monyer et al., 1992). Each NR2 subtype is expressed in the retina at some stage of development (Kalloniatis et al., 2004). At maturity, NR2A-containing receptors were localized to the synapse with AMPA receptors, whereas NR2B subunits were localized outside the synapse (J. Zhang & Diamond, 2009). Furthermore, NMDA receptors were typically localized at the synapse in OFF ganglion cells but outside the synapse in ON cells (Sagdullaev et al., 2006; J. Zhang & Diamond, 2009).

We tested for the presence of NR2B subunits in OFF cell responses by applying ifenprodil (10 μM), which has a >400-fold higher affinity for NMDA receptors comprised of NR2B subunits compared to those comprised of NR2A subunits (Williams, 1993). Puffing NMDA onto an OFF Alpha cell in the presence of bath-applied ifenprodil did not suppress the response (i.e., NMDA conductance at -62 mV) relative to baseline (control, 7.7 ± 2.2 nS; drug, 7.8 ± 2.2 nS; n = 7 cells; $p > 0.4$; paired *t*-test) (Figure 4.7A, C). However, the puff response in an OFF Delta cell was strongly suppressed (control, 4.8 ± 0.4 nS; drug, 0.19 ± 0.09 nS; n = 7 cells; $p < 0.001$; paired *t*-test) (Figure 4.7B, C). In two additional OFF Delta cells, the current evoked by the NMDA puff ($V_{hold}$ = ~-40 mV) was monitored continuously while applying ifenprodil and then washing it out; the block by ifenprodil was partially reversible (Figure 4.7D).

We next determined whether NR2B subunits contributed to the NMDA component of visual responses by presenting negative contrast in the presence of ifenprodil. In an OFF Alpha cell, a -50% contrast spot evoked a J-shaped conductance that largely persisted in the presence of ifenprodil (Figure 4.7E). Across cells, the fitted NMDA conductance declined slightly (control 5.4 ± 0.9 nS; ifenprodil, 4.8 ± 0.8 nS; $p > 0.15$; n = 7 cells) (Figure 4.7G). In an OFF Delta cell, a -50% contrast spot evoked a U-shaped conductance that was converted to a negative conductance (disinhibition) in the presence of ifenprodil (Figure 4.7F). Across cells, the NMDA conductance declined significantly in the presence of the drug (control 1.2 ± 0.4 nS; ifenprodil, -0.3 ± 0.09 nS; $p < 0.01$; n = 6 cells) (Figure 4.7G). Both NMDA puffing and light response measurements suggest that NR2B subunits explain the majority of the NMDA-mediated response in OFF Delta cells but not OFF Alpha cells.

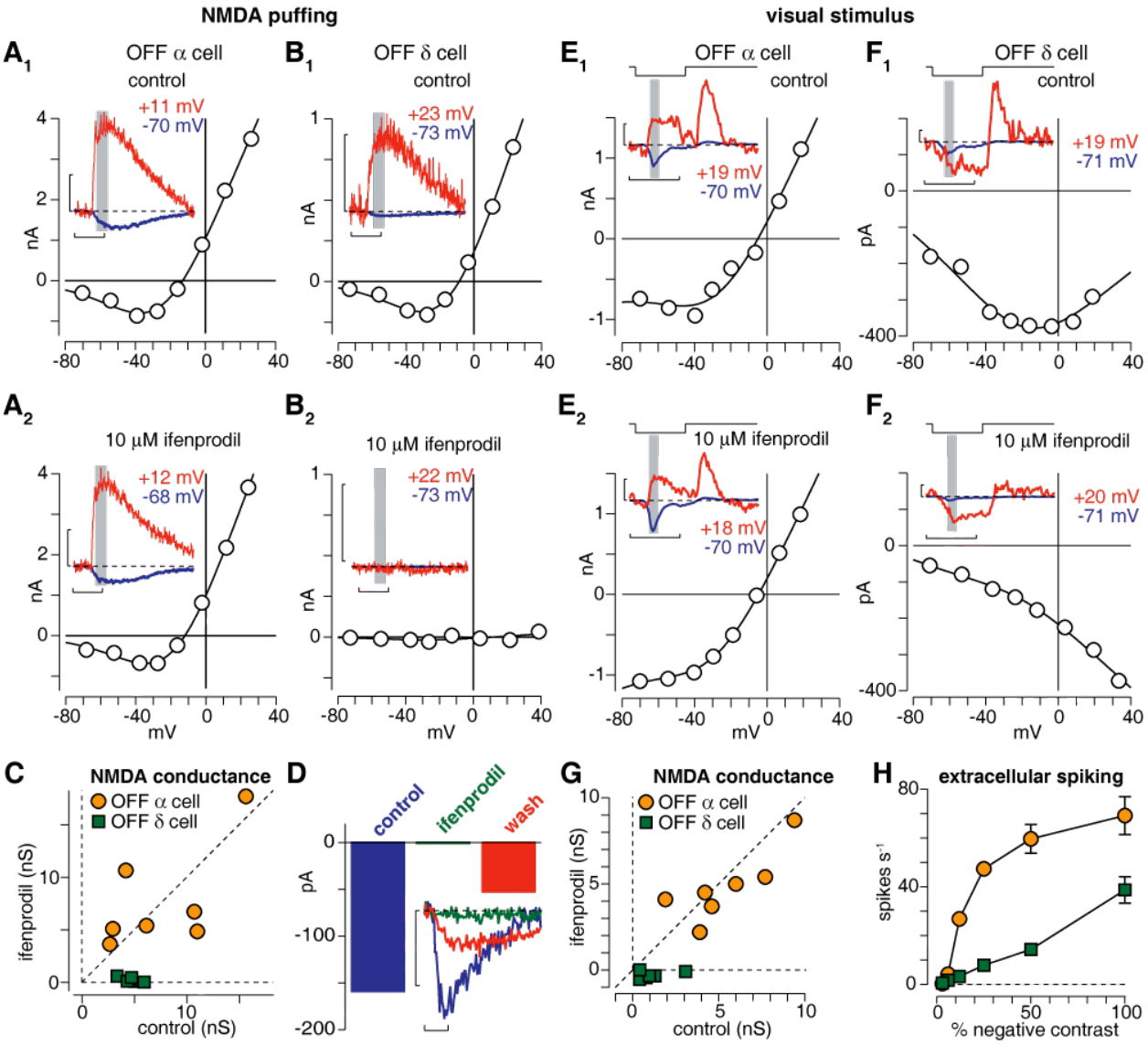


**Figure 4.7**. Distinct NMDA receptor subtypes contribute to OFF Alpha and Delta cell responses.
**A**, NMDA was puffed onto an OFF Alpha cell under control conditions (A1) and with NR2B subunits inhibited (ifenprodil; A2). Puff responses (inset; horizontal scale, 2 sec; vertical scale, 1000 pA) were also similar between conditions.
**B**, Ifenprodil suppressed the NMDA conductance in an OFF Delta cell (B2) compared to control (B1) (inset; horizontal scale, 2 sec; vertical scale, 1000 pA), suggesting expression of NR2B subunits.
**C**, Puff-evoked NMDA conductances for OFF Alpha (orange circles) and OFF Delta cells (green squares) under control conditions (*x*-axis) and in the presence of ifenprodil (*y*-axis).
**D,** Puff-evoked NMDA currents ($V_{hold}$, -40 mV) for two OFF Delta cells under control conditions (blue), in the presence of ifenprodil (green), and after washing

out ifenprodil (red). Responses for a single cell (inset; horizontal scale, 2 sec; vertical scale, 100 pA) show the average of six puffs.
**E**, An OFF Alpha cell was presented with a dark flash (contrast, -50%; duration, 200 ms; diameter, 0.2 mm). The flash elicited an inward current at -70 mV and an outward current positive to 0 mV (inset; horizontal scale, 200 ms; vertical scale, 1000 pA) under control (D1) and drug (D2) conditions.
**F**, An OFF Delta cell was presented with a dark flash (contrast, -100%; duration, 200 ms; diameter, 0.2 mm). The transient component of the response (inset, shaded area; horizontal scale, 200 ms; vertical scale, 100 pA) showed a relatively linear I-V relationship (i.e., primarily disinhibition) in the presence of ifenprodil.
**G**, The visually-evoked NMDA conductances for OFF □ and OFF □ cells under control (*x*-axis) and in the presence of ifenprodil (*y*-axis).
**H,** The extracellular (spike) contrast-response curves for OFF Alpha (orange circles; n = 16) and Delta (green squares; n = 8) cells show the spike rate (*y*-axis) as a function of contrast (*x*-axis).

## OFF Alpha and Delta cells show different degrees of contrast sensitivity in the firing response

We asked how the differences between OFF Alpha and Delta cells in their NMDA receptor function and subunit expression correlate with firing properties. Using loose-patch extracellular recordings, cells were stimulated with a spot stimulus (0.4-mm diameter) at various negative contrast levels (Figure 4.7H). OFF Alpha cells showed a relatively high gain at low contrast, as shown previously with a similar stimulus; responses then saturated above ~30% (Demb et al., 2004; Manookin et al., 2008). OFF Delta cells, by comparison, had a relatively low contrast gain with a roughly linear relationship between contrast and firing rate. Thus, the OFF Alpha cell's use of NMDA receptors to encode the full contrast range correlated with a relatively high gain in the firing response.

## Discussion

The results of this study show three ways in which ganglion cells encode contrast using iGluRs. ON Alpha cells lacked NMDA receptors and encoded contrast using only AMPA receptors (Figure 4.1, 3H). OFF Alpha cells expressed both AMPA and NMDA receptors and used both to encode the full contrast range (Figure 4.1, 3, 4). OFF Delta cells expressed both AMPA and NMDA receptors but used NMDA receptors only for the high contrast range (Figure 4.1, 3, 4).

The difference between the OFF Alpha and Delta cell NMDA-receptor-mediated responses suggests a possible difference in the receptor location (Figure 4.8A). Results suggest that OFF Alpha cells have NMDA receptors at the synapse, in which case the AMPA and NMDA receptors would experience stimulation at similar levels of contrast across the full range; whereas OFF Delta cells have NMDA receptors at an extrasynaptic location, in which case, the AMPA receptors would be stimulated across the full contrast range but NMDA receptors would be stimulated only at high contrast, when release spills over to extrasynaptic sites.

Spontaneous responses (i.e., mini EPSCs) from unknown types of OFF ganglion cells showed an NMDA-receptor component (Sagdullaev et al., 2006; J. Zhang & Diamond, 2009). These data are consistent with the OFF Alpha cell recordings to minimal contrast or spatial stimulation (Figures 4, 5), suggesting a synaptic location of the receptor. Recordings from unknown types of ON cells

and some OFF cells showed minis that were mediated exclusively by AMPA receptors, whereas evoked responses were mediated by both AMPA and NMDA receptors (Chen & Diamond, 2002; Kalbaugh et al., 2009; Matsui, Hosoi, & Tachibana, 1998; Mittman et al., 1990; Sagdullaev et al., 2006). These data are consistent with the OFF Delta cell recordings, where high rates of release (i.e., at high contrast) were required to generate an NMDA component to the response.

The apparent difference in location of NMDA receptors in OFF Alpha and Delta cells corresponded to a difference in NR2 subunit expression: the OFF Delta cell alone showed an NR2B component to the response (i.e., blocked by ifenprodil). The NR2B subunit is found primarily at extrasynaptic sites (J. Zhang & Diamond, 2009). Extrasynaptic NMDA receptors are found more commonly in ON ganglion cells, but they are found also in some OFF cells (J. Zhang & Diamond, 2009). Some OFF cells showed a mix of synaptic NR2A and extrasynaptic NR2B subunits in the same cell (J. Zhang & Diamond, 2009). Our results suggest that some OFF cell types have near exclusive (or dominant) expression of only one of these configurations.

Given that most mammalian ON ganglion cell types express the NMDA receptor (E. D. Cohen, 1998, 2000; Kalbaugh et al., 2009; Massey & Miller, 1988; Sagdullaev et al., 2006; J. Zhang & Diamond, 2009), it was surprising that the ON Alpha cell did not (Figures 1, 3). However, an *in vivo* study of the cat eye supports this conclusion: ON Y/Alpha cells (in the presence of bicuculline) did not respond to NMDA application ((Boos, Muller, & Wassle, 1990); but see (E. D. Cohen et al., 1994)). Furthermore, only a fraction of dissociated ganglion cells

(of unknown types) showed an NMDA response, suggesting that NMDA receptor expression is not uniform across cell types (Aizenman, Frosch, & Lipton, 1988; Karschin, Aizenman, & Lipton, 1988).

The lack of NMDA receptors in ON Alpha cells might be explained by the tonic rate of their presynaptic glutamate release. Recordings here and elsewhere suggest that the rate of glutamate release onto the ON Alpha cell is relatively high (Figure 4.3) (Murphy & Rieke, 2006; Trong & Rieke, 2008; Zaghloul et al., 2003). The exact rate is unknown. However, the number of glutamate receptors on ON and OFF Alpha cells is similar and so the relatively high tonic level of excitatory activity in the ON cell must correspond to a relatively high rate of basal release at each synapse (Xu, Vasudeva, Vardi, Sterling, & Freed, 2008). The high rate of glutamate release could saturate an NMDA receptor, rendering it useless for encoding increases above the basal rate. To illustrate the impact of basal release on AMPA versus NMDA receptors, we performed a simulation.

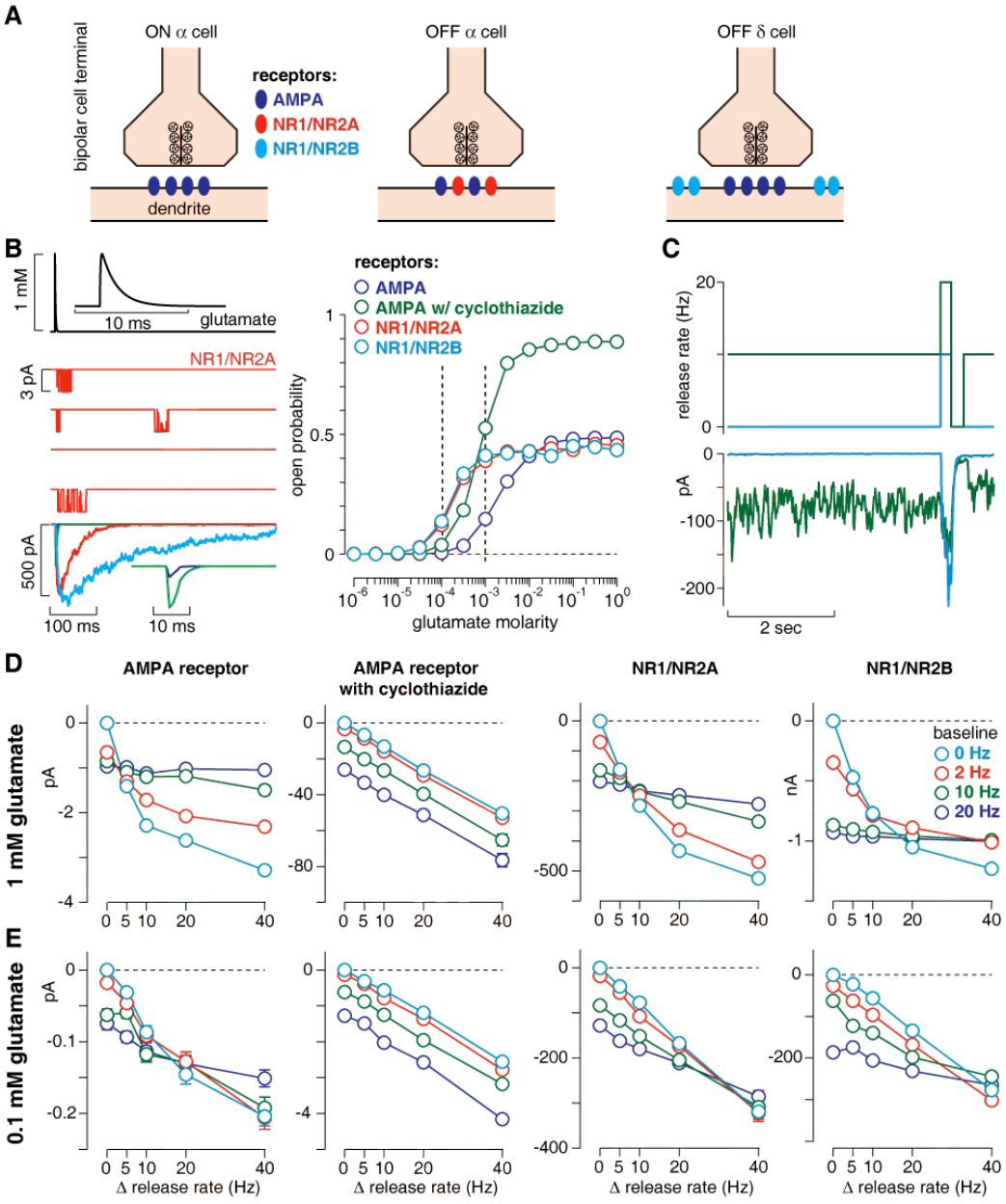


**Figure 4.8**

**A**, Model for AMPA and NMDA receptor expression in ON Alpha, OFF Alpha, and OFF Delta cells. OFF Delta cells alone express extrasynaptic NR2B-containing NMDA receptors.

**B**, Computational model of iGluR glutamate dose-response relationship. Presynaptic glutamate release was modeled as an instantaneous rise to a glutamate concentration followed by an exponential decay ($\tau$ = 1.2 ms). Single-channel responses from an NR2A-containing NMDA receptor (red) show current response to a 1 mM glutamate pulse. NMDA receptors showed greater sensitivity to glutamate than AMPA receptors, responding at lower glutamate

concentrations. NMDA receptors also saturated at lower glutamate concentrations than AMPA receptors.
**C**, Trains of glutamate pulses were presented at several baseline rates followed by a 200-ms increase in release rate. NR1/NR2A receptors responded to the 10-Hz increase from baseline with an inward current. The magnitude of the inward current was similar for the 0-Hz (cyan) and 10-Hz (green) backgrounds, but the increase relative to baseline was larger for the condition with low basal release.
**D**, Glutamate release trains were simulated for four iGluRs (peak molarity, 1 mM). The background release rate strongly influenced the ability of receptors to respond to a subsequent increase in glutamate concentration. The one exception, the non-desensitizing AMPA receptor, responded linearly across all conditions.
**E**, The trains were presented at a lower peak glutamate concentration (0.1 mM) to simulate conditions with lower open probability of single channels. Under this condition, iGluRs showed a more linear response and larger operating range.

### Glutamate receptor models show how high basal glutamate release can saturate responses and obscure contrast coding

In the simulation, release was random (Poisson; (Freed, 2000a, 2000b)) and increased in rate from zero to 40 Hz (Figure 4.8B); this range is consistent with the estimated range for ribbon synapses (DeVries, Li, & Saszik, 2006; Freed, 2000a, 2000b; Jackman et al., 2009; Singer, 2007; Singer et al., 2004). For simplicity, release events were modeled by exponential functions: instantaneous steps to a non-zero glutamate Molarity followed by a return to baseline with a time constant of 1.2 ms (Clements, Lester, Tong, Jahr, & Westbrook, 1992) (Figure 4.8B). Responses were modeled by summing across receptors (20 receptors/synapse) and synapses (50, total). Realistic single channel properties were based on published reports of an AMPA receptor with or without desensitization (i.e., in the absence or presence of cyclothiazide; (Dzubay & Jahr, 1999)), and NMDA receptors composed of the NR2A subunit

(Erreger et al., 2005) or NR2B subunit (Banke, Dravid, & Traynelis, 2005). The response time course and open probability for a single event are shown in Figure 4.8B.

We simulated the response to a contrast flash by increasing the release rate for 200 ms above a baseline level. The increment values were 5-40 Hz above the baseline values of 0-20 Hz (Figure 4.8C, D). Following the increment, the release was set to zero for 300 ms, which mimicked the apparent drop in release during the 'rebound' response. Increasing the release from the baseline level evoked an increase in inward current, but the gain (i.e., slope) of this increase depended strongly on the receptor type and the baseline release rate (Figure 4.8D). The non-desensitizing AMPA receptor, as expected, simply summed the events and so behaved linearly in all cases. For low baseline release rates (0 or 2 Hz), the desensitizing AMPA receptor and both NMDA receptors showed high gain for small increments (5-10 Hz) and saturation for large increments (20-40 Hz). For high baseline release rates (10 or 20 Hz), these three receptors all showed low gain across the full increment range or were saturated. We re-ran all models given a lower peak concentration in synaptic glutamate (0.1 mM), which effectively lowers the open probability of the channels and thus reduces the rate of receptor desensitization of individual channels (Figure 4.8E). This manipulation reduced response saturation across all models and conditions.

We draw several conclusions from the model. First, the saturation of the NMDA receptor component in the OFF Alpha cell response in the presence of

high basal release (L-AP4 + bicuculline condition, Figure 4.6) could be explained by the properties of the NMDA receptor (Figure 4.8D). Second, the OFF Alpha cell's ability to respond in the presence of high basal release with an AMPA receptor component suggests that these receptors are not strongly desensitizing (Figure 4.8D). Furthermore, the ON Alpha cell's ability to respond under control conditions in the presence of a high basal release of glutamate also suggests the use of a non-desensitizing AMPA receptor (Figure 4.3H).

OFF bipolar cells must also encode changes from a high basal release rate (i.e., ~20-40 Hz) (DeVries et al., 2006; Jackman et al., 2009; Singer, 2007; Singer et al., 2004) and apparently do so using several strategies. First, they do not employ NMDA receptors (Hartveit, 1997), which would apparently be saturated under high release conditions (Figure 4.8D). Second, they use AMPA receptors that show little desensitization or recover relatively quickly from desensitization (DeVries, 2000; Pang, Gao, Barrow, Jacoby, & Wu, 2008). Third, some OFF bipolar types use kainate receptors that recover slowly from desensitization, but these types position their dendrites relatively far from synaptic release sites effectively lowering the peak concentration of glutamate which can minimize the effects of desensitization (DeVries et al., 2006) (compare AMPA receptor in Figure 4.8D, E). The properties of AMPA receptors in specific ganglion cell types remain to be elucidated, but we predict that many types will use a non-desensitizing AMPA receptor similar to some OFF bipolar cells.

Why would there be a difference in the NMDA receptor expression and presumed receptor location between OFF Alpha and Delta cells? These cells

encode contrast in the firing rate differently (Figure 4.7G). OFF Alpha cells show high contrast gain, which requires sensitive responses at low contrast (Figure 4.7H). NMDA receptors are apparently recruited to support these responses. This may seem surprising given that the NMDA conductance is mostly blocked near $V_{rest}$. However, NMDA receptors in multiple systems contribute near $V_{rest}$ including responses to spontaneous release (Binshtok, Fleidervish, Sprengel, & Gutnick, 2006; Espinosa & Kavalali, 2009; Fleidervish, Binshtok, & Gutnick, 1998). Furthermore, an NMDA-receptor contribution may facilitate signal-to-noise at low contrast given the long time constant of the response (Demb et al., 2004). NMDA receptors also complement AMPA receptors in that, over the physiological range (-80 to -40 mV), the driving force on the two channels change in opposite directions. Thus, as the AMPA receptors lose driving force at high contrast, the NMDA-receptor conductance increases (Diamond & Copenhagen, 1993). The OFF Delta cell showed a linear contrast response curve, and thus the use of apparent extrasynaptic NMDA receptors may be useful for preventing a nonlinear response compression at high contrast. Future studies will be required to determine whether the three patterns of AMPA/NMDA receptor contributions at retinal synapses generalizes to the other cell types.

## Experimental Procedures

### Tissue preparation and electrophysiology

The experimental procedures have been described in detail previously (Demb et al., 1999; Manookin et al., 2008). Hartley guinea pigs were housed in a

12-h dark/light cycle. The animal was dark adapted for one hour before further procedures were carried out. The animal then was taken to a room illuminated with dim red light and anesthetized with an intramuscular injection of ketamine (100 mg/kg) and xylazine (10 mg/kg). While under anesthesia, the animal was decapitated and both eyes were removed in dim red light. All procedures conformed to National Institutes of Health and University of Michigan guidelines for use and care of animals in research. The retina was hemisected and the vitreous, lens, and cornea were removed and discarded. The back of the eye was cut into two pieces along the vertical midline and each piece was placed on a piece of filter paper and stored at room temperature in oxygenated (95% $O_2$, 5% $CO_2$) Ames' medium (Sigma-Aldrich, St. Louis, MO, USA). The tissue was stored in a light-tight container until the time of recording (storage time, 0.5-5 h). At the time of recording, the retina was placed in a chamber on a microscope stage and superfused (~6 ml $min^{-1}$) with oxygenated Ames' medium heated to 33–35◦C with an in-line heater (TC-344B, Warner Instruments, Hamden, CT, USA). In one experiment, synaptic transmission was blocked using $Cd^{2+}$. For this experiment, we used an extracellular Ringer solution containing (in mM) 1.15 $CaCl_2$, 1.24 $MgSO_4$, 3.1 KCl, 0.5 potassium methylsulfate, 120 NaCl, 6 glycine, 6 d-glucose, 0.2 D-serine, 22.6 $NaHCO_3$, 1 $CdCl_2$). We did not use the $Cd^{2+}$ puffing data for generating the NMDA receptor basis function as the Ringer was different from the Ames' solution used to record light responses.

The retina and electrode were visualized using a cooled CCD camera (Retiga 1300C, Qcapture software; Qimaging Corporation, Burnaby, British

Columbia, Canada) mounted on an Olympus BX51WI microscope (Olympus; Center Valley, PA, USA). We targeted ON and OFF Y-type/Alpha and OFF Delta ganglion cells by recording from the largest cell bodies in the ganglion cell layer (diameter: 20–25 □m). Cell type was confirmed by measuring light responses and in some cases by analyzing the stratification of the dendritic tree, as previously described (Manookin et al., 2008). OFF Alpha and Delta ells were readily distinguishable by their responses to full-contrast, square-wave spots: near $E_{Cl}$, the dark spot elicited an inward current of ~0.7-2 nA in OFF Alpha cells, whereas the inward current never exceeded 0.5 nA in OFF Delta cells. A glass electrode (tip resistance, 3–5 MΩ) was filled with Ames' solution for recording extracellular spiking or intracellular solution for whole-cell recording of membrane currents. Intracellular solution consisted of the following (in mM): 120 cesium methanesulphonate, 5 TEA-Cl, 10 HEPES, 3 NaCl, 10 BAPTA, 2 QX-314-Cl, 2 ATP-Mg, 0.3 GTP-Na with 0.10% Lucifer Yellow, titrated to pH 7.3. All chemicals were purchased from Sigma-Aldrich (St Louis, MO, USA) except for the following: BAPTA (Invitrogen; Eugene, OR, USA); strychnine (Fisher, Hampton, NH, USA); D-serine, D-AP5, and L-AP4 (Tocris; Bristol, UK).

Membrane current was amplified, sampled at 10 kHz, and stored on a computer using a MultiClamp 700A amplifier, Digidata 1322A analog–digital board and pCLAMP 9 software (Axon Instruments; Union City, CA, USA). Junction potential (-9 mV) was corrected in all cases. Light responses were analysed with custom programs written in Matlab (version 7.4; The Mathworks;

Natick, MA, USA). An error in the holding potential ($V_{hold}$) introduced by the series resistance was corrected by the formula:

$$V_{hold} = V_{hold,uncorr} - (I_{leak} * R_s * (1 - R_{S,correct})),$$

where $V_{hold,uncorr}$ is the apparent (uncorrected) holding potential (in mV), $I_{leak}$ is the leak current (in nA), $R_S$ is the series resistance (15.0 MΩ; S.D. = 4.5; $n$ = 171 cells) and $R_{S,correct}$ is the series resistance compensation. We excluded cells from the analysis with $R_S$ >25 MΩ. $R_{S,correct}$ was typically 0.4; higher values sometimes resulted in oscillations that destroyed the seal. The uncompensated series resistance was 9.4 MΩ (S.D. = 3.7). Using this technique, we corrected for the voltage error during the leak current, but the additional voltage error during the response was not corrected. To minimize the errors during a response, we excluded recordings with an uncompensated voltage drop of >10 mV during the response.

**Visual stimuli**

The stimulus was displayed on a miniature monochrome computer monitor (Lucivid MR1-103; Microbrightfield; Colchester, VT, USA) projected through the top port of the microscope through a 4× objective and focused on the photoreceptors (resolution, 640×480 pixels; 60 Hz vertical refresh). The relationship between gun voltage and monitor intensity was linearized in software with a lookup table. Stimuli were programmed in Matlab as previously described (Demb et al., 1999). All stimuli were centered on the cell body. Cells were recorded in the superior retina, where the cone distribution is ~95% M-cones and

~5% S-cones (Rohlich et al., 1994; Yin et al., 2006). During recording, the cell was exposed to stimuli that fluctuated around a constant mean luminance. Light level is described as the photoisomerization rate per photoreceptor (rod, M-cone or S-cone) per second: $P_R$*, $P_M$* and $P_S$*, respectively. Photoisomerization rates were calculated based on the spectral output of the monitor, the intensity of the monitor (W mm$^{-2}$) at the plane of the retina, and the photoreceptor properties described in Yin *et al.* (2006). The mean luminance evoked ~5×10$^3$ $P_R$*, ~10$^3$ $P_M$*, and ~10$^2$ $P_S$*. Under these conditions, M-cones and rods contribute about equally to the light response (Yin et al., 2006). At this light level, rod contributions presumably arise primarily through their gap junctions with cones but not through the rod bipolar circuit (Bloomfield & Dacheux, 2001; Manookin et al., 2008).

The primary stimulus was a spot (duration, 200 ms) centered on the cell body. In ON Alpha cells the spot diameter was 0.5 mm at all contrasts. In all other cells, the spot diameter varied with stimulus intensity. For high-contrast stimuli (contrast, 25-100%), a small spot (diameter, 0.2 mm) was used to decrease the response size and, thus, decrease the voltage drop across the pipette tip caused by the uncompensated series resistance. A larger spot (diameter, 0.4 mm) was used for low-contrast stimuli (contrast, 3-12%) to increase the signal-to-noise ratio. A spot was presented at each of nine holding potentials. A cell was held at a given holding potential for no more than 15 seconds. During the spot presentation, the stimulus program sent a transistor-transistor logic (TTL) pulse through the serial port at each frame presentation.

TTL pulses were recorded in Clampex and later analyzed to check for skipped frames and confirm proper alignment of the responses. The voltage output of the video card was also recorded in Clampex as a secondary control.

## Basis functions

The basis function for AMPA-receptors was determined from puffing experiments published previously (Beaudoin et al., 2008). The AMPA-receptor current was a linear function of membrane voltage,

$$I_{AMPA} = g_{AMPA}(V - E_{cation}),$$

where the current response (I) is the product of the conductance (g) and the electrical driving force (voltage, V; cation reversal potential, $E_{cation}$).

To determine the NMDA-receptor basis function, synaptic transmission was suppressed and NMDA was puffed onto the dendrites of a ganglion cell. In each cell, the conductance-voltage relationship was calculated and fit with the following equation (least-squares fit):

$$g_{NMDA} = \frac{1}{1+\frac{[Mg^{2+}]_o}{\beta} e^{\alpha V}}.$$

This equation reflects the relationship between the conductance (g) and voltage (V), where $[Mg^{2+}]_o$ is the extracellular magnesium concentration (1.2 mM). The constants representing voltage-dependence and the magnesium dependence of the NMDA-receptor ($\alpha$ and $\beta$, respectively) (Gerstner & Kistler, 2002; Jahr & Stevens, 1990a, 1990b) were free parameters in the fit (Figure 4.2).

In each cell, the g-V relationship was normalized to a maximal conductance of 1 nS. The fit was then performed on the normalized data across

cells. The fits produced values that became the NMDA-receptor basis function for OFF Alpha cells ($\alpha$, 0.059 $mV^{-1}$; $\beta$, 9.3 mM; n = 12 cells) and OFF Delta cells ($\alpha$, 0.055 $mV^{-1}$; $\beta$, 4.3 mM; n = 10 cells). The conductances were converted to currents using the following equation:

$$I_{NMDA} = g_{NMDA}\,(V - E_{cation}).$$

The $GABA_A$/glycine conductance-voltage relationship was modeled as an exponential function with an offset (b):

$$g_{GABA/glycine} = e^{aV} + b.$$

The function exponentially relates conductance (g) and voltage by two constants (a and b). Rebound data were fit for OFF Alpha (a, 3.9 x $10^{-3}$; b, 0.2060; n = 15 cells) and OFF Delta cells (a, 4 x $10^{-4}$; b, 0.1926; n = 6) (Figure 4.2E, 2F). The fitted equation was then used as the basis function for GABA/glycine receptors. The conductances were converted to currents using the following equation:

$$I_{GABA/glycine} = g_{GABA/glycine}\,(V - E_{Cl}),$$

where $E_{Cl}$ is the chloride reversal potential (-67 mV).

## Analysis

The current response to a contrast flash was determined by subtracting the leak current at baseline (first 500 ms). The flash response was measured by averaging over a 50-ms window centered on the peak excitatory response (~50-100 ms following flash onset). Responses were modeled as the sum of three

underlying ligand-gated currents mediated by AMPA, NMDA, and GABA/glycine receptors using the following equation (least-squares fit):

$$I_{total} = I_{AMPA} + I_{NMDA} + I_{GABA/glycine}.$$

We used this technique to estimate the ligand-gated conductances during the peak excitatory response. We also performed this analysis as a function of time (Figure 4.4E-H). The temporal current response was downsampled to 1 kHz and the analysis was performed on the current responses at each point in time (least-squares fit). For ON and ON-OFF cells, the OFF Alpha cell basis functions for GABA/glycine and NMDA receptors were used (e.g., Figure 4.3H).

The conductances were also fit as a function of time. In OFF cells, this analysis was specific to the excitatory portion of the response, as the 'rebound' response typically showed large amplitude currents with voltage errors >10 mV. Attempting to fit these portions often resulted in a negative AMPA conductance and a positive NMDA conductance that were perfectly anti-correlated over time. We assumed this pattern reflects an inability to model responses composed of very large currents at some holding potentials.

**Glutamate receptor modeling**

AMPA and NMDA receptors were modeled using Channel Lab (version 2; Synaptosoft, Inc, Decatur, GA). Presynaptic glutamate release was modeled as an instantaneous step to a peak glutamate concentration (0.1 or 1.0 mM) followed by an exponential decay ($\tau$ = 1.2 ms). The timing of presynaptic release was modeled as a Poisson process for each synapse (50 independent synapses)

with 20 receptors of each type per synapse. Synaptic release trains were generated in Matlab and run at a sample rate of 10 kHz in Channel Lab. The release rate increased for 200 ms to simulate the 200-ms contrast flash response. Each receptor was modeled as a state machine (Markov chain) containing several states and transitions between the states according to published values (Banke et al., 2005; Dzubay & Jahr, 1999; Erreger et al., 2005), and the model was run as a Monte Carlo simulation. All models were available with the Channel Lab software. The model predicted the current responses for the synaptic release trains at -62 mV—the approximate $V_{rest}$ for OFF cells.

# Chapter 5

## Conclusions

My thesis research focused on understanding how neural circuits and synapses encode information. The retina is an ideal system for studying information encoding in the brain as one can record responses to natural stimuli with the synaptic circuitry intact. The retina contains approximately 20 different classes of ganglion cell. Each cell type processes a particular aspect of a visual scene. This specialization suggests that each ganglion cell type has a unique combination of circuitry, receptors, and intrinsic properties. This thesis focused on the circuitry and receptors for ON $\alpha$, OFF $\alpha$, and OFF $\delta$ ganglion cells. These three cell types receive distinct patterns of excitatory and inhibitory input (Chapters 3 and 4), and they also show unique patterns of AMPA and NMDA receptor expression (Chapter 4). Furthermore, the spiking responses in these cell types reveal a distinct pattern of contrast encoding (Chapters 3 and 4).

Figure 3.4 illustrates the spiking response of ON $\alpha$ cells to bright flashes. The response shows a relatively high slope at low contrast; the response then saturates at high contrast. The contrast gain was relatively high at low contrast, suggesting that the ON $\alpha$ circuit is tuned to encoding low-contrast changes. The ON $\alpha$ cell also experienced a relatively high basal glutamate release, allowing the circuit to encode both increments and decrements in contrast (Chapter 4).

Furthermore, the circuit configuration for ON cells was a combination of excitation and feedforward inhibition at all contrasts tested (Chapters 3 and 4). Synaptically, this corresponded to functional expression of AMPA receptors to encode presynaptic glutamate release and GABA and/or glycine receptors to encode feedforward inhibition (Chapter 4). Our computational model for AMPA and NMDA receptors suggests that, given the high tonic rate of glutamate release onto the ON cell dendrites, these cells must express a non-desensitizing AMPA receptor (see Figure 4.8).

Spike responses in OFF $\alpha$ cells also reveal a steep slope at low contrast (Figures 3.4, 4.7), suggesting a high sensitivity to low contrast decrements. However, this high gain/sensitivity at low contrast causes the response to saturate at high contrast. The OFF $\alpha$ cell receives a relatively low rate of presynaptic glutamate release. Basal release is sufficient, however, that when removed following high-contrast stimulation, the OFF cell undergoes a period of reduced sensitivity—slow contrast adaptation (Chapter 2) (Manookin & Demb, 2006). Still the basal release rate is low relative to ON cells, allowing for the use of synaptic NMDA receptors (Chapter 4). Inhibitory synapses also play a fundamental role in the OFF $\alpha$ circuit (Manookin et al., 2008). Excitation in the OFF bipolar circuit (e.g. from a decrement in contrast) causes increased feedforward inhibition (through $GABA_A$ receptors) and disinhibition (through glycine receptors) (see Chapters 3 and 4). This disinhibition arises through the AII amacrine cell and plays a relatively large role in encoding low contrast stimuli.

The AII amacrine circuit plays an even greater role in OFF δ cells. OFF δ cells receive less excitatory input than OFF α cells and, thus, disinhibition plays a prominent role in encoding the full range of negative contrasts (Figure 4.4). These factors likely contribute to the δ cell's distinct contrast encoding. The δ cell contrast response reveals a linear relationship between contrast and spike rate (Figure 4.7). In other words, the gain at low contrast was identical to that at high contrast, suggesting an approximately equal sensitivity to all contrast decrements.

These data also suggest a possible correlation between high gain and excitatory synaptic input—gain was higher in cell types receiving relatively larger levels of presynaptic glutamate input (ON and OFF α cells), whereas gain was lower and contrast encoding was linear in the OFF δ cell, which was driven mostly by the removal of inhibitory glycine release. Experiments in other ganglion cell types are needed to elucidate such principles of circuit encoding.

**Slow contrast adaptation in ganglion cells arises largely from plasticity at the level of presynaptic bipolar cells.**

Several studies suggested that an intrinsic mechanism was responsible for slow contrast adaptation in retinal ganglion cells (Baccus & Meister, 2002; Solomon et al., 2004). This idea followed from research in the cortex, which demonstrated that in some neurons the afterhyperpolarization causing slow adaptation arose from an intrinsic mechanism (Sanchez-Vives et al., 2000a, 2000b). However, our ganglion cell recordings revealed a presynaptic

mechanism for slow contrast adaptation arising in bipolar cells (Manookin & Demb, 2006) (see Chapter 2).

Our findings are consistent with a model where, at the offset of high contrast, bipolar cell glutamate release drops below the normal background rate. This decrease in excitation hyperpolarizes the ganglion cell, resulting in an afterhyperpolarization and suppressed spiking. Bipolar cell glutamate release returns to baseline levels over several seconds, eventually returning the ganglion cell to the previous level of basal excitability.

**Disinhibition plays an important role in OFF cell contrast encoding**

The findings described in Chapter 3 present an unconventional role for the AII amacrine cell in visual coding. Previously, the prevailing view had stated that an AII amacrine cell drives visual processing under very dim light conditions where few photons are available for light encoding. Thus, the AII amacrine cell is often referred to as the 'rod amacrine cell' for its prominent role in scotopic vision. Here, we demonstrate that for OFF $\alpha$ cells, the AII amacrine cell plays a vital role in daylight (photopic) vision (Manookin et al., 2008). Other experiments have demonstrated that the AII also provides disinhibition to OFF $\delta$ cells (data not shown). These results suggest that ON bipolar cells should not show strong rectification, allowing them to signal both increments and decrements in light intensity to the AII amacrine cell. Indeed, the ON bipolar cell providing input to the ON $\alpha$ cell shows little rectification, having a high basal release near the middle of its operating range (Chapter 4).

Current flows from an ON cone bipolar cell to an AII amacrine cell through gap junctions. Thus, depolarizing an ON bipolar would, in turn, depolarize the AII cell; likewise, a dark flash would hyperpolarize an ON bipolar cell and, subsequently, an AII cell. Furthermore, recent findings provide physiological evidence (Manookin et al., 2008; Murphy & Rieke, 2008) for direct inhibitory (glycinergic) synapses from AII cells to OFF ganglion cells and presynaptic OFF bipolar terminals. The high rate of basal excitation in the ON pathway results in high basal AII cell activation, resulting in inhibition of OFF cells at baseline. Hyperpolarizing the ON pathway with a dark flash causes the AII cell to remove glycine release from OFF cell dendrites and presynaptic OFF bipolar terminals. In this way, the AII amacrine cell, an inhibitory neuron, extends the excitatory operating range of some OFF ganglion cells and, possibly, OFF bipolar cells.

### The roles of AMPA and NMDA receptors in contrast encoding

Excitatory input through glutamate receptors plays a prominent role in visual encoding. The results in Chapter 4 show three ways in which ganglion cells encode light information using AMPA and NMDA receptors. OFF $\alpha$ and $\delta$ cells showed functional expression of both receptor types. In OFF $\alpha$ cells, both receptors were utilized in encoding the full range of negative contrasts. However, in OFF $\delta$ cells, NMDA receptors contributed only at high contrast (> 25%). These findings are consistent with a synaptic NMDA receptor localization in OFF $\alpha$ cells and an extrasynaptic localization in OFF $\delta$ cells.

The distinction in apparent NMDA receptor location correlated with NR2 subunits in the OFF cells. OFF δ cells showed a striking bias toward NR2B subunit expression, as NMDA receptor currents were strongly suppressed in the presence of an NR2B antagonist (ifenprodil). Ifenprodil had little effect on OFF α cells, indicating that NR2B subunit expression was minimal in these cells.

The NMDA puffing and light stimulation experiments demonstrated that ON α cells do not express functional NMDA receptors. The lack of NMDA receptors in ON α cells might be explained by the high tonic rate of their presynaptic glutamate release. Recordings here and elsewhere suggest that the rate of glutamate release onto the ON α cell is relatively high (Figure 4.3) (Murphy & Rieke, 2006; Trong & Rieke, 2008; Zaghloul et al., 2003). The exact rate is unknown. However, the number of synapses on ON and OFF α cells is similar and so the relatively high tonic level of excitatory activity in the ON cell must correspond to a relatively high rate of basal release at each synapse (Xu et al., 2008). The high rate of glutamate release could saturate an NMDA receptor, rendering it useless for encoding increases above the basal rate. This conclusion was confirmed with computational models of AMPA and NMDA receptors (Figure 4.8).

## Future directions

### Mechanism for slow contrast adaptation in bipolar cells

The findings in Chapter 2 demonstrate that slow adaptation arises in bipolar cells. However, the mechanism remains an open question. One

hypothesis is that slow adaptation arises in bipolar cell synaptic terminals. This hypothesis could be tested with whole-cell recordings from bipolar cells. Sinusoidal current would be injected at 6 Hz and presynaptic release would be determined by measuring glutamate transporter currents. In this way, the amount of adaptation in the bipolar membrane potential and synaptic output could be compared and the source of adaptation could be isolated. Pharmacological experiments could also be done to isolate the specific cellular mechanism.

### The roles of NMDA receptors in contrast encoding

Another open question involves the function of NMDA receptors in OFF Alpha and Delta cells. In Chapter 4, I did not address the role of NMDA receptors in the spike response, but understanding spike encoding of contrast is my ultimate goal. Recording spike responses with NMDA receptors blocked could provide a great deal of insight into the function of NMDA receptors in spiking. Blocking NMDA receptors with D-AP-5 in the bath is not optimal due to possible circuit effects. However, in a separate experiment I was able to block NMDA receptors internally by adding 1 mM MK-801 to the pipette solution (data not shown). Preliminary results from this experiment suggest that NMDA receptors serve to keep the response gain high at low contrast in the OFF $\alpha$ cell.

### Receptor subunit expression

My thesis research used a variety of techniques (e.g. pharmacology, whole-cell recording) to infer the circuit and synaptic properties of ganglion cell inputs. However, the precise receptor profiles for ON and OFF ganglion cells remains an open question. For example, our recordings in the presence of an NR2B antagonist (ifenprodil) suggested that OFF $\alpha$ cells do not significantly express NR2B subunits, but this does not confirm the expression of NR2A subunits. In fact, NR2C, NR2D, and NR3A subunits are all expressed in retinal ganglion cells (Fletcher et al., 2000; Kalloniatis et al., 2004). These receptor subunits confer distinct kinetics, binding properties, and current responses on the NMDA receptor response (Nakanishi et al., 2009; Qian, Buller, & Johnson, 2005; Santucci & Raghavachari, 2008).

Receptor subunit expression could be determined using two techniques: single cell RT-PCR to determine mRNA expression and antibody staining to reveal receptor expression in dendritic membrane. The same techniques could also be used to determine AMPA receptor subunit composition in ON $\alpha$ cells, as these AMPA receptors should show minimal desensitization.

## Bibliography


Aizenman, E., Frosch, M. P., & Lipton, S. A. (1988). Responses mediated by excitatory amino acid receptors in solitary retinal ganglion cells from rat. *J Physiol, 396*, 75-91.

Albrecht, D. G., & Hamilton, D. B. (1982). Striate cortex of monkey and cat: contrast response function. *J Neurophysiol, 48*(1), 217-237.

Amthor, F. R., Takahashi, E. S., & Oyster, C. W. (1989). Morphologies of rabbit retinal ganglion cells with concentric receptive fields. *J Comp Neurol, 280*(1), 72-96.

Ascher, P., & Nowak, L. (1988). The role of divalent cations in the N-methyl-D-aspartate responses of mouse central neurones in culture. *J Physiol, 399*, 247-266.

Awatramani, G. B., & Slaughter, M. M. (2000). Origin of transient and sustained responses in ganglion cells of the retina. *J Neurosci, 20*(18), 7087-7095.

Awatramani, G. B., & Slaughter, M. M. (2001). Intensity-dependent, rapid activation of presynaptic metabotropic glutamate receptors at a central synapse. *J Neurosci, 21*(2), 741-749.

Baccus, S. A., & Meister, M. (2002). Fast and slow contrast adaptation in retinal circuitry. *Neuron, 36*(5), 909-919.

Baccus, S. A., & Meister, M. (2004). Retina versus cortex; contrast adaptation in parallel visual pathways. *Neuron, 42*(1), 5-7.

Banke, T. G., Dravid, S. M., & Traynelis, S. F. (2005). Protons trap NR1/NR2B NMDA receptors in a nonconducting state. *J Neurosci, 25*(1), 42-51.

Beaudoin, D. L., Manookin, M. B., & Demb, J. B. (2008). Distinct expressions of contrast gain control in parallel synaptic pathways converging on a retinal ganglion cell. *J Physiol, 586*(Pt 22), 5487-5502.

Berntson, A., & Taylor, W. R. (2000). Response characteristics and receptive field widths of on-bipolar cells in the mouse retina. *J Physiol, 524 Pt 3*, 879-889.

Binshtok, A. M., Fleidervish, I. A., Sprengel, R., & Gutnick, M. J. (2006). NMDA receptors in layer 4 spiny stellate cells of the mouse barrel cortex contain the NR2C subunit. *J Neurosci, 26*(2), 708-715.

Bloomfield, S. A., & Dacheux, R. F. (2001). Rod vision: pathways and processing in the mammalian retina. *Prog Retin Eye Res, 20*(3), 351-384.

Boos, R., Muller, F., & Wassle, H. (1990). Actions of excitatory amino acids on brisk ganglion cells in the cat retina. *J Neurophysiol, 64*(5), 1368-1379.

Boos, R., Schneider, H., & Wassle, H. (1993). Voltage- and transmitter-gated currents of all-amacrine cells in a slice preparation of the rat retina. *J Neurosci, 13*(7), 2874-2888.

Borg-Graham, L. J. (2001). The computation of directional selectivity in the retina occurs presynaptic to the ganglion cell. *Nat Neurosci, 4*(2), 176-183.
Borghuis, B. G., Sterling, P., & Smith, R. G. (2009). Loss of sensitivity in an analog neural circuit. *J Neurosci, 29*(10), 3045-3058.
Brainard, D. H. (1997). The Psychophysics Toolbox. *Spat Vis, 10*(4), 433-436.
Brown, S. P., & Masland, R. H. (2001). Spatial scale and cellular substrate of contrast adaptation by retinal ganglion cells. *Nat Neurosci, 4*(1), 44-51.
Calkins, D. J. (1999). Synaptic organization of cone pathways in the primate retina. In K. Gegenfurtner & L. T. Sharpe (Eds.), *Color vision: from genes to perception*. New York: Cambridge University Press.
Carandini, M., & Ferster, D. (1997). A tonic hyperpolarization underlying contrast adaptation in cat visual cortex. *Science, 276*(5314), 949-952.
Chander, D., & Chichilnisky, E. J. (2001). Adaptation to temporal contrast in primate and salamander retina. *J Neurosci, 21*(24), 9904-9916.
Chen, S., & Diamond, J. S. (2002). Synaptically released glutamate activates extrasynaptic NMDA receptors on cells in the ganglion cell layer of rat retina. *J Neurosci, 22*(6), 2165-2173.
Chichilnisky, E. J. (2001). A simple white noise analysis of neuronal light responses. *Network, 12*(2), 199-213.
Chun, M. H., Han, S. H., Chung, J. W., & Wassle, H. (1993). Electron microscopic analysis of the rod pathway of the rat retina. *J Comp Neurol, 332*(4), 421-432.
Clements, J. D., Lester, R. A., Tong, G., Jahr, C. E., & Westbrook, G. L. (1992). The time course of glutamate in the synaptic cleft. *Science, 258*(5087), 1498-1501.
Cohen, E., & Sterling, P. (1990). Convergence and divergence of cones onto bipolar cells in the central area of cat retina. *Philos Trans R Soc Lond B Biol Sci, 330*(1258), 323-328.
Cohen, E. D. (1998). Interactions of inhibition and excitation in the light-evoked currents of X type retinal ganglion cells. *J Neurophysiol, 80*(6), 2975-2990.
Cohen, E. D. (2000). Light-evoked excitatory synaptic currents of X-type retinal ganglion cells. *J Neurophysiol, 83*(6), 3217-3229.
Cohen, E. D. (2001). Synaptic mechanisms shaping the light-response in retinal ganglion cells. *Prog Brain Res, 131*, 215-228.
Cohen, E. D., & Miller, R. F. (1994). The role of NMDA and non-NMDA excitatory amino acid receptors in the functional organization of primate retinal ganglion cells. *Vis Neurosci, 11*(2), 317-332.
Cohen, E. D., & Miller, R. F. (1999). The network-selective actions of quinoxalines on the neurocircuitry operations of the rabbit retina. *Brain Res, 831*(1-2), 206-228.
Cohen, E. D., Zhou, Z. J., & Fain, G. L. (1994). Ligand-gated currents of alpha and beta ganglion cells in the cat retinal slice. *J Neurophysiol, 72*(3), 1260-1269.
Colbert, C. M., Magee, J. C., Hoffman, D. A., & Johnston, D. (1997). Slow recovery from inactivation of Na+ channels underlies the activity-

dependent attenuation of dendritic action potentials in hippocampal CA1 pyramidal neurons. *J Neurosci, 17*(17), 6512-6521.
Connors, B. W., & Prince, D. A. (1982). Effects of local anesthetic QX-314 on the membrane properties of hippocampal pyramidal neurons. *J Pharmacol Exp Ther, 220*(3), 476-481.
Croner, L. J., & Kaplan, E. (1995). Receptive fields of P and M ganglion cells across the primate retina. *Vision Res, 35*(1), 7-24.
Dacey, D., Packer, O. S., Diller, L., Brainard, D., Peterson, B., & Lee, B. (2000). Center surround receptive field structure of cone bipolar cells in primate retina. *Vision Res, 40*(14), 1801-1811.
Dacey, D. M. (1999). Primate retina: cell types, circuits and color opponency. *Prog Retin Eye Res, 18*(6), 737-763.
Dacheux, R. F., & Raviola, E. (1986). The rod pathway in the rabbit retina: a depolarizing bipolar and amacrine cell. *J Neurosci, 6*(2), 331-345.
Deans, M. R., Volgyi, B., Goodenough, D. A., Bloomfield, S. A., & Paul, D. L. (2002). Connexin36 is essential for transmission of rod-mediated visual signals in the mammalian retina. *Neuron, 36*(4), 703-712.
Demb, J. B. (2002). Multiple mechanisms for contrast adaptation in the retina. *Neuron, 36*(5), 781-783.
Demb, J. B., Haarsma, L., Freed, M. A., & Sterling, P. (1999). Functional circuitry of the retinal ganglion cell's nonlinear receptive field. *J Neurosci, 19*(22), 9756-9767.
Demb, J. B., Sterling, P., & Freed, M. A. (2004). How retinal ganglion cells prevent synaptic noise from reaching the spike output. *J Neurophysiol, 92*(4), 2510-2519.
Demb, J. B., Zaghloul, K., Haarsma, L., & Sterling, P. (2001). Bipolar cells contribute to nonlinear spatial summation in the brisk-transient (Y) ganglion cell in mammalian retina. *J Neurosci, 21*(19), 7447-7454.
Demb, J. B., Zaghloul, K., & Sterling, P. (2001). Cellular basis for the response to second-order motion cues in Y retinal ganglion cells. *Neuron, 32*(4), 711-721.
DeVries, S. H. (2000). Bipolar cells use kainate and AMPA receptors to filter visual information into separate channels. *Neuron, 28*(3), 847-856.
DeVries, S. H. (2001). Exocytosed protons feedback to suppress the Ca2+ current in mammalian cone photoreceptors. *Neuron, 32*(6), 1107-1117.
DeVries, S. H., & Baylor, D. A. (1995). An alternative pathway for signal flow from rod photoreceptors to ganglion cells in mammalian retina. *Proc Natl Acad Sci U S A, 92*(23), 10658-10662.
DeVries, S. H., Li, W., & Saszik, S. (2006). Parallel processing in two transmitter microenvironments at the cone photoreceptor synapse. *Neuron, 50*(5), 735-748.
Dhingra, N. K., Kao, Y. H., Sterling, P., & Smith, R. G. (2003). Contrast threshold of a brisk-transient ganglion cell in vitro. *J Neurophysiol, 89*(5), 2360-2369.
Diamond, J. S., & Copenhagen, D. R. (1993). The contribution of NMDA and non-NMDA receptors to the light-evoked input-output characteristics of retinal ganglion cells. *Neuron, 11*(4), 725-738.

Dingledine, R., Borges, K., Bowie, D., & Traynelis, S. F. (1999). The glutamate receptor ion channels. *Pharmacol Rev, 51*(1), 7-61.
Dumitrescu, O. N., Protti, D. A., Majumdar, S., Zeilhofer, H. U., & Wassle, H. (2006). Ionotropic glutamate receptors of amacrine cells of the mouse retina. *Vis Neurosci, 23*(1), 79-90.
Dzubay, J. A., & Jahr, C. E. (1999). The concentration of synaptically released glutamate outside of the climbing fiber-Purkinje cell synaptic cleft. *J Neurosci, 19*(13), 5265-5274.
Enroth-Cugell, C., & Freeman, A. W. (1987). The receptive-field spatial structure of cat retinal Y cells. *J Physiol, 384*, 49-79.
Enroth-Cugell, C., & Robson, J. G. (1966). The contrast sensitivity of retinal ganglion cells of the cat. *J Physiol, 187*, 517-552.
Erreger, K., Chen, P. E., Wyllie, D. J., & Traynelis, S. F. (2004). Glutamate receptor gating. *Crit Rev Neurobiol, 16*(3), 187-224.
Erreger, K., Geballe, M. T., Dravid, S. M., Snyder, J. P., Wyllie, D. J., & Traynelis, S. F. (2005). Mechanism of partial agonism at NMDA receptors for a conformationally restricted glutamate analog. *J Neurosci, 25*(34), 7858-7866.
Espinosa, F., & Kavalali, E. T. (2009). NMDA receptor activation by spontaneous glutamatergic neurotransmission. *J Neurophysiol, 101*(5), 2290-2296.
Famiglietti, E. V., Jr., & Kolb, H. (1975). A bistratified amacrine cell and synaptic cirucitry in the inner plexiform layer of the retina. *Brain Res, 84*(2), 293-300.
Feigenspan, A., Teubner, B., Willecke, K., & Weiler, R. (2001). Expression of neuronal connexin36 in AII amacrine cells of the mammalian retina. *J Neurosci, 21*(1), 230-239.
Field, G. D., & Chichilnisky, E. J. (2007). Information Processing in the Primate Retina: Circuitry and Coding. *Annu Rev Neurosci*.
Fleidervish, I. A., Binshtok, A. M., & Gutnick, M. J. (1998). Functionally distinct NMDA receptors mediate horizontal connectivity within layer 4 of mouse barrel cortex. *Neuron, 21*(5), 1055-1065.
Fletcher, E. L., Hack, I., Brandstatter, J. H., & Wassle, H. (2000). Synaptic localization of NMDA receptor subunits in the rat retina. *J Comp Neurol, 420*(1), 98-112.
Fletcher, E. L., Koulen, P., & Wassle, H. (1998). GABAA and GABAC receptors on mammalian rod bipolar cells. *J Comp Neurol, 396*(3), 351-365.
Freed, M. A. (2000a). Parallel cone bipolar pathways to a ganglion cell use different rates and amplitudes of quantal excitation. *J Neurosci, 20*(11), 3956-3963.
Freed, M. A. (2000b). Rate of quantal excitation to a retinal ganglion cell evoked by sensory input. *J Neurophysiol, 83*(5), 2956-2966.
Gerstner, W., & Kistler, W. (2002). *Spiking neuron models*. Cambridge, UK: Cambridge University Press.
Grunert, U., Haverkamp, S., Fletcher, E. L., & Wassle, H. (2002). Synaptic distribution of ionotropic glutamate receptors in the inner plexiform layer of the primate retina. *J Comp Neurol, 447*(2), 138-151.

Gustafson, E. C., Stevens, E. R., Wolosker, H., & Miller, R. F. (2007). Endogenous D-serine contributes to NMDA-receptor-mediated light-evoked responses in the vertebrate retina. *J Neurophysiol, 98*(1), 122-130.
Hack, I., Peichl, L., & Brandstatter, J. H. (1999). An alternative pathway for rod signals in the rodent retina: rod photoreceptors, cone bipolar cells, and the localization of glutamate receptors. *Proc Natl Acad Sci U S A, 96*(24), 14130-14135.
Han, Y., & Massey, S. C. (2005). Electrical synapses in retinal ON cone bipolar cells: subtype-specific expression of connexins. *Proc Natl Acad Sci U S A, 102*(37), 13313-13318.
Hartveit, E. (1997). Functional organization of cone bipolar cells in the rat retina. *J Neurophysiol, 77*(4), 1716-1730.
Hochstein, S., & Shapley, R. M. (1976). Linear and nonlinear spatial subunits in Y cat retinal ganglion cells. *J Physiol, 262*(2), 265-284.
Imai, S., Suzuki, T., Sato, K., & Tokimasa, T. (1999). Effects of quinine on three different types of potassium currents in bullfrog sympathetic neurons. *Neurosci Lett, 275*(2), 121-124.
Jackman, S. L., Choi, S. Y., Thoreson, W. B., Rabl, K., Bartoletti, T. M., & Kramer, R. H. (2009). Role of the synaptic ribbon in transmitting the cone light response. *Nat Neurosci, 12*(3), 303-310.
Jacoby, R. A., Wiechmann, A. F., Amara, S. G., Leighton, B. H., & Marshak, D. W. (2000). Diffuse bipolar cells provide input to OFF parasol ganglion cells in the macaque retina. *J Comp Neurol, 416*(1), 6-18.
Jahr, C. E., & Stevens, C. F. (1990a). A quantitative description of NMDA receptor-channel kinetic behavior. *J Neurosci, 10*(6), 1830-1837.
Jahr, C. E., & Stevens, C. F. (1990b). Voltage dependence of NMDA-activated macroscopic conductances predicted by single-channel kinetics. *J Neurosci, 10*(9), 3178-3182.
Kalbaugh, T. L., Zhang, J., & Diamond, J. S. (2009). Coagonist release modulates NMDA receptor subtype contributions at synaptic inputs to retinal ganglion cells. *J Neurosci, 29*(5), 1469-1479.
Kalloniatis, M., Sun, D., Foster, L., Haverkamp, S., & Wassle, H. (2004). Localization of NMDA receptor subunits and mapping NMDA drive within the mammalian retina. *Vis Neurosci, 21*(4), 587-597.
Kaplan, E., & Shapley, R. M. (1982). X and Y cells in the lateral geniculate nucleus of macaque monkeys. *J Physiol, 330*, 125-143.
Karschin, A., Aizenman, E., & Lipton, S. A. (1988). The interaction of agonists and noncompetitive antagonists at the excitatory amino acid receptors in rat retinal ganglion cells in vitro. *J Neurosci, 8*(8), 2895-2906.
Kier, C. K., Buchsbaum, G., & Sterling, P. (1995). How retinal microcircuits scale for ganglion cells of different size. *J Neurosci, 15*(11), 7673-7683.
Kim, K. J., & Rieke, F. (2001). Temporal contrast adaptation in the input and output signals of salamander retinal ganglion cells. *J Neurosci, 21*(1), 287-299.
Kim, K. J., & Rieke, F. (2003). Slow Na+ inactivation and variance adaptation in salamander retinal ganglion cells. *J Neurosci, 23*(4), 1506-1516.

Kohn, A., & Movshon, J. A. (2003). Neuronal adaptation to visual motion in area MT of the macaque. *Neuron, 39*(4), 681-691.
Kohn, A., & Movshon, J. A. (2004). Adaptation changes the direction tuning of macaque MT neurons. *Nat Neurosci, 7*(7), 764-772.
Kolb, H. (1979). The inner plexiform layer in the retina of the cat: electron microscopic observations. *J Neurocytol, 8*(3), 295-329.
Kolb, H., & Famiglietti, E. V. (1974). Rod and cone pathways in the inner plexiform layer of cat retina. *Science, 186*(4158), 47-49.
Kolb, H., & Nelson, R. (1993). OFF-alpha and OFF-beta ganglion cells in cat retina: II. Neural circuitry as revealed by electron microscopy of HRP stains. *J Comp Neurol, 329*(1), 85-110.
Koulen, P., Brandstatter, J. H., Kroger, S., Enz, R., Bormann, J., & Wassle, H. (1997). Immunocytochemical localization of the GABA(C) receptor rho subunits in the cat, goldfish, and chicken retina. *J Comp Neurol, 380*(4), 520-532.
Kwon, Y. H., Nelson, S. B., Toth, L. J., & Sur, M. (1992). Effect of stimulus contrast and size on NMDA receptor activity in cat lateral geniculate nucleus. *J Neurophysiol, 68*(1), 182-196.
Lee, E. J., Han, J. W., Kim, H. J., Kim, I. B., Lee, M. Y., Oh, S. J., et al. (2003). The immunocytochemical localization of connexin 36 at rod and cone gap junctions in the guinea pig retina. *Eur J Neurosci, 18*(11), 2925-2934.
Lee, E. J., Kim, H. J., Kim, I. B., Park, J. H., Oh, S. J., Rickman, D. W., et al. (2003). Morphological analysis of disabled-1-immunoreactive amacrine cells in the guinea pig retina. *J Comp Neurol, 466*(2), 240-250.
Levitt, J. B., Schumer, R. A., Sherman, S. M., Spear, P. D., & Movshon, J. A. (2001). Visual response properties of neurons in the LGN of normally reared and visually deprived macaque monkeys. *J Neurophysiol, 85*(5), 2111-2129.
Li, W., Keung, J. W., & Massey, S. C. (2004). Direct synaptic connections between rods and OFF cone bipolar cells in the rabbit retina. *J Comp Neurol, 474*(1), 1-12.
Lin, B., Jakobs, T. C., & Masland, R. H. (2005). Different functional types of bipolar cells use different gap-junctional proteins. *J Neurosci, 25*(28), 6696-6701.
Llinas, R., & Lopez-Barneo, J. (1988). Electrophysiology of mammalian tectal neurons in vitro. II. Long-term adaptation. *J Neurophysiol, 60*(3), 869-878.
Maffei, L., Fiorentini, A., & Bisti, S. (1973). Neural correlate of perceptual adaptation to gratings. *Science, 182*(116), 1036-1038.
Malenka, R. C., & Bear, M. F. (2004). LTP and LTD: an embarrassment of riches. *Neuron, 44*(1), 5-21.
Manookin, M. B., Beaudoin, D. L., Ernst, Z. R., Flagel, L. J., & Demb, J. B. (2008). Disinhibition combines with excitation to extend the operating range of the OFF visual pathway in daylight. *J Neurosci, 28*(16), 4136-4150.
Manookin, M. B., & Demb, J. B. (2006). Presynaptic mechanism for slow contrast adaptation in mammalian retinal ganglion cells. *Neuron, 50*(3), 453-464.

Marc, R. E. (1999a). Kainate activation of horizontal, bipolar, amacrine, and ganglion cells in the rabbit retina. *J Comp Neurol, 407*(1), 65-76.
Marc, R. E. (1999b). Mapping glutamatergic drive in the vertebrate retina with a channel-permeant organic cation. *J Comp Neurol, 407*(1), 47-64.
Margolis, D. J., & Detwiler, P. B. (2007). Different mechanisms generate maintained activity in ON and OFF retinal ganglion cells. *J Neurosci, 27*(22), 5994-6005.
Masland, R. H. (2001). The fundamental plan of the retina. *Nat Neurosci, 4*(9), 877-886.
Massey, S. C., & Miller, R. F. (1988). Glutamate receptors of ganglion cells in the rabbit retina: evidence for glutamate as a bipolar cell transmitter. *J Physiol, 405*, 635-655.
Massey, S. C., & Miller, R. F. (1990). N-methyl-D-aspartate receptors of ganglion cells in rabbit retina. *J Neurophysiol, 63*(1), 16-30.
Matsui, K., Hosoi, N., & Tachibana, M. (1998). Excitatory synaptic transmission in the inner retina: paired recordings of bipolar cells and neurons of the ganglion cell layer. *J Neurosci, 18*(12), 4500-4510.
Mayer, M. L., Westbrook, G. L., & Guthrie, P. B. (1984). Voltage-dependent block by Mg2+ of NMDA responses in spinal cord neurones. *Nature, 309*(5965), 261-263.
Menger, N., Pow, D. V., & Wassle, H. (1998). Glycinergic amacrine cells of the rat retina. *J Comp Neurol, 401*(1), 34-46.
Miller, R. F. (2008). Cell communication mechanisms in the vertebrate retina the proctor lecture. *Invest Ophthalmol Vis Sci, 49*(12), 5184-5198.
Mills, S. L., & Massey, S. C. (1995). Differential properties of two gap junctional pathways made by AII amacrine cells. *Nature, 377*(6551), 734-737.
Mills, S. L., O'Brien, J. J., Li, W., O'Brien, J., & Massey, S. C. (2001). Rod pathways in the mammalian retina use connexin 36. *J Comp Neurol, 436*(3), 336-350.
Mittman, S., Taylor, W. R., & Copenhagen, D. R. (1990). Concomitant activation of two types of glutamate receptor mediates excitation of salamander retinal ganglion cells. *J Physiol, 428*, 175-197.
Molnar, A., & Werblin, F. (2007). Inhibitory feedback shapes bipolar cell responses in the rabbit retina. *J Neurophysiol, 98*(6), 3423-3435.
Monyer, H., Sprengel, R., Schoepfer, R., Herb, A., Higuchi, M., Lomeli, H., et al. (1992). Heteromeric NMDA receptors: molecular and functional distinction of subtypes. *Science, 256*(5060), 1217-1221.
Movshon, J. A., & Lennie, P. (1979). Pattern-selective adaptation in visual cortical neurones. *Nature, 278*(5707), 850-852.
Muller, F., Wassle, H., & Voigt, T. (1988). Pharmacological modulation of the rod pathway in the cat retina. *J Neurophysiol, 59*(6), 1657-1672.
Murphy, G. J., & Rieke, F. (2006). Network variability limits stimulus-evoked spike timing precision in retinal ganglion cells. *Neuron, 52*(3), 511-524.
Murphy, G. J., & Rieke, F. (2008). Signals and noise in an inhibitory interneuron diverge to control activity in nearby retinal ganglion cells. *Nat Neurosci*.

Myme, C. I., Sugino, K., Turrigiano, G. G., & Nelson, S. B. (2003). The NMDA-to-AMPA ratio at synapses onto layer 2/3 pyramidal neurons is conserved across prefrontal and visual cortices. *J Neurophysiol, 90*(2), 771-779.

Nakajima, Y., Iwakabe, H., Akazawa, C., Nawa, H., Shigemoto, R., Mizuno, N., et al. (1993). Molecular characterization of a novel retinal metabotropic glutamate receptor mGluR6 with a high agonist selectivity for L-2-amino-4-phosphonobutyrate. *J Biol Chem, 268*(16), 11868-11873.

Nakanishi, N., Tu, S., Shin, Y., Cui, J., Kurokawa, T., Zhang, D., et al. (2009). Neuroprotection by the NR3A subunit of the NMDA receptor. *J Neurosci, 29*(16), 5260-5265.

Nelson, S. B., & Sur, M. (1992). NMDA receptors in sensory information processing. *Curr Opin Neurobiol, 2*(4), 484-488.

Nomura, A., Shigemoto, R., Nakamura, Y., Okamoto, N., Mizuno, N., & Nakanishi, S. (1994). Developmentally regulated postsynaptic localization of a metabotropic glutamate receptor in rat rod bipolar cells. *Cell, 77*(3), 361-369.

Nowak, L., Bregestovski, P., Ascher, P., Herbet, A., & Prochiantz, A. (1984). Magnesium gates glutamate-activated channels in mouse central neurones. *Nature, 307*(5950), 462-465.

O'Brien, B. J., Isayama, T., Richardson, R., & Berson, D. M. (2002). Intrinsic physiological properties of cat retinal ganglion cells. *J Physiol, 538*(Pt 3), 787-802.

Palmer, M. J., Hull, C., Vigh, J., & von Gersdorff, H. (2003). Synaptic cleft acidification and modulation of short-term depression by exocytosed protons in retinal bipolar cells. *J Neurosci, 23*(36), 11332-11341.

Palmer, M. J., Taschenberger, H., Hull, C., Tremere, L., & von Gersdorff, H. (2003). Synaptic activation of presynaptic glutamate transporter currents in nerve terminals. *J Neurosci, 23*(12), 4831-4841.

Pan, F., Mills, S. L., & Massey, S. C. (2007). Screening of gap junction antagonists on dye coupling in the rabbit retina. *Vis Neurosci*, 1-10.

Pang, J. J., Abd-El-Barr, M. M., Gao, F., Bramblett, D. E., Paul, D. L., & Wu, S. M. (2007). Relative contributions of rod and cone bipolar cell inputs to AII amacrine cell light responses in the mouse retina. *J Physiol, 580*(Pt 2), 397-410.

Pang, J. J., Gao, F., Barrow, A., Jacoby, R. A., & Wu, S. M. (2008). How do tonic glutamatergic synapses evade receptor desensitization? *J Physiol, 586*(Pt 12), 2889-2902.

Pang, J. J., Gao, F., & Wu, S. M. (2003). Light-evoked excitatory and inhibitory synaptic inputs to ON and OFF alpha ganglion cells in the mouse retina. *J Neurosci, 23*(14), 6063-6073.

Peichl, L. (1989). Alpha and delta ganglion cells in the rat retina. *J Comp Neurol, 286*(1), 120-139.

Pelli, D. G. (1997). The VideoToolbox software for visual psychophysics: transforming numbers into movies. *Spat Vis, 10*(4), 437-442.

Perry, V. H., Oehler, R., & Cowey, A. (1984). Retinal ganglion cells that project to the dorsal lateral geniculate nucleus in the macaque monkey. *Neuroscience, 12*(4), 1101-1123.
Pugh, E. N., Jr., Nikonov, S., & Lamb, T. D. (1999). Molecular mechanisms of vertebrate photoreceptor light adaptation. *Curr Opin Neurobiol, 9*(4), 410-418.
Qian, A., Buller, A. L., & Johnson, J. W. (2005). NR2 subunit-dependence of NMDA receptor channel block by external Mg2+. *J Physiol, 562*(Pt 2), 319-331.
Rieke, F. (2001). Temporal contrast adaptation in salamander bipolar cells. *J Neurosci, 21*(23), 9445-9454.
Rohlich, P., van Veen, T., & Szel, A. (1994). Two different visual pigments in one retinal cone cell. *Neuron, 13*(5), 1159-1166.
Roska, B., Molnar, A., & Werblin, F. S. (2006). Parallel processing in retinal ganglion cells: how integration of space-time patterns of excitation and inhibition form the spiking output. *J Neurophysiol, 95*(6), 3810-3822.
Roska, B., & Werblin, F. (2001). Vertical interactions across ten parallel, stacked representations in the mammalian retina. *Nature, 410*(6828), 583-587.
Sagdullaev, B. T., McCall, M. A., & Lukasiewicz, P. D. (2006). Presynaptic inhibition modulates spillover, creating distinct dynamic response ranges of sensory output. *Neuron, 50*(6), 923-935.
Sakaba, T., Ishikane, H., & Tachibana, M. (1997). Ca2+ -activated K+ current at presynaptic terminals of goldfish retinal bipolar cells. *Neurosci Res, 27*(3), 219-228.
Sakai, H. M., Wang, J. L., & Naka, K. (1995). Contrast gain control in the lower vertebrate retinas. *J Gen Physiol, 105*(6), 815-835.
Sanchez-Vives, M. V., Nowak, L. G., & McCormick, D. A. (2000a). Cellular mechanisms of long-lasting adaptation in visual cortical neurons in vitro. *J Neurosci, 20*(11), 4286-4299.
Sanchez-Vives, M. V., Nowak, L. G., & McCormick, D. A. (2000b). Membrane mechanisms underlying contrast adaptation in cat area 17 in vivo. *J Neurosci, 20*(11), 4267-4285.
Santucci, D. M., & Raghavachari, S. (2008). The effects of NR2 subunit-dependent NMDA receptor kinetics on synaptic transmission and CaMKII activation. *PLoS Comput Biol, 4*(10), e1000208.
Sassoe-Pognetto, M., Wassle, H., & Grunert, U. (1994). Glycinergic synapses in the rod pathway of the rat retina: cone bipolar cells express the alpha 1 subunit of the glycine receptor. *J Neurosci, 14*(8), 5131-5146.
Schiller, P. H. (1992). The ON and OFF channels of the visual system. *Trends Neurosci, 15*(3), 86-92.
Schubert, T., Degen, J., Willecke, K., Hormuzdi, S. G., Monyer, H., & Weiler, R. (2005). Connexin36 mediates gap junctional coupling of alpha-ganglion cells in mouse retina. *J Comp Neurol, 485*(3), 191-201.
Singer, J. H. (2007). Multivesicular release and saturation of glutamatergic signalling at retinal ribbon synapses. *J Physiol, 580*(Pt 1), 23-29.

Singer, J. H., & Diamond, J. S. (2003). Sustained Ca2+ entry elicits transient postsynaptic currents at a retinal ribbon synapse. *J Neurosci, 23*(34), 10923-10933.

Singer, J. H., & Diamond, J. S. (2006). Vesicle depletion and synaptic depression at a mammalian ribbon synapse. *J Neurophysiol*.

Singer, J. H., Lassova, L., Vardi, N., & Diamond, J. S. (2004). Coordinated multivesicular release at a mammalian ribbon synapse. *Nat Neurosci, 7*(8), 826-833.

Slaughter, M. M., & Miller, R. F. (1981). 2-amino-4-phosphonobutyric acid: a new pharmacological tool for retina research. *Science, 211*(4478), 182-185.

Smirnakis, S. M., Berry, M. J., Warland, D. K., Bialek, W., & Meister, M. (1997). Adaptation of retinal processing to image contrast and spatial scale. *Nature, 386*(6620), 69-73.

Smith, R. G., Freed, M. A., & Sterling, P. (1986). Microcircuitry of the dark-adapted cat retina: functional architecture of the rod-cone network. *J Neurosci, 6*(12), 3505-3517.

Solomon, S. G., Peirce, J. W., Dhruv, N. T., & Lennie, P. (2004). Profound contrast adaptation early in the visual pathway. *Neuron, 42*(1), 155-162.

Soucy, E., Wang, Y., Nirenberg, S., Nathans, J., & Meister, M. (1998). A novel signaling pathway from rod photoreceptors to ganglion cells in mammalian retina. *Neuron, 21*(3), 481-493.

Srinivas, M., Hopperstad, M. G., & Spray, D. C. (2001). Quinine blocks specific gap junction channel subtypes. *Proc Natl Acad Sci U S A, 98*(19), 10942-10947.

Sterling, P. (2004). How retinal circuits optimize the transfer of visual information. In L. M. Chalupa & J. S. Werner (Eds.), *The Visual Neurosciences* (Vol. 1, pp. 234-259). Cambridge, MA: MIT Press.

Strettoi, E., Raviola, E., & Dacheux, R. F. (1992). Synaptic connections of the narrow-field, bistratified rod amacrine cell (AII) in the rabbit retina. *J Comp Neurol, 325*(2), 152-168.

Tagawa, Y., Sawai, H., Ueda, Y., Tauchi, M., & Nakanishi, S. (1999). Immunohistological studies of metabotropic glutamate receptor subtype 6-deficient mice show no abnormality of retinal cell organization and ganglion cell maturation. *J Neurosci, 19*(7), 2568-2579.

Taylor, W. R., Chen, E., & Copenhagen, D. R. (1995). Characterization of spontaneous excitatory synaptic currents in salamander retinal ganglion cells. *J Physiol, 486 ( Pt 1)*, 207-221.

Taylor, W. R., Mittman, S., & Copenhagen, D. R. (1996). Passive electrical cable properties and synaptic excitation of tiger salamander retinal ganglion cells. *Vis Neurosci, 13*(5), 979-990.

Taylor, W. R., & Vaney, D. I. (2002). Diverse synaptic mechanisms generate direction selectivity in the rabbit retina. *J Neurosci, 22*(17), 7712-7720.

Trexler, E. B., Li, W., & Massey, S. C. (2005). Simultaneous contribution of two rod pathways to AII amacrine and cone bipolar cell light responses. *J Neurophysiol, 93*(3), 1476-1485.

Trong, P. K., & Rieke, F. (2008). Origin of correlated activity between parasol retinal ganglion cells. *Nat Neurosci, 11*(11), 1343-1351.
Troy, J. B., & Enroth-Cugell, C. (1993). X and Y ganglion cells inform the cat's brain about contrast in the retinal image. *Exp Brain Res, 93*(3), 383-390.
Tsukamoto, Y., Morigiwa, K., Ueda, M., & Sterling, P. (2001). Microcircuits for night vision in mouse retina. *J Neurosci, 21*(21), 8616-8623.
van Wyk, M., Taylor, W. R., & Vaney, D. I. (2006). Local edge detectors: a substrate for fine spatial vision at low temporal frequencies in rabbit retina. *J Neurosci, 26*(51), 13250-13263.
van Wyk, M., Wassle, H., & Taylor, W. R. (2009). Receptive field properties of ON- and OFF-ganglion cells in the mouse retina. *Vis Neurosci, 26*(3), 297-308.
Veruki, M. L., & Hartveit, E. (2002). Electrical synapses mediate signal transmission in the rod pathway of the mammalian retina. *J Neurosci, 22*(24), 10558-10566.
Vidyasagar, T. R. (1990). Pattern adaptation in cat visual cortex is a co-operative phenomenon. *Neuroscience, 36*(1), 175-179.
Volgyi, B., Abrams, J., Paul, D. L., & Bloomfield, S. A. (2005). Morphology and tracer coupling pattern of alpha ganglion cells in the mouse retina. *J Comp Neurol, 492*(1), 66-77.
von Gersdorff, H., & Borst, J. G. (2002). Short-term plasticity at the calyx of held. *Nat Rev Neurosci, 3*(1), 53-64.
von Gersdorff, H., Schneggenburger, R., Weis, S., & Neher, E. (1997). Presynaptic depression at a calyx synapse: the small contribution of metabotropic glutamate receptors. *J Neurosci, 17*(21), 8137-8146.
Walraven, J., Enroth-Cugell, C., Hood, D. C., Macleod, D. I., & Schnapf, J. L. (1990). The control of visual sensitivity: receptoral and postreceptoral processes. In L. Spillmann & J. S. Werner (Eds.), *Visual perception: the neurophysiological foundations* (pp. 53-101). San Diego: Academic Press.
Wang, L. Y., & Kaczmarek, L. K. (1998). High-frequency firing helps replenish the readily releasable pool of synaptic vesicles. *Nature, 394*(6691), 384-388.
Wassle, H. (2004). Parallel processing in the mammalian retina. *Nat Rev Neurosci, 5*(10), 747-757.
Wassle, H., Koulen, P., Brandstatter, J. H., Fletcher, E. L., & Becker, C. M. (1998). Glycine and GABA receptors in the mammalian retina. *Vision Res, 38*(10), 1411-1430.
Wassle, H., Puller, C., Muller, F., & Haverkamp, S. (2009). Cone contacts, mosaics, and territories of bipolar cells in the mouse retina. *J Neurosci, 29*(1), 106-117.
Wassle, H., Schafer-Trenkler, I., & Voigt, T. (1986). Analysis of a glycinergic inhibitory pathway in the cat retina. *J Neurosci, 6*(2), 594-604.
Werblin, F. S., & Dowling, J. E. (1969). Organization of the retina of the mudpuppy, Necturus maculosus. II. Intracellular recording. *J Neurophysiol, 32*(3), 339-355.

Williams, K. (1993). Ifenprodil discriminates subtypes of the N-methyl-D-aspartate receptor: selectivity and mechanisms at recombinant heteromeric receptors. *Mol Pharmacol, 44*(4), 851-859.
Xia, Y., & Nawy, S. (2003). The gap junction blockers carbenoxolone and 18beta-glycyrrhetinic acid antagonize cone-driven light responses in the mouse retina. *Vis Neurosci, 20*(4), 429-435.
Xin, D., & Bloomfield, S. A. (1999). Comparison of the responses of AII amacrine cells in the dark- and light-adapted rabbit retina. *Vis Neurosci, 16*(4), 653-665.
Xu, Y., Vasudeva, V., Vardi, N., Sterling, P., & Freed, M. A. (2008). Different types of ganglion cell share a synaptic pattern. *J Comp Neurol, 507*(6), 1871-1878.
Yamada, E. S., Bordt, A. S., & Marshak, D. W. (2005). Wide-field ganglion cells in macaque retinas. *Vis Neurosci, 22*(4), 383-393.
Yin, L., Smith, R. G., Sterling, P., & Brainard, D. H. (2006). Chromatic properties of horizontal and ganglion cell responses follow a dual gradient in cone opsin expression. *J Neurosci, 26*(47), 12351-12361.
Zaghloul, K. A., Boahen, K., & Demb, J. B. (2003). Different circuits for ON and OFF retinal ganglion cells cause different contrast sensitivities. *J Neurosci, 23*(7), 2645-2654.
Zaghloul, K. A., Boahen, K., & Demb, J. B. (2005). Contrast adaptation in subthreshold and spiking responses of mammalian Y-type retinal ganglion cells. *J Neurosci, 25*(4), 860-868.
Zhang, A. J., & Wu, S. M. (2009). Receptive fields of retinal bipolar cells are mediated by heterogeneous synaptic circuitry. *J Neurosci, 29*(3), 789-797.
Zhang, J., & Diamond, J. S. (2009). Subunit- and pathway-specific localization of NMDA receptors and scaffolding proteins at ganglion cell synapses in rat retina. *J Neurosci, 29*(13), 4274-4286.
Zhang, J., Li, W., Hoshi, H., Mills, S. L., & Massey, S. C. (2005). Stratification of alpha ganglion cells and ON/OFF directionally selective ganglion cells in the rabbit retina. *Vis Neurosci, 22*(4), 535-549.